ROLES OF SOD1 IN NON–SMALL CELL LUNG CANCER

by

XIAOWEN WANG

A dissertation submitted to the

School of Graduate Studies

Rutgers, The State University of New Jersey

In partial fulfillment of the requirements

For the degree of

Doctor of Philosophy

Graduate Program in Cellular and Molecular Pharmacology

Written under the direction of

X. F. Steven Zheng

And approved by

_____

_____

_____

_____

New Brunswick, New Jersey

January, 2019

ABSTRACT OF THE DISSERTATION

ROLES OF SOD1 IN NON–SMALL CELL LUNG CANCER

by XIAOWEN WANG

Dissertation Director:

X. F. Steven Zheng

ABSTRACT

Reactive oxygen species play many important roles in cell growth, metabolism, and survival. Elucidation of the key regulatory mechanisms of cellular redox homeostasis and defense against oxidative stress are fundamentally important for biology and medicine. Superoxide dismutase 1 (SOD1), which rapidly converts superoxide anion to H_2O_2, is a critical component of the cellular antioxidant defense system. However, its role in cancer is not well understood. In this study, I established a physiologically-relevant, non-small cell lung cancer (NSCLC) mouse model, driven by oncogenic K-RAS and p53 knockout (KP), to determine the function and significance of SOD1 in cancer and examine the underlying mechanisms. This study demonstrates that acute ablation of Sod1 accelerates KP tumor initiation and suppresses KP tumor maintenance *in vivo*. Curiously, although the dismutase activity of SOD1 was essential for SOD1 to sustain the growth of KP tumor-derived cells *in vitro*, loss of SOD1 did not significantly enhance global ROS levels. This result suggests a novel function for SOD1 in redox signaling that is critical for the growth of KP tumors. Consistently, nuclear SOD1, rather than cytosolic SOD1, was found to be essential for KP tumor growth, indicating that SOD1 modulates nuclear redox signaling to sustain KP cell

growth. The results from the transcriptome and metabolomics analyses provide additional evidence that specifically nuclear SOD1 function supports tumor maintenance. Collectively, these studies elucidate novel functions of SOD1 that are essential for lung carcinogenesis.

ACKNOWLEDGEMENT

First and foremost, I would like to express my sincere gratitude to my advisor Dr. X. F. Steven Zheng for the continuous support of my Ph.D. study and related research, for his patience, motivation, and immense knowledge. He has provided me with such a wonderful opportunity to advance my scientific knowledge as well as personal improvement. I would like to thank him for being encouraging and for allowing me to grow as an all-around research scientist. His advice on both research as well as on my career have been invaluable.

I would like to thank members of my thesis committee, Drs. Eileen White, Ping Xie, and Michael Verzi for serving as my committee members. Each of the members has offered me insightful comments and suggestions on my work. I am especially thankful to my committee members for taking your time and meet with me individually to discuss my project as well as career development in-between the committee meetings. I benefit enormously from these meetings. A special mention of thanks to Dr. Yanxiang (Jessie) Guo, for offering so many valuable suggestions and discussion that helped me critically during my research. I would like to thank my Program Director, Dr. Marc Gartenberg, and Department Chair, Dr. Nancy Walworth, for their unreserved support during my graduate studies. I also would like to thank Dr. Xiaoyang Su from the Metabolomics shared resource for his guidance with the metabolomics study.

I am also grateful to those I have had the pleasure to work with during this and other related projects. I would like to thank Drs Chen Liu, Evita Sadimin, Christine Minerowicz, Malik Deen for teaching me physiopathology and their contribution to this work. Dr. Christine Minerowicz performed pathological scoring of the mouse tumors. I thank Dr. Wenjing Chen from Biomedical

Imaging Center for Biomedical Imaging & Informatics at CINJ. Dr. Chen established the program for tumor burden quantification with Dr. Evita Sadimin advised on tumor lesion identification. All pictures of tissue staining were taken by the microscope at the Biomedical Imaging Center for Biomedical Imaging & Informatics at CINJ. I would like to thank Shafiq Bhat and Lucyann Franciosa from the histopathology core at CINJ for mouse tissue processing and embedding, as well as performing H&E staining. I would like to thank Arthur Roberts from the Flow Cytometry and Cell Sorting shared resource for advising on Flow Cytometry analysis.

I am also thankful for the members of the Zheng lab. I thank Mengqin Cai for breeding the quadruple mutant mice (over a year long process) and Justin Wong for his hard work in maintaining the mouse colony.

I would like to thank my friends from the CINJ and the broader Rutgers community, for all your help and support throughout my graduate study. Finally, but by no means least, thanks go to my parents for their unconditional support. I dedicate this thesis to them.

Contents

ABSTRACT ---- ii

ACKNOWLEDGEMENT ---- iv

LIST OF TABLES ---- viii

LIST OF ILLUSTRATIONS ---- ix

ABBREVIATIONS ---- xi

CHAPTER I Introduction ---- 1

1.1 Lung cancer ---- *2*

1.1.1 Lung cancer epidemiology and classification ---- 2

1.1.2 The genetic landscape of NSCLC ---- 3

1.1.3 Advances in NSCLC therapy ---- 4

1.1.4 KRAS mutation lung cancer etiology and therapy ---- 5

1.2 Reactive oxygen species and their roles in cancer ---- *7*

1.2.1 Reactive oxygen species and antioxidants ---- 7

1.2.2 Cellular redox signaling ---- 10

1.2.3 The dual role of ROS in cancer initiation and development ---- 12

1.3 Superoxide Dismutase 1 in normal physiology and cancer ---- *14*

1.3.1 Superoxide Dismutase 1 ---- 14

1.3.2 SOD1 and ALS ---- 15

1.3.3 Functional study of SOD1 in bacteria and yeast ---- 16

1.3.4 Functional study of SOD1 in mouse ---- 17

1.3.5 Role of SOD1 in redox signaling ---- 19

1.3.6 SOD1 as an anticancer therapeutic target ---- 20

CHAPTER II SOD1 is required for KP lung cancer maintenance ---- **25**

Rationale ---- *26*

MATERIALS AND METHODS ---- *28*

EXPERIMENTAL RESULTS ---- *32*

2.1 Establishment of an inducible Sod1-knockout mouse model ---- *32*

2.2 Physiology and histopathology analysis of conditional whole body Sod1 knockout mice. ---- *34*

2.3 Generation of a KP lung cancer mouse model with inducible Sod1 knockout. ---- *34*

2.4 SOD1 suppresses KP tumor initiation but is required for tumor development/maintenance ---- *35*

DISCUSSION ---- *37*

CHAPTER III SOD1 is required for KP cells proliferation and survival *in vitro* ---- **55**

MATERIALS AND METHODS ---- *56*

EXPERIMENTAL RESULTS ---- *63*

3.1 Loss of SOD1 suppresses KP Cell Proliferation ---- *63*

3.2 Loss of SOD1 does not increase basal ROS in KP TDCLs but potentiate the cells to oxidative stress. ---- *64*

3.3 Dismutase activity is required for SOD1 to sustain KP cell proliferation. ---- *66*

3.4 Nuclear SOD1, rather than cytosolic SOD1, is important for KP cell proliferation ---- *67*

3.5 Analysis of transcriptome alteration in Sod1 knockout KP TDCLs ---- *68*

3.6 Analysis of the metabolomics alteration in Sod1 knockout KP TDCLs ---- *69*

DISCUSSION ---- *70*

OVERALL CONCLUSION AND FUTURE DIRECTIONS ---- **93**

REFERENCES ---- **95**

APPENDICS: PUBLISHED PAPER ---- **114**

LIST OF TABLES

Table 1.1 Summary of clinical trials for SOD1 inhibitors and mimetics 24

Table 3.1.1 Summary of apoptosis in data from Figure 3.1.2 77

Table 3.1.2 Summary of cell cycle data from in Figure 3.1.3. 77

Table 3.1.3 Summary of cell cycle data from Figure 3.1.3 77

Table 4 Nuclear Fe-S cluster containing genes in mouse. 92

LIST OF ILLUSTRATIONS

Figure 1.1 Generation and deposition of reactive oxygen species 23

Figure 2.1.1 Schematic diagram of *Sod1* locus for the conditional knockout in mouse 42

Figure 2.1.2 Genetic analysis of conditional Sod1-knockout mice carrying various combinations of the wild type and mutant alleles 43

Figure 2.1.3 Schematic diagram of *Sod1* conditional knockout mouse and genotyping primer design. 44

Figure 2.1.4 Induction of UBC-Cre-ERT2-facilitated global SOD1 knockout in $Sod1^{Flox/Flox}$ mice by tamoxifen. 45

Figure 2.1.5 Induction of UBC-Cre-ERT2-facilitated global SOD1 knockout in $Sod1^{Flox/Flox}$ mice. (IHC) 46

Figure 2.2.1 Physiology and histopathology of conditional whole body *Sod1* knockout mice. 48

Figure 2.3.1 Scheme for creation of an inducible *Sod1* knockout KP lung cancer model. 49

Figure 2.4.1 Acute *Sod1* ablation accelerates KP tumor initiation and suppresses KP tumor maintenance 50

Figure 2.4.2 Loss of SOD1 suppresses KP lung tumor proliferation. 52

Figure 3.1.1 Loss of SOD1 suppresses KP Cell Proliferation *in vitro* 75

Figure 3.1.2 Loss of SOD1 induces apoptosis in KP TDCLs. 78

Figure 3.1.3 4OH-Tam causes KP TDCLs to arrest at G2/M independent of SOD1 status. 80

Figure 3.1.4 Loss of SOD1 does not induce senescence in KP TDCLs. 81

Figure 3.2.1 Loss of SOD1 does not increase ROS level in KP cells. 82

Figure 3.2.2 Antioxidants do not rescue KP proliferation from loss of SOD1. 84

Figure 3.2.3 Loss of SOD1 in KP TDCLs does not alter the MAP kinase pathway. 85

Figure 3.3 Dismutase activity is required for SOD1 to sustain KP cells proliferation. 86

Figure 3.4 Nuclear SOD1 is important for KP cell proliferation. 87

Figure 3.5 Changes in KP TDCLs transcriptome following loss of SOD1..... 90

Figure 3.6 Metabolomics analysis of KP TDCLs after loss of SOD1. 91

ABBREVIATIONS

4HT or **4OH-TAM** 4-OH-Tamoxifen

ADC Adenocarcinoma

ALS Amyotrophic lateral sclerosis

DHE Dihydroethidium

GSH Glutathione

NAC N-acetylcysteine

NSCLC Non-small cell lung cancer

SCC Squamous cell carcinoma

SOD Superoxide dismutase

TDCL Tumor derived cell line

TMX tamoxifen

ROS Reactive oxygen species

CHAPTER I Introduction

INTRODUCTION

1.1 Lung cancer

1.1.1 Lung cancer epidemiology and classification

Lung cancer is the most commonly diagnosed of all cancers and the deadliest. In 2018, there were an estimated 2 million new diagnoses, and 1.7 million deaths from lung cancer globally[1]. The high mortality rate makes lung cancer a major cause of cancer-related deaths in the US and globally. In the US alone, it is estimated that in 2018 over 230,000 cases of lung cancer will be diagnosed and more than 150,000 lung cancer-related deaths will occur, accounting for a quarter of all cancer deaths. (Data from the Surveillance, Epidemiology, and End Results (SEER) Program, National Cancer Institute.) Lung cancer incidence is gender-biased, affecting males at higher rates than females. In females, lung cancer is the third most commonly diagnosed cancer, outranked only by breast cancer and colorectal cancer. However, mortality rates are similar for both genders.

Tobacco smoking is the most common cause of lung cancer, accounting for 80% cases worldwide. Among never-smokers, lung cancer incidence is higher in women, and in the general East Asian population; the etiology for these groups is associated with exposure to second-hand smoke, pollution, occupational carcinogen exposure, and inherited genetic susceptibility[2]. Owing to the absence of clinical symptoms and the lack of effective screening programs, lung cancers are often diagnosed at a late stage, which may contribute to the poor prognosis. The 5-year survival rate for lung cancer remains under 20%.

Lung cancer is largely classified according to histopathological characteristics. The most common type of lung cancer is non-small cell lung cancer (NSCLC), comprising 85% of lung cancer incidence. The other 15% of lung cancer cases are small-cell lung cancer (SCLC). There are three

common histotypes of NSCLC: 30% are lung squamous cell carcinoma (SCC) and 70% are non-squamous. Of non-squamous lung cancer cases, 90% are lung adenocarcinomas (ADC) and 10% are large-cell carcinomas[3]. Thus, more than 50% of all cases diagnosed are lung adenocarcinomas. Although all major types of lung cancer are associated with smoking, the association is stronger with SCLC and SCC than with ADC. ADC is the most common histotype found in never-smoker patients[4].

1.1.2 The genetic landscape of NSCLC

Advances in high-throughput genomic profiling such as next-generation sequencing (NGS) has enabled scientists to describe cancers in ways beyond histopathology, including at the molecular and genetic levels. With NGS, individual patient's tumors can be sequenced quickly and cost-effectively to yield information on the particular genetic alterations present in the cancer cells. This method is being applied more frequently, allowing the accumulation of vast amounts of data about individual tumors. With this information, large databases characterizing the molecular profiles of human tumors have been compiled and continue to expand. This information helps to identify the most common mutations in the various histotypes of lung cancer, and correlate them with clinical characteristics of the tumors. Understanding the key genetic features that drive tumorigenesis or determine tumor vulnerability is critical to developing more effective cancer therapies.

KRAS mutation was the first oncogenic mutation identified in lung cancer,[5] followed by the discovery of *BRAF*[6] and *ERBB2*[7] in lung cancer patients. The discovery of a mutation in epidermal growth factor receptor (*EGFR*)[8] in ADC patients, and the association between *EGFR* mutation and EGFR inhibitor response has furthered our understanding of oncogene addiction in NSCLC.[9] Other targetable genetic alterations identified in NSCLC include *MET* amplification[10], *FGFR1*

amplificaiton[11], *NTRK1* amplification[12], and *PDGFRα* mutation[13], and gene translocations such as NGR1 fusion[14], *RET* fusion[15], and *ALK* fusion[16]. A comprehensive list of potential important genetic alterations identified in ADC and SCC was published by Chen *et al.* in 2014[17].

Also published in 2014, was a benchmark TCGA genome-wide integrative genetic analysis on lung tumors, which revealed a comprehensive array of genetic alteration events found in ADC[18]. More than 400 adenocarcinoma cases were analyzed for messenger RNA, microRNA and DNA sequences, and integrated with an analysis of copy number, methylation status, and proteomics. *TP53* was found to be the most commonly mutated gene (46% of all cases). *KRAS* mutations (33%) were mutually exclusive with *EGFR* mutations (14%) in this study. However, *KRAS* and *EGFR* co-mutation does exist in rare cases[19]. Commonly studied oncogenes that were mutated in ADC also include: *BRAF* (10%), *PIK3CA* (7%), and *MET* (7%). Commonly mutated tumor suppressors include *STK11* (17%), *KEAP1* (17%), *NF1* (11%), *RB1* (4%) and *CDKN2A* (4%). The chromatin modifying genes SETD2 (9%), ARID1A (7%), and SMARCA4 (6%) and the RNA splicing genes RBM10 (8%) and U2AF1 (3%) were also observed with significant incidence. Loss-of-function *MGA* mutations, though not previously reported, were also found in this study and were mutually exclusive with *MYC* amplification.

1.1.3 Advances in NSCLC therapy

Efforts to uncover targetable genetic alterations in lung cancer have significantly reshaped the clinical management of lung cancer, and the therapeutic options have expanded beyond genotoxic agents to targeted therapy and immunotherapy[2]. FDA-approved targeted therapies include EGFR tyrosine kinase inhibitors (TKIs) for EGFR mutated cases[20], and ALK inhibitors for lung cancer with *ALK* or *ROS1* fusions[21]. For lung cancer patients with *BRAF* mutations, BRAF and MET inhibitors are available as either single-agent or combination treatment. On the other hand,

immune checkpoint proteins, such as PD-1, PD-L1 and CTLA4 downregulate T-cell activation and thus promote immune escape by tumors[22]. Antibodies targeting PD-1 and PD-L1 have been approved for treating some types of NSCLCs. Nivolumab (anti-PD-1) was approved for patients with metastatic squamous NSCLC with progression during or after platinum-based chemotherapy. Pembrolizumab (anti-PD-1) in combination with pemetrexed and carboplatin was approved for the treatment of patients with previously untreated metastatic non-squamous NSCLC. Atezolizumab (anti-PD-L1) is indicated for patients with metastatic NSCLC who have disease progression during or following platinum-containing chemotherapy.

1.1.4 KRAS mutation lung cancer etiology and therapy

KRAS (Kirsten ras oncogene homolog) belongs to the RAS family (which also includes HRAS and NRAS). The *KRAS* gene encodes a small GTPase. Over 30% of lung adenocarcinomas harbor KRAS point mutations. However, the KRAS mutation rate is lower in the Asian population (13%)[23,24] and in lung cancer patients who are never smokers (4%)[4]. In addition, KRAS mutations are rare in SCC[25] and SCLC[26]. KRAS mutations are predominantly found at the Gly 12 residue[27]. Mutation at Gly 12 residue impairs the intrinsic and GAP-facilitated GTP hydrolytic activity of KRAS. This allows persistent KRAS-GTP binding, resulting in constitutive activation of KRAS. Activated KRAS regulates various downstream effectors and thus controls diverse cellular processes including cell proliferation, differentiation, and survival.

In a review of eleven different RAS effectors by Vigil et al.[28], functional studies validated that at least six of these effector pathways are responsible for RAS-dependent cancer initiation and/or maintenance[29]. Among the many RAS effector pathways, the RAF/MEK/ERK pathway is considered the key driver of RAS-driven tumorigenesis[30,31]. In particular, the CRaf-MEK1/2-ERK1/2 pathway is uniquely essential for KRAS-mediated lung cancer tumorigenesis[30]. The PI3K-AKT-

mTOR pathway is also a well validated RAS effector pathway. Disrupting RAS mediated PI3K activation almost completely ablates tumor initiation and leads to regression of KRAS-mediated lung cancer in mouse models[32]. Activation of the PI3K pathway is sufficient to maintain tumor growth in the absence of oncogenic Ras[33].

Despite enormous efforts made to examine Ras, targeting mutant *KRAS* has proven to be very difficult clinically. Cox et al.[27] reviewed in 2014 (updated in 2017[34]) the efforts and challenges in targeting RAS. There are generally five possible anti-RAS strategies: 1. Direct inhibition of RAS. Directly inhibiting Ras small GTPase with GTP competitive inhibitors is challenging due to the picomolar affinity of GTP-RAS (in contrast, ATP binds protein kinases with micromolar affinity). Taking advantage of the unique nucleophilicity of cysteine thiols, covalent G12C specific Inhibitors[35,36] have been developed to target cancers bearing KRAS the G12C mutation (44% of lung adenocarcinomas[25]). 2. Targeting the association of RAS with the plasma membrane. RAS activation requires c-terminal prenylation-dependent membrane association to be functional. The predominant KRAS splice variant, KRAS4B, differs from the other splice variants, KRAS4A, HRAS and NRAS, in that it can be alternatively modified by farnesylation or geranylgeranylation, and does not require palmitoylation.[37] Failure to appreciate this difference has led to the failure of farnesyltransferase inhibitors clinical trials. A recent identified potential target, prenyl-binding protein phosphodiesterase δ (PDEδ), facilitates the shuttling and recycling of RAS protein between endosomal vesicles and the plasma membrane[38]. PDEδ inhibitors were found to suppress oncogenic KRAS signaling and impair the tumorigenic growth of KRAS-mutant cancer cells[39,40]. 3. Inhibition of RAS downstream signaling pathways. This is the most intensely pursued strategy. Numerous inhibitors of each component of the RAF/MEK/ERK and PI3K/AKT/mTOR pathways have been developed and are currently under clinical evaluation. A key problem lies in the complicated compensatory and feedback mechanism, which has made it difficult for single-target

inhibitors to exert lasting anti-cancer effects. Inhibitors that simultaneously affect several effector proteins, or combination regimens that target several proteins, are being developed but have shown disappointing results in clinical trials, partially due to toxicity. 4. Targeting synthetic lethal interactors of mutant RAS, and 5. Targeting RAS-mediated metabolic pathways that are critical in cancer cells. Recent advances and successes in cancer immunotherapy have spurred great interest in identifying optimal biomarkers for predicting sensitivity to immunotherapy (such as immune checkpoint blockade therapy) sensitivity. Tumor mutational burden (TMB) has been proposed as a potential marker for responsiveness to immune checkpoint inhibitors in advanced NSCLC[41,42]. Lung adenocarcinoma has a high TMB, at 8.87 mutations per megabase (Mb) of DNA[18]. In addition, lung cancers harboring *KRAS* mutations may be more likely to respond to immune blockade therapy[41,43]. In particularly, TP53/KRAS co-mutated lung cancer have been found to express increased levels of programmed death-ligand 1 (PD-L1), and a large proportion of $PD\text{-}L1^{+}/CD8A^{+}$ expression, and demonstrate a remarkable clinical response to PD-1 inhibitors[44].

1.2 Reactive oxygen species and their roles in cancer

1.2.1 Reactive oxygen species and antioxidants

Until the so called “Great Oxidation Event” that took place about 2.4 billion year ago, the level of atmospheric oxygen was only 0.001% of what it is today.[45] It is widely accepted that the emergence of photosynthesis led to a dramatic rise in O_2 in the atmosphere. The dioxygen molecule (O_2) generated from photosynthesis thus shaped the atmosphere that we all live in today. The transfer of electrons through biological matter is one of the key steps by which cells harvest, store and utilize cellular energy. O_2 is a four-electron oxidizing agent and an ideal electron donor for many biological processes, such as oxidative phosphorylation. Electron reduction of O_2

leads to the formation of reactive oxygen species (ROS). Similar nitrogen-containing oxidants, such as nitric oxide, are called reactive nitrogen species (RNS).

The three major types of ROS are superoxide ($O_2^{\cdot-}$), hydrogen peroxide (H_2O_2) and hydroxyl radicals (•HO), which are the all intermediates generated when O_2 is reduced to H_2O in four sequential one-electron steps. Of these three ROS, •HO is the most potent oxidizing molecule, whereas $O_2^{\cdot-}$ is not reactive unless protons are available to stabilize the O_2^{2-} as $O_2^{\cdot-}$ receives the electron from oxidation[46]. Superoxide does not oxidize most organic substrates, such as proteins, lipids, nucleic acids or carbohydrates. It is a short-lived free radical as it is rapidly converted to H_2O_2 by the superoxide dismutase (SOD) family protein. This dismutase activity occurs with high efficiency (rate constant $>10^9$ M^{-1} s^{-1})[46], whereas the rate constant of superoxide self-disproportionation at pH 7 is about 1000-fold less (10^6 M^{-1} s^{-1})[47]. Superoxide carries a negative charge at physiological pH (p*K*a = 4.8), therefore does not pass through cellular membranes by diffusion. However, it can cross the membrane through the anion channel[48]. Superoxide anion can rapidly react with nitric oxide (•NO), which is a signal transducing free radical, and gives rise to the strong oxidant, peroxynitrite ($ONOO^-$). Peroxynitrite, in turn, promotes oxidation and nitration reactions that affect various biomolecules such as proteins and lipids[49]. Peroxynitrite can also profoundly influence cellular processes such as inflammatory responses[50].

Aerobic organisms are constantly exposed to endogenous ROS from various sources. Mitochondria are the major source of superoxide in the cell. The mitochondrial respiratory complex leaks a certain amount of electrons to oxygen from the Qo and Qi intermediates, thus generating superoxide[51,52]. Superoxide is then released on both sides of the mitochondrial intermembrane[53]. Peroxisomes are another key ROS-generating organelles, particularly of H_2O_2, contributed mainly by β-oxidation of fatty acids. Among at least ten H_2O_2-generating oxidases located in peroxisomes, xanthine oxidase, catalyzes the oxidation of hypoxanthine to xanthine

and generates superoxide radicals and hydrogen peroxide during this process.[54,55] Studies have suggested that oxidative protein folding at the endoplasmic reticulum is also an important source of ROS production[56]. Cytochrome P450 superfamily proteins at the endoplasmic reticulum are responsible for oxidizing a wide spectrum of drugs and xenobiotics, as well as carrying out hormone synthesis. However, uncoupling of the catalytic cycle results in continuous production of ROS.[57] Another class of oxidants is the NADPH oxidase (NOX) family proteins consisting of seven members: NOX1 - NOX5, Duox1 and Duox2. NOX proteins are professional ROS-producing enzymes. Among them, Nox1, Nox2, Nox3 and Nox5 produce primarily superoxide, which may be converted into H_2O_2 by dismutase. In contrast, Nox4, Duox1 and Duox2 produce H_2O_2 directly[58]. Lastly, the nitric oxide synthases (NOS) generate the relatively stable and signal-transducing free radical, nitric oxide (•NO).

Most ROS are highly reactive molecules that can readily act on vital cellular components (i.e., nucleic acids, proteins, lipids, and sugars) potentially causing irreversible damage. Therefore, organisms that are capable of cohabitating with or even utilizing ROS have an evolutionary advantage. The earliest existing antioxidant genes were superoxide dismutase (SOD), catalase (CAT), and peroxiredoxin (PRX)[59]. Accumulated superoxide can damage and inactivate proteins, especially those containing iron-sulfur (Fe-S) clusters[60,61]. The resultant H_2O_2 can in turn react with ferrous iron (Fe^{2+}) or copper ion (Cu^{+}) and give rise to hydroxyl radicals. H_2O_2 is also reactive to protein cysteine residues at physiological pH. This reaction oxidizes the cysteine thiolate anion ($Cys\text{-}S^{-}$) to the sulfenic form (Cys-SOH), causing allosteric changes in the protein that alter its function. Such H_2O_2-induced allosteric changes in proteins have also been shown to represent a mechanism for sensing oxidative stress, and for activating the survival response.[62-64] Oxidized cysteine can be reduced by the disulfide reductases, thioredoxin (TRX) and glutaredoxin (GRX). Peroxiredoxins (PRXs) and glutathione peroxidase (GPXs) function to prevent accumulation of

intracellular H_2O_2 in the first place. These redoxins and peroxidases are eventually reduced by NADPH and glutathione (GSH), which therefore represent the ultimate ROS scavengers within the cell (Figure 1.1).

1.2.2 Cellular redox signaling

Elevated levels of ROS create oxidative stress, causing damage to both DNA and protein, leading to an accumulation of damaged biological molecules. Excessive ROS is thought to be the one of the main causes of many pathologic conditions, such as neurodegenerative diseases, atherosclerosis and aging. At physiological levels, however, ROS can serve as a signaling molecule, triggering and regulating biological processes[60,61,65,66].

The oxidative stress response mechanism allows cells to "measure" the cellular ROS level, then activate or induce the corresponding antioxidant system. In prokaryotic cells, SoxR and OxyR are responsible for sensing O_2^- and H_2O_2 respectively. High reactivity of O_2^- towards the [Fe-S] center of SoxR enables the specific superoxide response regulation[67]. H_2O_2 facilitates an intramolecular disulfide bond between Cys199 and Cys 208 in OxyR and triggers the activation of OxyR dependent genes[68,69]. While SoxR does not exist in eukaryotes, ROS-mediated protein activity modulation through reversible oxidation of cysteine residues is a conserved mechanism for redox signaling transduction.

Hypoxia-inducible factor 1 (HIF-1) is a transcription factor that mediates adaptive responses to changes in tissue oxygenation[70,71]. HIF-1 is a heterodimer consisting of HIF-1β and HIF-1α. The HIF-1β level is constant, while the HIF-1α level is tightly regulated through protein synthesis and degradation. Under normoxic conditions, O_2-dependent hydroxylation of HIF-1α enables its binding to von Hippel–Lindau (VHL) tumor-suppressor protein, and can then be recognized by the

ubiquitin-proteasome for degradation. Under hypoxic conditions, HIF-1α is not hydroxylated and therefore stabilized as a result of decelerated degradation[72-74]. O_2-dependent hydroxylation of an asparagine residue of HIF-1α disrupts its binding of the p300 transcriptional coactivator, limiting its transcriptional activation potential[75].

The transcription factor "nuclear factor erythriod 2-related factor 2" (Nrf2) is the master regulator of the cellular antioxidant response, detoxification and anti-inflammatory cytoprotective genes[76]. Nrf2 controls the transcription of an array of antioxidant response element (ARE) dependent genes to regulate cellular redox homeostasis[77]. Kelch-like erythroid cell-derived protein with CNC homology-associated protein 1 (Keap1) forms an E3-ubiquitin ligase with Cullin-3/Rbx1 and targets Nrf2 for proteasome-mediated degradation[78-80]. Oxidation of cysteine residues in Keap1 disrupte the ubiquitination of Nrf2 and leads to Nrf2 accumulation, and, in turn, the induction of transcription of Nrf2-dependent genes[78,81]. Ataxia telangiectasia mutated (ATM) protein kinase is a master regulator of the DNA damage response. ATM coordinates checkpoint activation, DNA repair, and metabolic changes in response to double-strand breaks and oxidative stress in eukaryotic cells[82]. Loss of ATM leads to chronic oxidative stress in both mice and patients with ataxia telangiectasia[83-85]. ATM can be directly activated by oxidation-induced homodimerization in the absence of DNA damage[62,86].

Cells have been able to harness the same mechanism of reversible oxidation of protein cysteine thiols by oxidants such, as H_2O_2, in order to modulate cellular processes other than for sensing oxidative stress. Growth factors employ H_2O_2 as a signaling molecule to transmit downstream growth signals.[87-91] Inhibition by H_2O_2-induced oxidation is a common phenomenon among several protein tyrosine phosphatases.[92,93] Through Phosphatidylinositol 3-Kinase (PI3K)/Rac1, epidermal growth factor (EGF) and platelet-derived growth factor (PDGF) can transiently

stimulate NOXs to produce ROS[90,94]. Peroxiredoxin can be inactivated locally in response to growth factor signaling or immune receptors and allows for transient accumulation of H_2O_2[89]. H_2O_2 accumulation at the cellular membrane inactivates protein-tyrosine phosphatase 1B (PTP1B) by oxidizing the catalytic cysteine to a sulfenic moiety[87]. PTP1B dephosphorylates tyrosine residues of EGFR, and so inactivation of PTP1B leads to the activation of EGFR[91,95]. Similarly, Src homology region 2-containing protein tyrosine phosphatase 2 (SHP-2) can be inhibited through oxidation, thus allowing the activation of PDFGR pathway[93]. Phosphatase and tensin homolog (PTEN) is a tumor suppressor that negatively regulates the P13K/AKT pathway through its lipid phosphatase activity. Pten can be transiently inactivated by oxidation following cellular stimulation by EGF, PDGF, or insulin[97]. Loss of SOD1 results in reduced PTP oxidation and therefore attenuates phosphatases dependent growth factor signaling activation[98].

1.2.3 The dual role of ROS in cancer initiation and development

ROS is considered a driving factor of carcinogenesis[99]. At elevated levels, ROS can act as a direct DNA mutagen or cause genomic instability, and thus contribute to tumorigenesis[100,101]. Antioxidant function of p53 is thought to be critical for its tumor suppressor role. Loss of p53 results in increased ROS level in both cultured tumor cells and primary splenocytes and thymocytes[102]. Prepartum administration of the antioxidant, N-acetylcysteine (NAC), extended life and blunted lymphoma formation in p53-deficient murine offspring[102]. Mutant $p53^{3KR/3KR}$, which lacks the capacity to mediate cell cycle arrest, apoptosis and senescence, but is capable of regulating ROS production, was found to confer resistance to early-onset spontaneous tumorigenesis[103]. The homozygous loss of breast cancer-associated gene-1 (BRCA1) also caused elevated ROS levels, sensitizing cells to oxidative stress and leading to increased tumor susceptibility[104]. Mitochondria ROS is particularly critical for tumorigenesis[105,106]. Oncogene

transformation increases overall mitochondrial metabolism[107]. Mitochondria ROS preferentially accumulates potentially oncogenic signaling pathways[108]. Inhibition of mitochondrial ROS in murine sarcoma cells by overexpression of mitochondrial SOD was found to suppress radiation-induced transformation[109,110]. Oncogenic Kras was shown to increase oxidative stress in the mitochondria matrix, and mitochondria-derived ROS is required for tumor cell proliferation[111].

High ROS levels are nonetheless cytotoxic to cancer cells[112-114]. Multiple studies have demonstrated that antioxidants can have tumor-promoting effects. For example, NAC was shown to promote tumorigenesis in several mouse models of lung cancer. ROS reduction by NAC protected the tumor cells from DNA damage, prevented p53 activation, and promoted proliferation[115]. In addition, synthesis of the antioxidant glutathione (GSH) has been demonstrated to be required for tumor initiation. The GSH and TXN antioxidant pathways synergistically support tumor cell survival[116]. And loss of the antioxidant master regulator Nrf2 was also found to inhibit tumorigenesis in models of lung and pancreatic cancer[117,118].

This evidence highlights the crucial role of ROS in the regulation of cancer initiation and maintenance. Cancer cells manifest with increased rates of ROS production due to aberrant metabolism and protein translation[119-121]. Accumulation of ROS can eventually lead to cancer cell apoptosis. Under survival pressure, however, cancer cells can evolve a network that is different from the canonical signaling pathway, through which the cancer cells are more tolerant to oxidative stress and therefore thrive under conditions of elevated ROS[122]. For instance, oncogenic Kras promotes lung and pancreatic cancer initiation and maintenance through activating Nrf2 to promote and sustain mRNA translation as well as mitogenic signaling[117,118].

HIF-1α is frequently found to be upregulated in cancer[123-125]. Intratumoral hypoxia is a major mechanism underlying the increased levels of HIF-1α. More strikingly, through genetic alteration

such as VHL mutation in renal cell carcinoma or mutations in the Wnt/β-catenin signaling pathway in colon carcinoma[126], tumor cells exhibit elevated levels of HIF-1α under normoxic conditions[127]. Activated HIF-1α protects tumor cells beyond hypoxia stress. HIF-1α regulates various aspect of cancer development, including proliferation, angiogenesis, apoptosis, autophagy, metabolism, DNA damage response, extracellular matrix remodeling, cell migration and invasion[126,128]. Furthermore, HIF-1α overexpression promotes tumorigenesis, and high HIF-1α levels are associated with poor prognosis[129].

Oncogenes modulate redox homeostasis in tumor cells by reprograming cellular metabolism to promote tumorigenesis[130]. Ras mutant tumor cells are "addicted" to glutamine. Oncogenic Ras reprograms glutamine metabolism to maintain redox homeostasis and support cell survival and growth[111,131-133]. Oncogenic Kras reprograms glutamine metabolism, resulting in an increased $NADPH/NADP^+$ ratio, which maintains the cellular redox state[133,134]. Kras-Keap1 mutant lung tumor cells are dependent on increased glutaminolysis and are sensitive to glutaminase inhibition[132,135]. A cancer-specific isoform of pyruvate kinase, pyruvate kinase M2 isoform, muscle (PKM2), has minimal kinase activity[136-138]. PKM2 converts phosphoenolpyruvate (PEP) to ATP and pyruvate less efficiently, and therefore diverts the flow of upstream glycolytic intermediates into the pentose phosphate pathway (PPP), where NADPH are generated to support the antioxidant system. High ROS can inhibit PKM2 through oxidation, and thereby promote NADPH generation[64].

1.3 Superoxide Dismutase 1 in normal physiology and cancer

1.3.1 Superoxide Dismutase 1

SOD1 was first isolated from bovine erythrocytes as a blue copper-containing protein named "hemocuprein" in 1939[139]. In 1969, its enzymatic function was discovered and it was appropriately

renamed as superoxide dismutase[140]. SOD1 (Cu/Zn-SOD) is located in the cytosol and mitochondrial intermembrane space (IMS), while SOD2 (Mn-SOD) localizes to the mitochondrial matrix. SOD3 (EC-SOD), also a copper-zinc-containing SOD, is secreted into the extracellular space.

All aerobic organisms produce superoxide dismutase[141]. The crystal structures of the fully metallated state of SOD1 from various species show a highly conserved structure that contains eight strands of *β*-barrel, and binds one atom of copper and one atom of zinc. It also possesses two large functionally important loops, the electrostatic loop and zinc loop. SOD1 functions as a homodimer of two proteins of 154 amino acids. The copper ion, bound by conserved histidine residues His 46, His 48, His 63, and His 120, is at the center of the catalytic reaction. The zinc ion, bound by conserved residues His 63, His 71, His 80, and Asp 83, is not necessary for the enzymatic activity, but it is structurally critical for the catalytic center. A highly conserved intramolecular disulfide bond between Cys 57 and Cys 146 (human SOD1 numbering) is also essential for its enzymatic activity.

Maturation of SOD1 is considered to require three critical steps: zinc and copper acquisition, disulfide bond formation, and dimerization. Copper insertion and disulfide bond formation are facilitated by the chaperone protein, Copper Chaperone For Superoxide Dismutase (CCS). CCS largely determines SOD1 activity and regulates cellular distribution of SOD1 into the cytosol or mitochondria[142,143]. However, loss of CCS does not fully abrogate SOD1 activity, or disulfide bond formation, indicating that a CCS-independent mechanism exists SOD1 to incorporate Cu[144-146]. The mechanism for zinc incorporation into SOD1 is unknown.

1.3.2 SOD1 and ALS

Amyotrophic lateral sclerosis (ALS) is an adult-onset progressive neurodegenerative disease affecting motor neurons in the brain and spinal cord. SOD1 mutation accounts for about 20% of

familiar ALS (fALS) cases (which comprises 1~2% of all ALS cases) and 2-7% of sporadic cases. Although the mechanism underlying mutant SOD1 dependent motor neuron death is still not well understood, there is strong evidence supporting the hypothesis that loss of dismutase function by SOD1 is not the cause. Transgenic expression in mice of a mutant form of SOD1 discovered in human ALS cases leads to neuronal disease that is comparable to ALS. But SOD1 deletion in mice, however, does not lead to motor neuron diseases[147]. More than 160 different fALS mutations have now been identified in the SOD1 sequence according to the Amyotrophic Lateral Sclerosis Online genetics Database (ALSoD; http://alsod.iop.kcl.ac.uk/). Most of these SOD1 mutations lead to misfolded proteins that can then aggregate to form inclusions in the lower motor neuron, which was believed to cause disease pathogenesis. However, activity analysis on fALS SOD1 mutations revealed that many of these SOD1 mutants retain dismutase activity, such as hSOD1 G37R[148], hSOD1 G93A[149,150], hSOD1 G85R[151]. Indeed, gain-of-function mutation in SOD1 that results in toxic downstream effects on many cellular processes is the prevalent hypothesis for the etiology of mutant SOD1-associated fALS.

1.3.3 Functional study of SOD1 in bacteria and yeast

Superoxide alone is not reactive to macromolecules such as peptides, lipids and DNA. Studies on SOD null *E. coli* have provided evidence and mechanisms by which superoxide may damage cellular components[152]. The *sodAsodB* mutant *E. coli* stain cannot survive in aerobic conditions unless provided with branched-chain, sulfur-containing, and aromatic amino acids. Superoxide activity was found responsible for these phenotypical defects. Superoxide shuts down the branched-chain amino acid biogenesis pathway by critically inactivating the penultimate step, which is catalyzed by dihydroxy acid dehydratase, a [4Fe-4S]-containing enzyme[153]. It was proposed that superoxide generates •HO and release Fe^{2+} by oxidizing [4Fe-4S]-cluster-containing

proteins[154]. Indeed, superoxide was found to be capable of inactivating several [4Fe-4S]-cluster-containing proteins in *E. coli*, such as aconitase, 6-phosphogluconate dehydratase, and fumarases A and B[155,156]. Superoxide inactivation of transketolase in the aromatic amino acid biosynthesis pathway is thought to be the cause of aromatic-amino-acid auxotrophy[157]. The auxotrophy for sulfur-containing amino acid is believed to be related to the phenomenon of superoxide alteration of cell membrane permeability, which leads to the leakage of metabolic intermediates such as sulfite[158].

1.3.4 Functional study of SOD1 in mouse

Mice with constitutive *Sod1* knockout were generated almost two decades ago. Distinct from *Sod2* knockout, which leads to perinatal death in mice[159], mice with *Sod1* deficiency are viable and develop relatively similar to wild type mice[160,161]. However, *Sod1*-deficient mice have a reduced lifespan[162,163], and manifest premature aging related phenotypes, such as accelerated hearing loss[164], neurological degeneration[161], macular degeneration[165-167], and enhanced age-related cataracts[168]. Aging has been associated with elevated level of ROS. Indeed, analysis of mice with global constitutive *Sod1* deficiency showed widespread oxidative damage[162,163,169]. Accompanying this increased oxidative stress, SOD1-deficient mice show increased mutation accumulation and cellular apoptosis[162,170]. Elevated ROS has been linked to myriad pathologies, and, similarly, many of the deleterious phenotypes observed in *Sod1*-null mice are associated with increased ROS levels. Female *Sod1*-null mice have impaired reproductive function due to compromised ovarian function[171]. A follow-up study showed that *Sod1*-deficient oocytes arrest at the two-cell stage as a result of intrinsic oxidative stress[172]. ROS is also found at elevated levels in red blood cells in *Sod1*-deficient mice, which are associated with an anemic phenotype[172-174]. *Sod1* deficiency in combination with Fanconi anemia complementation group C (Fancc) resulted in defective

hematopoiesis and hepatic steatosis, and was accompanied by Increased superoxide production by Fancc$^{-/-}$Sod1$^{-/-}$ liver cell cultures[175]. Furthermore, downregulation of *Sod1* in neuronal cells led to cell death caused by accumulated superoxide reacting with nitric oxide to form cytotoxic peroxynitrite[176,177].

Increased superoxide is found in the arteries and micro vessels in *Sod1*-deficient mice and is associated with vascular dysfunction[178]. Elevated superoxide level and impairment of endothelial function have been observed in *Sod1*$^{+/-}$ mice[179]. Deficiency in *Sod1* caused enhanced angiotensin II-mediated impairment of endothelial function, which was prevented by overexpression of *Sod1*[180]. Similar effects were observed in cerebral arterioles: a gene-dosing effect of *Sod1* increases superoxide, and leads to induction of cerebral vascular hypertrophy and vascular dysfunction[181].

Muscle atrophy and weakness observed in young *Sod1* null mice resembles that which is observed in older wildtype mice[165]. *Sod1* null mice show age-dependent skeletal muscle atrophy[166], accompanied by impaired neurotransmitter release and neuromuscular junction destabilization[167]. *Sod1* deficits in the motor neuron and muscle both contribute to the sarcopenia phenotype. Neuron-specific expression of *Sod1* prevents the muscle mass loss in *Sod1* knockout mice[182], but neuron-specific deletion of *Sod1* does not fully recapitulate the sarcopenia phenotype[183]. A specific redox shift in the catalytic Cys47 residue of peroxiredoxin 6 was identified in the peripheral nerves of *Sod1* null mice, suggesting impaired redox signaling may play a key role in the development of *Sod1*-deficiency induced sarcopenia[184].

Whole body constitutive knockout in mice results the development neoplastic diseases such as lymphoma, hepatocellular carcinoma, lung tumors, and hemangiomas in the liver and spleen[162,163]. Aged *Sod1* knockout mice develop hepatocellular carcinomas (HCC)[162]. This may

develop similarly as non-alcoholic fatty liver disease (NAFLD) progression to HCC[185]. *Sod1* deficiency causes hepatosteatosis in mice. Degradation of apoB protein in *Sod1* deficient mice may account for the lipid accumulation due to impaired lipoprotein secretion[186]. *Sod1* knockout mice also exhibit altered hepatic glycolysis, gluconeogenesis, and lipogenesis[187]. The observed accumulation of hepatic collagen suggests that liver fibrosis is greatly expected to occur in *Sod1* knockout mice[188].

The immune-modulating function of SOD1 was revealed using *Sod1*-deficient mice, which were found to produce less caspase-1-dependent cytokines and were less susceptible to lipopolysaccharide-induced septic shock[189]. *Sod1*-deficient macrophages have high superoxide production and altered redox potential. This leads to specific inhibition of caspase-1 through oxidation of cysteine residues[189]. Modulation of the cellular redox balance is also critical for viral infection-associated tissue damage. SOD1 was demonstrated to provide protection for hepatocytes from virus-induced oxidative stress and cell death, reinforcing the concept that innate immunity can be a driver for tissue pathology[190].

1.3.5 Role of SOD1 in redox signaling

At physiological levels, ROS is known to act as a signaling molecule. Among various forms of ROS, $O_2^{\bullet -}$ and especially H_2O_2 are well-appreciated as redox signaling molecules[191]. The oxidation of specific redox-sensitive cysteine residues is the best-studied mechanism of redox signaling. Examples of redox signaling that depend on SOD1-derived H_2O_2 include regulation of inflammation, angiogenesis and vascular function.

SOD1 has been suggested to participate in IL-1β signaling at the endosome. SOD1 is recruited to endosomes following IL-1β simulation, where it converts IL-1β-induced $O_2^{\bullet -}$ to H_2O_2, activating IL-1β-dependent IKK and leading to NF-κB activation[192,193]. SOD1 also facilitates IL-1β maturation

by specifically regulating caspase-1 oxidation at Cys397 and Cys362. Loss of SOD1 resulted in decreased caspase-1 dependent cytokines production in mice and decreased susceptibility to septic shock[189].

SOD1 also facilitates a self-regulating redox sensor for Nox2-derived $O_2^{\bullet-}$ production. Redox sensitive binding of SOD1 to Rac1 maintains Rac1 activation as well as Rac1-dependent $O_2^{\bullet-}$ production by Nox2. Locally accumulated H_2O_2 from dismutation of $O_2^{\bullet-}$ dissociates SOD1 from Rac1 leading to inactivation and thereby inactivation of Nox2[194]. Phosphatase inactivation by SOD1-mediated H_2O_2 production is critical for FGF-2 and VEGF signaling in endothelial cells[98].

SOD1 is critical for endothelium function. SOD1 produced H_2O_2 act as an endothelium-derived hyperpolarization factor (EDHF) to regulate endothelial function such as EDHF-mediated relaxations and hyperpolarizations and coronary flow response[195]. Increases H_2O_2 production from overexpression of SOD1 can enhance VEGF synthesis, indicating the involvement of ROS in signaling downstream of VEGF stimulation[196].

1.3.6 SOD1 as an anticancer therapeutic target

Multiple large-sample gene expression profile studies of primary tumors have revealed slightly but statistically significant increased *SOD1* levels in NSCLCs[197]. Analysis of human primary breast cancers found that SOD1 is overexpressed in 70% of mammary tumors, as well as in the tumor tissue of several breast cancer mouse models[198]. Targeting SOD1 in the clinical treatment of multiple types of cancers has been explored with the use of chemical inhibitors[197,199-202]. SOD1 mimetics or recombinant SOD1 have been developed for clinical management of radiation-related adverse effects owing to the anti-inflammatory activity[203,204] as well as the radioprotective effects of SOD1[205] (Summarized in Table 1.3.1).

Tetrathiomolybdate is a copper chelator that was first developed as a copper managing agent to treat Wilson's disease[206]. Wilson's disease is a genetic disorder of copper deposition in the body that is caused by a defect in the *ATP7B* gene. ATP7B is a copper-transporting P-type ATPase transmembrane protein that is expressed mainly in hepatocytes[207-209]. Deletion or loss-of-function of *ATP7B* causes excessive copper accumulation in the liver, and ultimately other organs, which can lead to severe and life-threatening symptoms[210]. Tetrathiomolybdate forms a tripartite complex with protein, copper and itself[211], thus limiting copper availability in the cells. Copper directly stimulates the proliferation and migration of cultured endothelial cells and is essential for promoting angiogenesis[212,213]. *In vivo*, tetrathiomolybdate has been found to suppress tumor growth by inhibiting angiogenesis[200,214-217]. When administered in murine breast cancer models, tetrathiomolybdate resulted in impaired tumor growth and angiogenesis through its inhibition of vascular endothelial growth factor (VEFG), FGF2 fibroblast growth factor, and several cytokines including interleukin (IL)-1α, IL-6 and IL-8. Nuclear factor (NF)κB levels and transcriptional activity were similarly suppressed by tetrathiomolybdate[214]. Continued study of copper chelators using the second-generation tetrathiomolybdate analogue, ATN-224 (a bis-choline tetrathiomolybdate) revealed that SOD1 is a target for ATN-224. SOD1 inhibition by ATN-224 leads to reduced endothelial cell proliferation *in vitro*, and attenuation of angiogenesis *in vivo*[200,218]. ATN-224 has been tested in clinical trials in patients with solid tumors, hematological malignancies, breast cancer, and prostate cancer[218-221]. ATN-224 was shown to selectively kill lung cancer cells through H_2O_2-dependent p38 MAPK activation and decreased anti-apoptotic factor MCL1 in oncogenic *Kras*-driven cancer[199]. Ammonium tetrathiomolybdate has also been reported to inhibit MEK1/2 kinase activity and the growth of oncogenic BRAF-driven cancer[222,223].

2-Methoxyoestradiol (2-ME), is an estrogen derivative that cannot bind the estrogen receptor and was reported to induce p53 activation and apoptosis in lung cancer cell lines[224]. 2-ME also

showed selective toxicity towards human leukaemia cells but not normal lymphocytes, regardless of p53 status. Further study identified SOD1 as a possible target for 2-ME. By inhibiting SOD, 2-ME causes accumulation of cellular O_2^- and leads to apoptosis of cancer cells[201]. However, 2-ME was later demonstrated not to bind to SOD1, but rather interfere with the SOD activity assay[225]. The *in vitro* liquid assay for measuring SOD activity uses hypoxanthine and xanthine oxidase to produce superoxide radical. Compounds that interfere with xanthine oxidase activity are likely to produce false-positive results.

LCS-1 was discovered in a lung cancer drug screen to inhibit SOD1 and was shown to prevent the growth of lung adenocarcinoma cell lines harboring mutations in epidermal growth factor receptor (EGFR) or KRAS[197]. Chemical inhibition of SOD1 by LCS-1 was shown to compromise the antioxidant system in the cell, raising cellular ROS levels, in turn leading to the cell death of lung cancer cells, both *in vitro* and *in vivo*[197].

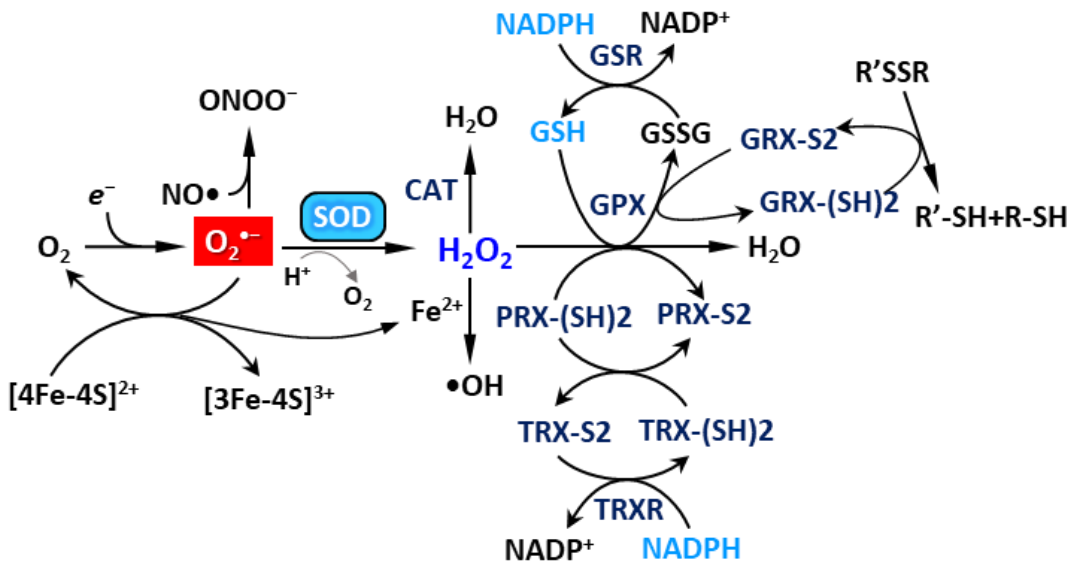

Figure 1.1 Generation and deposition of reactive oxygen species

Abbreviations: Superoxide dismutase, SOD; Catalase, CAT; Glutathione, GSH; Glutathione disulfide, GSSG; Glutathione peroxidase, GPX; Glutathione-Disulfide Reductase, GSR; Thioredoxin, TRX; Thioredoxin reductase, TrxR; Peroxiredoxin, Prx; Glutaredoxin, Grx.

Table 1.1 Summary of clinical trials for SOD1 inhibitors and mimetics

Year started	ClinicalTrials.gov Identifier	Condition	Intervention	Phase
SOD1 inhibitor				
2013	NCT01837329	Metastatic Non-small Cell Lung Cancer	Tetrathiomolybdate	Phase 1
2008	NCT00674557	Breast Cancer	ATN-224	Phase 2
2008	NCT00352742	Multiple Myeloma	ATN-224 + bortezomib	Phase 1&2
2008	NCT00674557	Postmenopausal Women With Recurrent or Advanced Breast Cancer	ATN-224 + exemestane	Phase 2
2007	NCT00560495	Stage I, Stage II, or Stage III Non-Small Cell Lung Cancer	Tetrathiomolybdate+radiation	Phase 1
2006	NCT00405574	Prostate Cancer	ATN-224	Phase 2
2006	NCT00383851	Advanced Melanoma	ATN-224 + Temozolomide	Phase 2
2006	NCT00805805	Primary Biliary Cirrhosis	Tetrathiomolybdate	Phase 3
2003	NCT00189176	Idiopathic Pulmonary Fibrosis	Tetrathiomolybdate	Phase 1&2
2003	NCT00195091	Breast Cancer	Tetrathiomolybdate	Phase 2
2001	NCT00176800	Esophageal Carcinoma	Tetrathiomolybdate	Phase 2
2001	NCT00150995	Hormone Refractory Prostate Cancer	Tetrathiomolybdate	Phase 2
2000	NCT00006332	Hepatocellular Carcinoma	Tetrathiomolybdate	Phase 2
1994	NCT00004339	Wilson Disease	Tetrathiomolybdate	Phase 3
SOD1 mimics				
2015	NCT02508389	Radiation Induced Oral Mucositis	GC4419	Phase 2
2013	NCT01921426	Squamous Cell Carcinoma of the Oral Cavity Squamous Cell Carcinoma of the Oropharynx	GC4419	Phase 1
Recombinant SOD1				
2013	NCT01513278	Radiation Induced Dermatitis	Liposomal Recombinant Human SOD1	Phase 2
2012	NCT01771991	Treat Radiation Induced Fibrosis	Topical Sodermix Dismutase in the form of Sodermix (SOD)	
2005	NCT00264186	Inflammation-Induced Impairment of Vascular Reactivity	Recombinant Human SOD1	
2005	NCT00800995	Age Related Macular Degeneration	SOD	Phase 3

CHAPTER II SOD1 is required for KP lung cancer maintenance

Rationale

Oncogenic mutations in *KRAS* and *TP53* (including *TP53* null) are the most frequent gene alteration in lung cancers. Over 30% of lung adenocarcinomas harbor a *KRAS* mutation[226]. Targeted therapy using specific inhibitors has shown superior clinical benefits over traditional chemotherapy for several classes of mutations, including EGFR tyrosine kinase inhibitors (TKIs) for EGFR mutation cases, and ALK inhibitors for lung cancers harboring *ALK* or *ROS1* fusions[20,21]. However, *KRAS* mutant tumors are generally resistant to these drugs and no therapy targeting *KRAS* mutant tumors is currently available.

The SOD1 inhibitor ATN-224 has been shown to induce apoptosis in KP tumor cells by activating p38 MAPK pathway and reduce tumor burden in mice bearing KP lung tumors[199]. As a copper chelator, however, ATN-224 is mechanistically non-specific, potentially affecting many Cu-containing proteins besides SOD1, and therefore cannot be used to accurately probe the role of SOD1 in KP tumors. Therefore, genetic deletion of *Sod1* should offer more direct and conclusive evidence about the role of SOD1 in KP tumor initiation and development. In breaking down superoxide, SOD1 generates H_2O_2, thus replacing one form of ROS with another. Inhibition of SOD1 increases the steady-state levels of superoxide and reduces H_2O_2 levels. Constitutive deletion of *Sod1* leads to increased oxidative damage and tumorigenesis with a long latency (11–29 months of age). Moreover, non-cell-autonomous or compensatory mechanisms may occur at an early embryonic stage allowing reestablishment of normal redox potential. In contrast, inducible knockout of *Sod1* in adult mice, which bypasses the developmental stage and therefore provides a model that is more appropriate for studying the true biological functions of SOD1 and for evaluating potential therapeutic effects.

To better understand the role of SOD1 in cancer, particularly in lung cancer initiation and development, I established a mouse model that allows inducible acute *Sod1* knockout in an established inducible lung cancer model to provide a highly specific and flexible tool and conclusively define the role of SOD1 in tumorigenesis and tumor maintenance. This model should also provide important information for targeting SOD1 as a potential cancer therapy.

MATERIALS AND METHODS

Mice

All animal care and treatments were carried out in compliance with Rutgers University Institutional Animal Care and Use Committee guidelines. UBC-Cre-ERT2 mice[227] (JAX stock #007001) and *Sod1*$^{Flox/Flox}$ mice (kindly provided by Dr. Van Remmen H, Oklahoma Medical Foundation [228]) were crossbred to generate *UBC-Cre-ERT2*$^{-/+}$*; Sod1*$^{Flox/Flox}$ mice. To assess the consequences of SOD1 deletion on tumorigenesis, Ubc-CreERT2; Sod1 mice were bred with *K-ras*$^{FSF-G12D/+}$ mice (JAX stock #008653) and *Trp53*$^{frt/frt}$ mice (JAX stock #017767) to generate *UBC-Cre-ERT2*$^{-/+}$*; K-ras*$^{FSF-G12D/+}$*; Trp53*$^{frt/frt}$*; Sod1*$^{+/+}$ mice and *UBC-Cre-ERT2*$^{-/+}$*; K-ras*$^{FSF-G12D/+}$*; Trp53*$^{frt/frt}$*; Sod1*$^{Flox/Flox}$ mice.

Genomic DNA extraction from ear clips

Genomic DNA extraction from ear clips for routine genotyping followed the Hot Shot Method from Tylor Jacks' lab. (https://jacks-lab.mit.edu/protocols/dna_isolation_hot_shot_method) Briefly, ear clips are collected in PCR strip tubes, and 75 µl of Alkaline Lysis Buffer (14 µl 50% sodium hydroxide and 14 µl 0.5M EDTA, pH 8.0, in 10 ml sterile deionized water) is added to each tube. The tubes are then placed into a thermocycler and incubated for 30 min at 95° C, followed by cooling to 4°C. The lysates are promptly removed from the thermocycler and neutralized with 75 µl of Neutralization Buffer (40 mM Tris-HCl, pH = 5). The DNA is then used for genotyping PCR or stored indefinitely at 4°C.

Genomic DNA extraction from tail tissue

Fresh or frozen tail tissue (up to 5 mm) was snap frozen in liquid nitrogen and then ground in a pre-chilled pestle and mortar. The ground tissue was then collected in a microcentrifuge tube and the genomic DNA extracted using the NucleoSpin Tissue Kit (Macherey-Nagel, REF 740952.10).

Tamoxifen treatment

Tamoxifen was used to activate Cre-ERT2 and initiate Cre/loxP recombination. Tamoxifen (Sigma, T5648) was dissolved in sunflower seed oil (Sigma, 88921) with 2% ethanol at 20 mg/ml. Mice were given 160 mg/kg tamoxifen by intraperitoneal injection once a day for 5 consecutive days.

Lung cancer induction

To activate K-ras^{G12D} and delete Trp53 in the lung and produce tumors, mice were infected intranasally with recombinant, replication-deficient Ad-FlpO (University of Iowa Adenoviral Core) at 1.2 x 10^8 pfu while under anesthesia by isoflurane inhalation.[229]

Histology

Mouse tissues were fixed in 10% neutral buffered Formalin solution (Sigma, HT501640) overnight. Fixed tissues were transferred to 75% ethanol and then embedded in paraffin. For frozen sections, tissues were fixed in 10% neutral buffered Formalin solution overnight, transferred into 15% sucrose until sinking, and then placed in 30% sucrose overnight. Antibodies used for immunohistochemistry were: SOD1 (Abcam, ab16831), Ki-67 (Thermo Scientific, MA5-14520), cleaved Caspase-3 (Cell Signaling, 9664), phospho-histone H2A.X (Cell Signaling, 9718), and ApopTag® Plus Peroxidase In Situ Apoptosis Kit (EMD Millipore, S7101).

Tumor burden quantification

H&E stained lung tissue sections were scanned at 20x. Tumor burden was defined as the ratio of tumor area over total lung area. Tumor area and total lung area were outlined and measured using Visiopharm. Dr. Evita Sadimin provided help in pathological identification of tumor regions and Dr. Wenjin Chen established the Visiopharm analyzing protocol at the Center for Biomedical imaging & informatics, Rutgers Cancer Institute of New Jersey.

Tissue protein extraction

Tissues were snap frozen in liquid nitrogen and lysed in Lysis Buffer (50 mM HEPES, 150 Mm NaCl, 2 mM EDTA, 1% Triton X-100) with PhosSTOP (Sigma, 4906845001) and cOmplete™ Protease Inhibitor Cocktail (Sigma, 11697498001).

RNA extraction and RT-qPCR

Messenger RNA extraction was performed using the RNeasy Mini Kit (Qiagen, cat 74104) following the manufacturer's instructions. Reverse transcription of mRNA used the High-Capacity cDNA Reverse Transcription Kit (ThermoFisher, Cat# 4368813). The Sybr Green method was used for mRNA quantification. PCR reaction used PowerUp™ SYBR™ Green Master Mix (ThermoFisher, Cat# A25742)

Primers for qPCR

Gene	Sense	Antisense
SOD1	GGGTTCCACGTCCATCAGTAT	ACACATTGGCCACACCGTC
ACTB	TGAGCGCAAGTACTCTGTGTGGAT	ACTCATCGTACTCCTGCTTGCTGA
Pck1	TGCCCCAGGCAGTGAGGAAGTT	GTCAGTGAGAGCCAGCCAACAGT
G6pc	TCTGTCCCGGATCTACCTTG	GCTGGCAAAGGGTGTAGTGT

Fasn	CTGCGGAAACTTCAGGAAATG	GGTTCGGAATGCTATCCAGG
Scd1	TCTTCCTTATCATTGCCAACACCA	GCGTTGAGCACCAGAGTGTATCG
Ppara	TATTCGGCTGAAGCTGGTGTAC	CTGGCATTTGTTCCGGTTCT
Pparg	ATTCTGGCCCACCAACTTCGG	TGGAAGCCTGATGCTTTATCCCCA
Hmgcr	ATCATGTGCTGCTTCGGCTGCAT	AAATTGGACGACCCTCACGGCT
Srebf1	CACTTCTGGAGACATCGCAAAC	ATGGTAGACAACAGCCGCATC
Slc27a1	TGCACAGCAGGTACTACCGCAT	TGCGCAGTACCACCGTCAAC
PDK4	TTCACACCTTCACCACATGC	GAAGGACGGTTTTCTTGATG
CPT1A	AGGACCCTGAGGCATCTATT	ATGACCTCCTGGCATTCTCC

Statistical Analysis

Statistical analyses were carried out using GraphPad Prism 7 software. Unless otherwise indicated, differences between treatment groups were compared using two-tailed Student's t test.

EXPERIMENTAL RESULTS

2.1 Establishment of an inducible *Sod1*-knockout mouse model

The conditional *Sod1* knockout cassette contains two LoxP sites inserted flanking *Sod1* exons 3 and 4 in *Sod1*$^{Flox/Flox}$ mice[228]. The Cre-LoxP strategy was used to facilitate recombination and deletion of exons 3 and 4 at the Sod1 locus (Figure 2.1.1A). *Sod1*$^{Flox/Flox}$ mice were bred with transgenic mice carrying one copy of *Cre-ERT2* gene under control of the human ubiquitin C (UBC) promoter (*UBC-Cre-ERT2*$^{+}$). *Cre-ERT2* is a fusion gene of Cre and ERT2; the Cre recombinase was fused to a G400V/M543A/L544A triple mutation of the human estrogen receptor ligand-binding domain[230]. Because attempts to breed homozygous *UBC-Cre-ERT2*$^{+}$ mice have failed (a result consistent with a report from Jackson Laboratory), all mice used in this study carry a single copy of *Cre-ERT2*. Upon injection of TMX, these *UBC-Cre-ERT2*$^{+}$*; Sod1*$^{Flox/Flox}$ mice ubiquitously express ERT2-Cre, inducing the knockout of Sod1 and thus resulting in a sustained loss of S*od*1 protein in all tissues (*Sod1*$^{\Delta/\Delta}$ mice).

***Sod1*$^{Flox/Flox}$ strain recovery.** Immunoblot revealed that some of the *Sod1*$^{flox/flox}$ mice did not express SOD1 protein before TMX treatment (Figure 2.1.2A). After systematic analysis of their genomic DNA, it was discovered that two types of non-expressing *Sod1* alleles exist in the cohort. One is the allele that has already gone through Cre/loxP recombination, and the other allele has a neomycin resistance (neoR) cassette at the intron between exon 2 and exon 3 (Figure 2.1.1). It is known that the gene encoding neomycin resistance mediates a cis-acting negative effect on proximal promoters, resulting in decreased expression[231]. Primers were designed to identify these two types of alleles, as well as the wild type and floxed alleles (Figures 2.1.3A and B), as follows.

Primer set #1 (Figure 2.1.3A): The amplicon size for the corresponding alleles are wildtype, 675 bp; Floxed, 951 bp; Cre-recombined, 419 bp; and NeoR, 504 bp.

SOD1 Floxed F1: 5’-TGAGCTGTGCCTTGTGACTGGC -3’;

SOD1 Floxed R1: 5’-CCAGCAATACTACAGACTTAAATACTAGC-3’;

SOD1 Gseq R6: 5’-CGCCGGGCCACCATGTTTCTTA-3’;

SOD1 PolyA R2: 5’-AGATCTCTCGTGGGATCATTGT-3’.

Primer set #2 (Figure 2.1.3B). The amplicon sizes for the corresponding alleles are wildtype, 312 bp; Floxed, 587 bp; Cre-recombined, 346 bp; and NeoR, 431 bp.

SOD1 Floxed 6F: 5’-CAGCCCTGGCCCTTGGGAACAA-3’;

SOD1 Floxed 6R: 5’-ACAGTGTCTCACTACTACAGCTCAGG-3’;

SOD1 Floxed R1: 5’-CCAGCAATACTACAGACTTAAATACTAGC-3’;

SOD1 PolyA R2: 5’-AGATCTCTCGTGGGATCATTGT-3’.

UBC-Cre-ERT2^{+}; *Sod1*$^{Flox/Flox}$ and *UBC-Cre-ERT2*$^{-}$; *Sod1*$^{Flox/Flox}$ mice were sacrificed two weeks after initiating TMX administration. By performing genotyping PCR on the tail genomic DNA sample from TMX-treated mice, SOD1 knockout efficiency could be evaluated at the DNA level without sacrificing the animal. Good recombination efficiency was observed on analyzing the genomic DNA (Figure 2.1.4A). SOD1 protein expression level was then measured in several tissues: lung, liver, spleen, thymus, kidney, heart, pancreas, large intestine (colon), small intestine, stomach, brain, muscle (skeletal), and fat (white adipose tissue). Tissues were collected and SOD1 protein levels determined by western blot (Figure 2.1.4B) and IHC analysis (Figure 2.1.5). Decreased SOD1 protein expression was observed in all twelve different tissues analyzed. Variation between them is likely to be due to incomplete induction of the Cre recombinase and variations in the SOD1

turnover rate in different tissues. The mosaic pattern of SOD1 expression after TMX injection is evident in IHC staining of SOD1.

2.2 Physiology and histopathology analysis of conditional whole body *Sod1* knockout mice.

UBC-Cre-ERT2$^{+/-}$*; Sod1*$^{Flox/Flox}$ and *UBC-Cre-ERT2*$^{-/-}$*; Sod1*$^{Flox/Flox}$ mice were given TMX at 6 - 8 weeks of age, and body weight was monitored for up to 12 months post TMX treatment (Figure 2.2.1A). There was no difference observed in body weight at the time of TMX treatment. However, the loss of SOD1 resulted in lower body weight for both male and female mice up to 8 months post TMX treatment. By 9 months, however, there was no difference in body weight in male mice. Female mice body weight was not monitored after 8 months post TMX. Similarly treated mice were sacrificed at 5 months after TMX treatment and major tissues were harvested and processed for pathophysiological analysis. Tissues collected included lung, liver, spleen, thymus, kidney, heart, pancreas, large intestine (colon), small intestine, stomach, brain, skeletal muscle, and fat (white adipose tissue) (Figure 2.2.1B). The only discernable abnormality detected in any of the tissues was hepatosteatosis, observed in the livers of *Sod1* knockout mice (Figure 2.2.1C). Hepatosteatosis was observed as early as 3 months post-TMX injection. Lipid droplets were confirmed with Oil Red O staining (Figure 2.2.1C).

2.3 Generation of a KP lung cancer mouse model with inducible *Sod1* knockout.

The inducible KP lung cancer mouse model was generated as follows. One allele of the *Kras* gene was knocked in with the G12D mutation following a Frt-flanked stop sequence (*FSF-Kras*$^{G12D/+}$). Two Frt sites were knocked-in to flank critical exons of *Tp53* (*TP53*$^{Frt/Frt}$). Upon intranasal administration of adenovirus that expresses a codon-optimized version of Flp recombinase (FlpO), the recombination results in *Kras*^{G12D} gene expression and *Tp53* knockout (*Kras*$^{G12D/+}$; *Tp53*$^{-/-}$).

Oncogenic *Kras* alone can initiate tumorigenesis, and loss of p53 drives the malignant transformation. Mice were bred to carry all four mutant genes in order to achieve independent inducible *Sod1* knockout and lung cancer development. These mice are designated as *Ubc-CreERT2+*; *Sod*$^{Flox/Flox}$; *FSF-Kras*$^{G12D/+}$; *Tp53*$^{Frt/Frt}$. Mice with genotypes *Ubc-CreERT2+*; *Sod1*$^{+/+}$; *FSF-Kras*$^{G12D/+}$; *Tp53*$^{Frt/Frt}$ and *Ubc-CreERT2-*; *Sod1*$^{Flox/Flox}$; *FSF-Kras*$^{G12D/+}$; *Tp53*$^{Frt/Frt}$ served as controls (Figure 2.3.1A). Consistent with previous reports that SOD1 is slightly but significantly increased in lung tumor tissue[197], SOD1 protein level was found to be upregulated in KP tumor (Figure 2.3.1 B). Effective SOD1 knockout in KP tumor was confirmed by IHC (Figure 2.3.1 C).

2.4 SOD1 suppresses KP tumor initiation but is required for tumor development/maintenance

To determine the effect of acute loss of *Sod1* on KP lung cancer initiation, the quadruple mutant *Sod1*$^{\Delta/\Delta}$ mice (*Ubc-CreERT2+*; *Sod1*$^{Flox/Flox}$; *FSF-Kras*$^{G12D/+}$; *Tp53*$^{Frt/Frt}$) and *Sod1*$^{+/+}$ controls (*Ubc-CreERT2+*; *Sod1*$^{+/+}$; *FSF-Kras*$^{G12D/+}$; *Tp53*$^{Frt/Frt}$) were first injected with TMX at around 8 -10 weeks of age to induce deletion of *Sod1*. One month after TMX injection, mice were inoculated with FlpO to induce *Kras* mutation and *p53* deletion (Figure 2.4.1 A). At 5 weeks after infection, greater tumor burden was observed in the *Sod1* knockout group (Figure 2.4.1 B). This suggests that *Sod1* suppresses tumor initiation, provided that loss of *Sod1* does not alter adenovirus infection efficiency. However, at 14 weeks after infection, a significant reduction in tumor burden was observed in *Sod1* knockout group (Figure 2.4.1 B), suggesting that SOD1 is required for tumor development/maintenance. This observation was confirmed when the alternative arm of experiment was tested. In this case, the quadruple mutant mice and controls were first infected with FlpO at 8-10 weeks of age, and TMX was injected 10 weeks later to induce *Sod1* knockout (Figure 2.4.1 E). Consistently, loss of SOD1 resulted in inhibited tumor growth. At 6 weeks post TMX treatment, tumor burden in the *Sod1* knockout group was significantly less than that in the

control group. Comparing tumor burden at 4 and 6 weeks after *Sod1* knockout, tumors in the control group almost doubled in size, whereas tumor growth for the *Sod1* knockout group was insignificant (Figure 2.4.1 F). Accordingly, Ki67 staining was used to confirm the reduced cell proliferation in SOD1 null tumors (Figures 2.4.2 A and B). Inhibition of proliferation, rather than apoptosis induction, is likely the main cause of reduced tumor burden in SOD1-knockout mice, as no increase of cleaved caspase 3 staining was found in *Sod1* null tumors (Figures 2.4.2 A and C). Furthermore, no difference was found in the TUNEL assay or γH2AX staining, indicating that loss of SOD1 does not induce DNA damage *in vivo* (Figure 2.4.2 A). Although tumors lacking SOD1 exhibit retarded growth, there was no difference in aggressiveness as evaluated by histopathology of the tumors with or without SOD1 (Figures 2.4.1 C and G, and Figure 2.4.3). In addition, loss of *Sod1* did not improve the overall survival rate of KP lung cancer mice (Figures 2.4.1 D and H).

DISCUSSION

In this chapter, the physiological consequences of acute global knockout of *Sod1* in adult mice were evaluated. Except for hepatic steatosis, no obvious abnormality was observed among the major organs that were analyzed. It was found that hepatic steatosis is associated with acute *Sod1* knockout induced in adult mice, which is consistent with what has been observed in constitutive *Sod1* knockout mice. Also, the anti-cancer function of SOD1 was demonstrated using an inducible *Sod1* knockout mouse model in an oncogenic *Kras* and *p53* deficient lung cancer background.

SOD1 is expressed ubiquitously throughout the body. IHC and western blot analysis of various mouse tissues confirmed SOD1 protein expression in all major organs, with the levels varying between different tissues. It has been reported previously that liver expresses the greatest amounts of SOD1[232]. Indeed, among all the tissues analyzed, the highest levels of SOD1 were detected in the liver (Figure 2.1.4 B and C). Thus, it is not surprising that the earliest phenotype in both constitutive and inducible Sod1 knockout mice is observed in the liver. Interestingly, increased oxidative stress is implicated in the development of non-alcoholic fatty liver disease (NAFLD) [233-236], while decreased SOD activity has been observed in an experimental non-alcoholic steatohepatitis (NASH) mouse model[237]. Mice with global knockout of *Sod2* (the mitochondrial matrix form) exhibit massive lipid accumulation in the liver, and death at the neonatal stage[237]. *Sod2* knockout mice exhibited massive lipid accumulation in the liver and neonatal death[159]. However, liver-specific *Sod2* knockout does not yield hepatic steatosis[238]. *Sod1*-deficient mice developed hepatocellular carcinoma later in life[162], and are also more sensitive to alcohol-induced liver damage[239]. These results inspired the focused examination of hepatic physiology of *Sod1* deficient mice[186]. Indeed, loss of *Sod1* resulted increases in lipid peroxidation and triglyceride in the liver of *Sod1* knockout and *Sod1*/*Sod2* double knockout mice but not in the liver of *Sod2* knockout mice. Furthermore, degradation of apolipoprotein B (ApoB) was observed in the liver

and plasma of *Sod1*-KO mice. ApoB is a critical component and an important player in the development of NAFLD[240,241]. Degradation of apoB resulting from loss of SOD1 may result in impaired secretion of lipoprotein from the liver and eventually lead to the development of hepatic steatosis[186].

It has been suggested that oxidative stress created by loss of SOD1 is the underlying cause of lipid accumulation in hepatic steatosis[186]. In fact, increased superoxide levels were found to be associated with hepatic steatosis, and administration of superoxide scavengers or SOD mimics was shown to suppress superoxide generation and inhibit liver steatosis[237]. In addition to impaired lipid secretion from liver, this study shows acute loss of *Sod1* enhanced the amount of sterol-regulatory binding protein 1 (SREBP1) transcription in the liver (Figure 2.2.1 D). This is consistent with previous observations of SREBP1 expression in *Sod1*-deficient mice[187]. SREBP-1c is a transcription factor that regulates *de novo* lipogenesis in the liver[242]. However, genes in the fatty acid synthesis pathway such as *Fasn*, *Scd1*, and *Accα* are down regulated in *Sod1* deficient liver (Figure 2.2.1 D). It is likely that increased fatty acid synthesis is not elevated in *Sod1* null liver, despite upregulated SREBP1 transcription. Activation of SREBPs require post-translational cleavage and transportation through the Golgi complex[243]. Further experiments needed to determine the upstream regulator of SOD1 loss induced SREBP1 transcription and its downstream effectors.

The focus of this chapter is the effect of SOD1 on the development of lung cancer. In humans, SOD1 and SOD2 activity are lower in lung than in several other vital organs such as liver, kidney, heart, and brain. Lung has the highest SOD3 activity among the major organs[232]. In this work, analysis of mouse tissues revealed similar expression levels of SOD1. (Figures 2.1.4 B and C) SOD1 has been shown to be highly expressed in alveolar type II (AT2) epithelial cells[244,245], which are

considered the cell-of-origin for lung adenocarcinomas[17,246,247]. Two independent datasets reveal that the *SOD1* RNA levels are slightly higher in tumors than in normal lung tissue[197]. In the current study, slightly increased protein levels of SOD1 were detected in the lung tumors of KP mice, compared to normal adjacent tissue (Figure 2.3 B). This suggests that SOD1 may provide an evolution advantage to tumor cells. This resulted in the enrichment of high SOD1-expressing cells under selection pressure during tumorigenesis. It is also plausible that high SOD1-expressing cells such as AT2 overpopulate the tumors, while in normal adjacent tissue, the apparent expression level detected by western blot is the average level of several cell types. Nonetheless, the elevated SOD1 expression level is associated with tumorigenesis.

The antitumor function of SOD1 was directly probed by genetic knockout *Sod1* in the KP lung cancer model. When lung tumors are induced in *Sod1*-null mice, larger tumor burdens can be observed 5 weeks after tumor induction, compared to wild type controls. It is unlikely due to higher viral infection rate in the *Sod1* null lungs, since no report suggested loss of *Sod1* promote viral infection. In fact, SOD1 was shown to protect virus-induced liver damage[190]. (This is unlikely to be due merely to higher viral infection rates in the *Sod1*-null lungs, since no reports suggest that loss of *Sod1* promotes viral infection, and in fact, SOD1 has been shown to protect liver from virus-induced damage[190].) This suggests that SOD1 may have a suppressive effect on early-stage tumorigenesis. However, SOD1 is critically needed to sustain tumor cells growth. At later stages, *Sod1*-null mice exhibited reduced tumor burden compared to the control group. The tumor-promoting function of SOD1 was confirmed when *Sod1* was knocked out in established tumors; loss of *Sod1* in mice bearing KP lung tumors led to retarded tumor growth. Overall, these data validate on the genetic level that SOD1 may be a viable target in the treatment of lung cancer.

SOD1 has been suggested as a cancer target in many studies that used a copper chelators to inhibit SOD1. The copper chelator ATN-224 was shown to induce apoptosis in KP lung cancer cells and reduce tumor burden[199]. The strong pro-apoptotic effect was not seen in my genetic knockout approach. This discrepancy is likely due to the distinct kinetics of chemical inhibition of SOD1 compared to genetic knockout. SOD1 is a stable protein with a long half-life[248]. SOD1 protein ablation by genetic knockout is a relatively slow process compared to almost instant protein deactivation by chemical means. The gradual loss of SOD1 may provide cells an opportunity to activate the survival pathway or a compensatory response. This may explain the weaker cytotoxic effect of SOD1-knockout compared to that of ATN-224 administration. In addition, copper chelators are likely to affect many other copper-dependent enzymes. For instance, SOD3 also requires copper and zinc for its catalytic center, and is highly expressed in lung[232]. Loss of *Sod3* in mice is reported to cause acute lung damage and immune infiltration by granulocytes, T cells and natural killer cells[249]. It is plausible that inhibition of SOD3 can thus induce an immune response, contributing to the overall anticancer effect of ATN-224.

While ROS play an important role in cancer development, the exact effects of interventions to reduce ROS activity on tumor initiation and development are not clear. Depending on which antioxidant gene is manipulated to modulate ROS levels, and in which tissue it occurs, the effect can be either anti-tumor or pro-tumor. Oftentimes, inhibition of ROS can actually support tumor development: mice heterozygous for Sod2 have increased oxidative damage and increased cancer incidence[250]; mice lacking Prx1 are predisposed to certain hematopoietic cancers[251]; and Gpx2 null mice have microflora-associated intestinal cancer[252]. On the other hand, targeting catalase at the mitochondria suppresses invasive breast cancer in mice[253]; Txn1 transgenic mice show elevated skin cancer incidence[254]; and Gpx4 null mice have a reduced cancer risk[255]. In addition, increased oxidative stress resulting from inhibition of synthesis of the antioxidant, glutathione, hinders KP

sarcoma initiation[116]. There is great controversy over whether Nrf2, a master transcription factor for antioxidant genes, has an overall tumor suppressive effect, or, conversely, is oncogenic. Nrf2 induces detoxification and antioxidant genes, and these can be advantageous to tumor cell initiation. Yet, Nrf2-knockout increases susceptibility to inflammation-related colorectal cancer[256,257]. On the other hand, activation of Nrf2 through upregulated transcription, acquired gain-of-function mutation in Nrf2, or loss-of-function mutations in Keap1 is associated with tumor promotion. Loss of Nrf2 impairs EGFR signaling and mRNA translation, and eventually leads to inhibition of cancer cell proliferation[117,118,258].

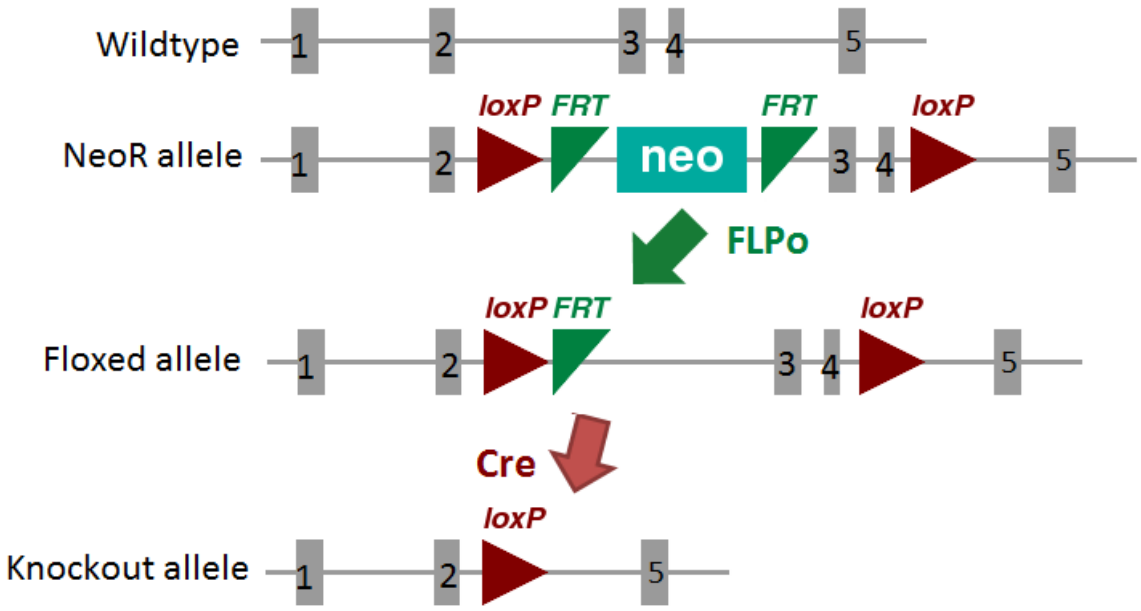

Figure 2.1.1 Schematic diagram of *Sod1* locus for the conditional knockout in mouse

The Sod1 gene locus is shown schematically at each stage of genetic rearrangement, starting with wildtype allele; NeoR allele: LoxP site knockin allele with neomycin cassette; Floxed allele: LoxP site knockin allele without neomycin cassette after induction by virus (FLPo); and knockout allele: *Sod1* genomic locus after Cre/loxP recombination

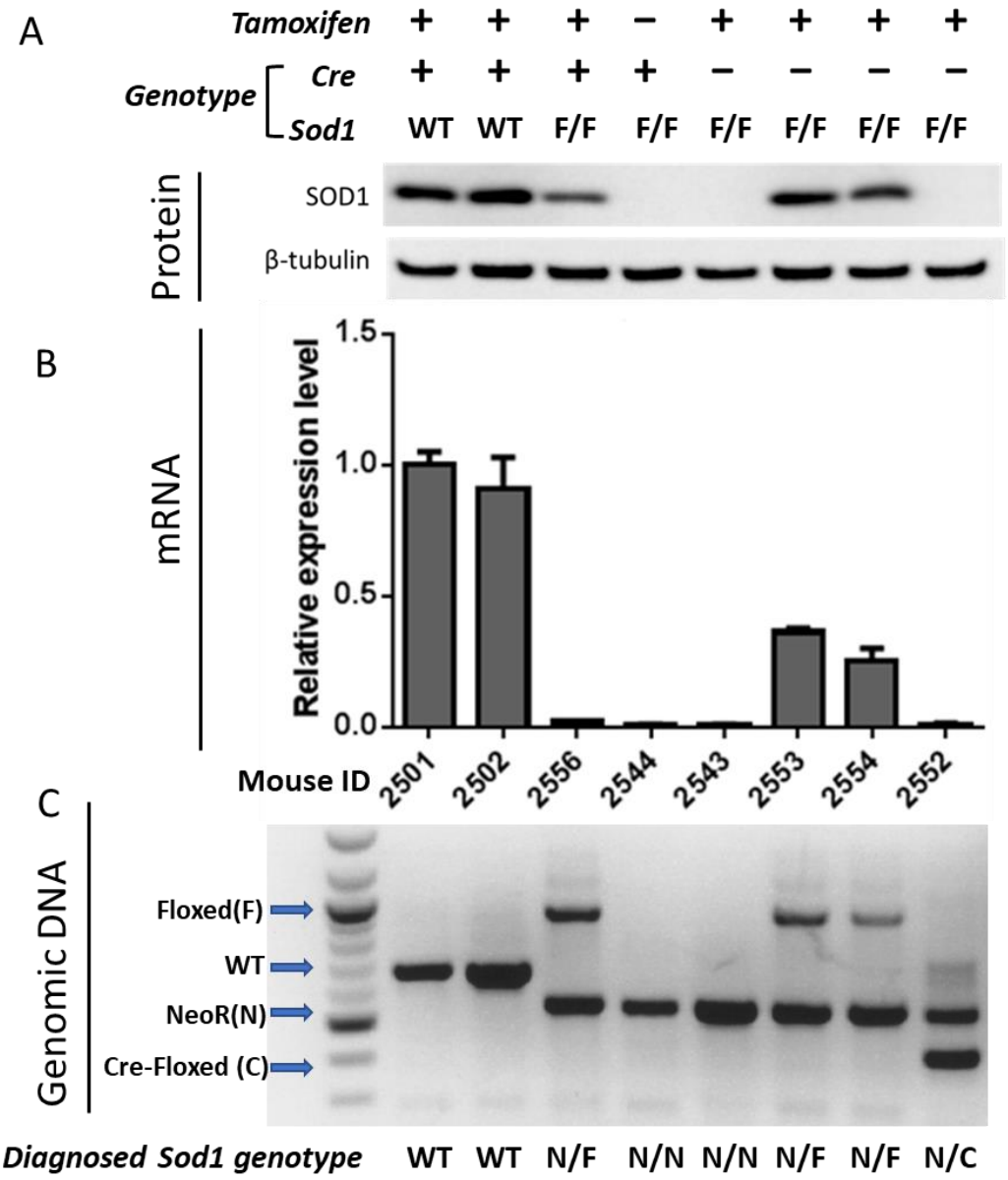

Figure 2.1.1 Genetic analysis of conditional Sod1-knockout mice carrying various combinations of the wild type and mutant alleles

(A) western blot analysis of SOD1 protein levels in lung tissue from mice with the indicated genotype, treated with or without tamoxifen. (B) Relative mRNA levels of *Sod1* from the same lung tissues as in A. Data are shown as mean ± SD. n = 2 (C) Genotyping PCR analysis of genomic DNA from ear clippings from the same mice as in A, performed with primer set #1 (see text).

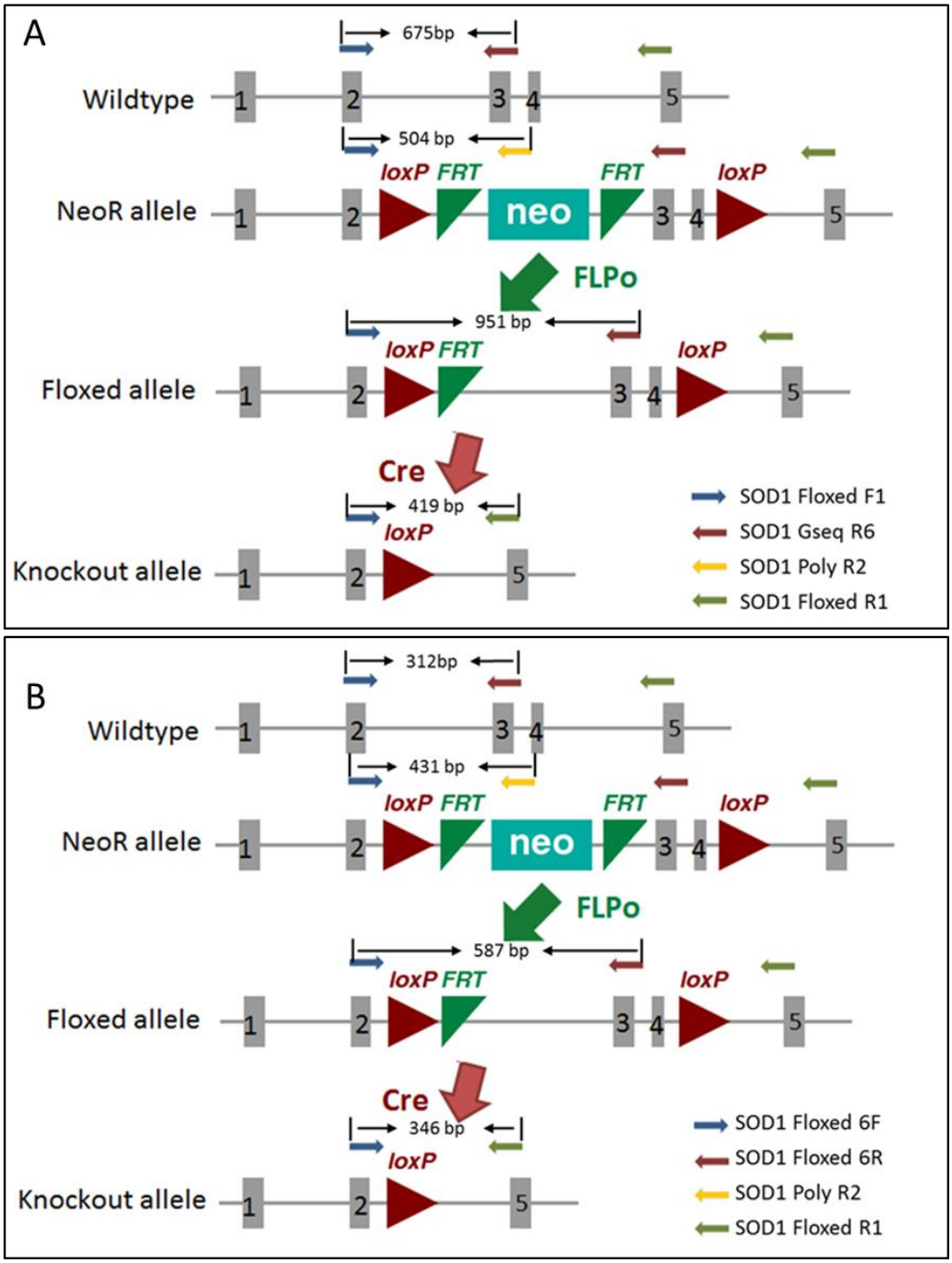

Figure 2.1.3 Schematic diagram of *Sod1* conditional knockout mouse and genotyping primer design.

(A) Conducted using primer set #1, or (B) Primer set #2 (see text).

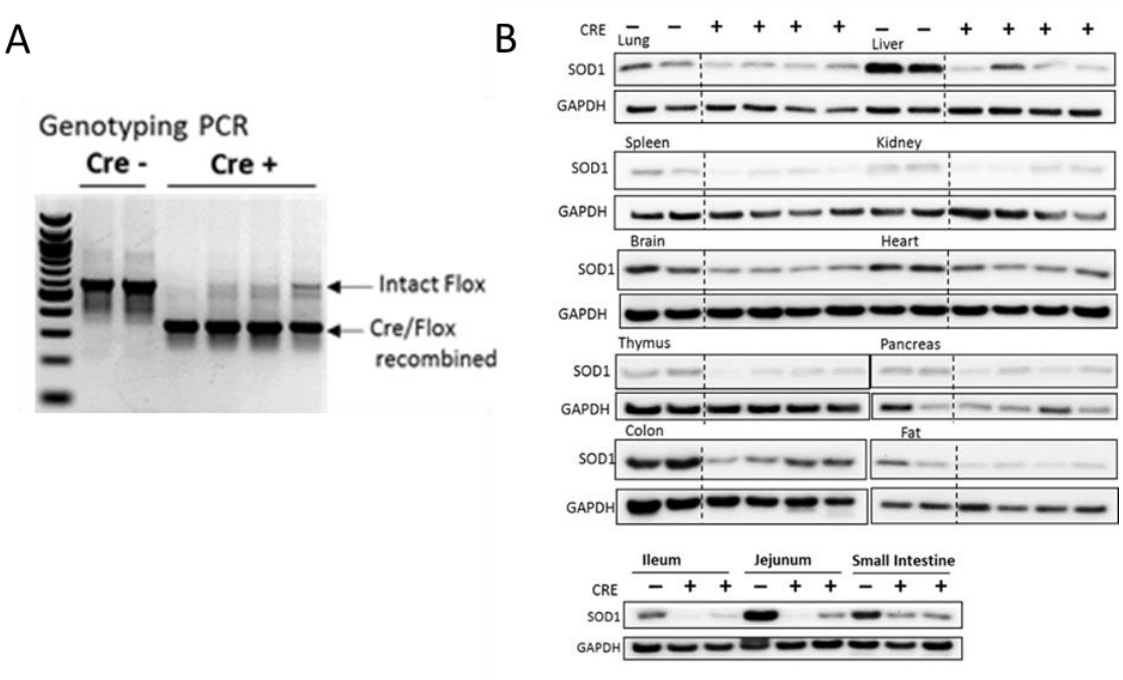

Figure 2.1.4 Induction of UBC-Cre-ERT2-facilitated global SOD1 knockout in Sod1$^{Flox/Flox}$ mice by tamoxifen.

(A) Genotyping PCR analysis of tail genomic DNA using genotyping primer set #2. (B) Western blot analysis showing SOD1 protein levels in various tissues from *Sod1*$^{Flox/Flox}$ mice with or without the UBC-Cre-ERT2 cassette, two weeks after TMX injection.

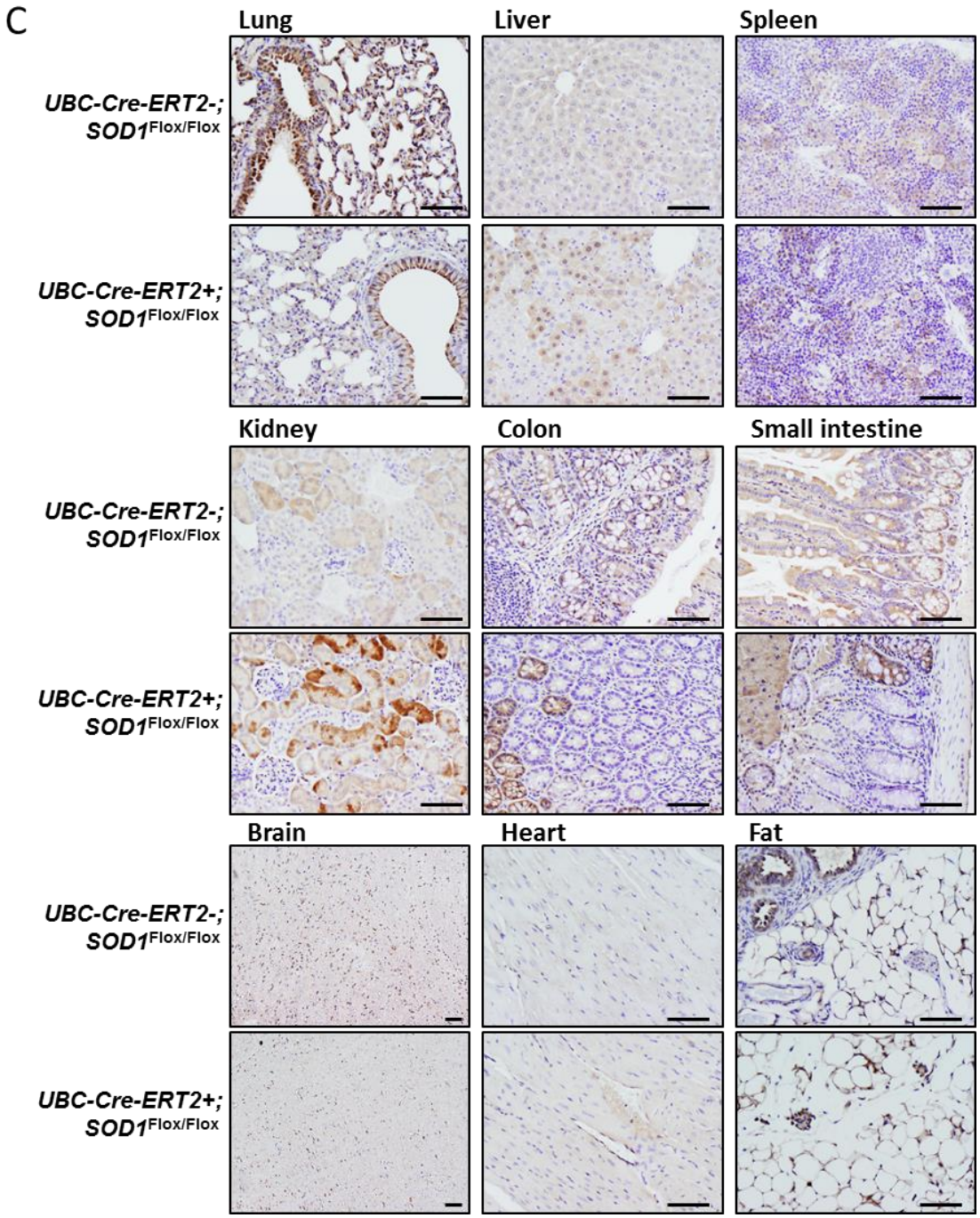

Figure 2.1.5 Induction of UBC-Cre-ERT2-facilitated global SOD1 knockout in *Sod1*$^{Flox/Flox}$ mice. (IHC)

IHC Analysis of SOD1 protein levels in various tissues from *Sod1*$^{Flox/Flox}$ mice with or without UBC-Cre-ERT2 two weeks after tamoxifen injection. Scale bar, 100 μm.

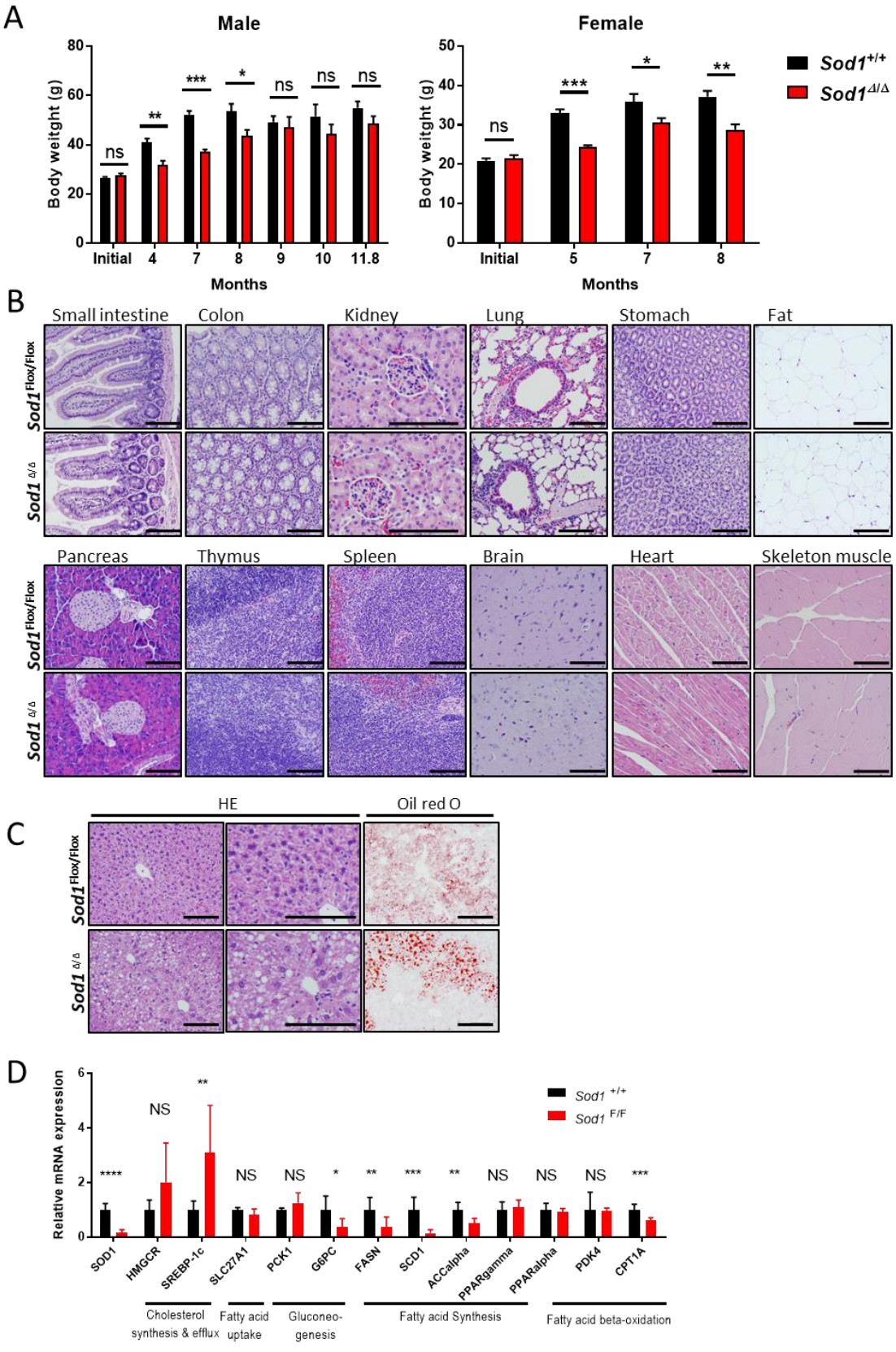
A
Male
Female
Body weitght (g)
Months
Initial
Sod1+/+
Sod1Δ/Δ
B
Small intestine
Colon
Kidney
Lung
Stomach
Fat
Pancreas
Thymus
Spleen
Brain
Heart
Skeleton muscle
Sod1Flox/Flox
Sod1Δ/Δ
C
HE
Oil red O
D
Relative mRNA expression
Sod1 +/+
Sod1 F/F
SOD1
HMGCR
SREBP-1c
SLC27A1
PCK1
G6PC
FASN
SCD1
ACCalpha
PPARgamma
PPARalpha
PDK4
CPT1A
Cholesterol synthesis & efflux
Fatty acid uptake
Gluconeo-genesis
Fatty acid Synthesis
Fatty acid beta-oxidation

Figure 2.2.1 Physiology and histopathology of conditional whole body *Sod1* knockout mice.

(A) Body weight of *Sod1* knockout mice and control mice was monitored for up to 9 months post TMX injection. Data presented as mean ± SEM; *p<0.05, **p<0.001, ***p<0.0001. (B) Representative H&E staining of the indicated mouse tissues at 5-months post TMX injection. Scale bar: 100 µm. (C) H&E and oil red O staining of mouse liver tissue at 3-months post TMX injection. Scale bar: 67.5 µm. (D) qPCR analysis of mRNA levels of key lipid metabolism enzymes in the liver tissue of $Sod1^{+/+}$ and $Sod1^{\Delta/\Delta}$ mice at 3 months post TMX injection. Data presented as mean ± SD; *p<0.05, **p<0.001, ***p<0.0001; NS, not significant.

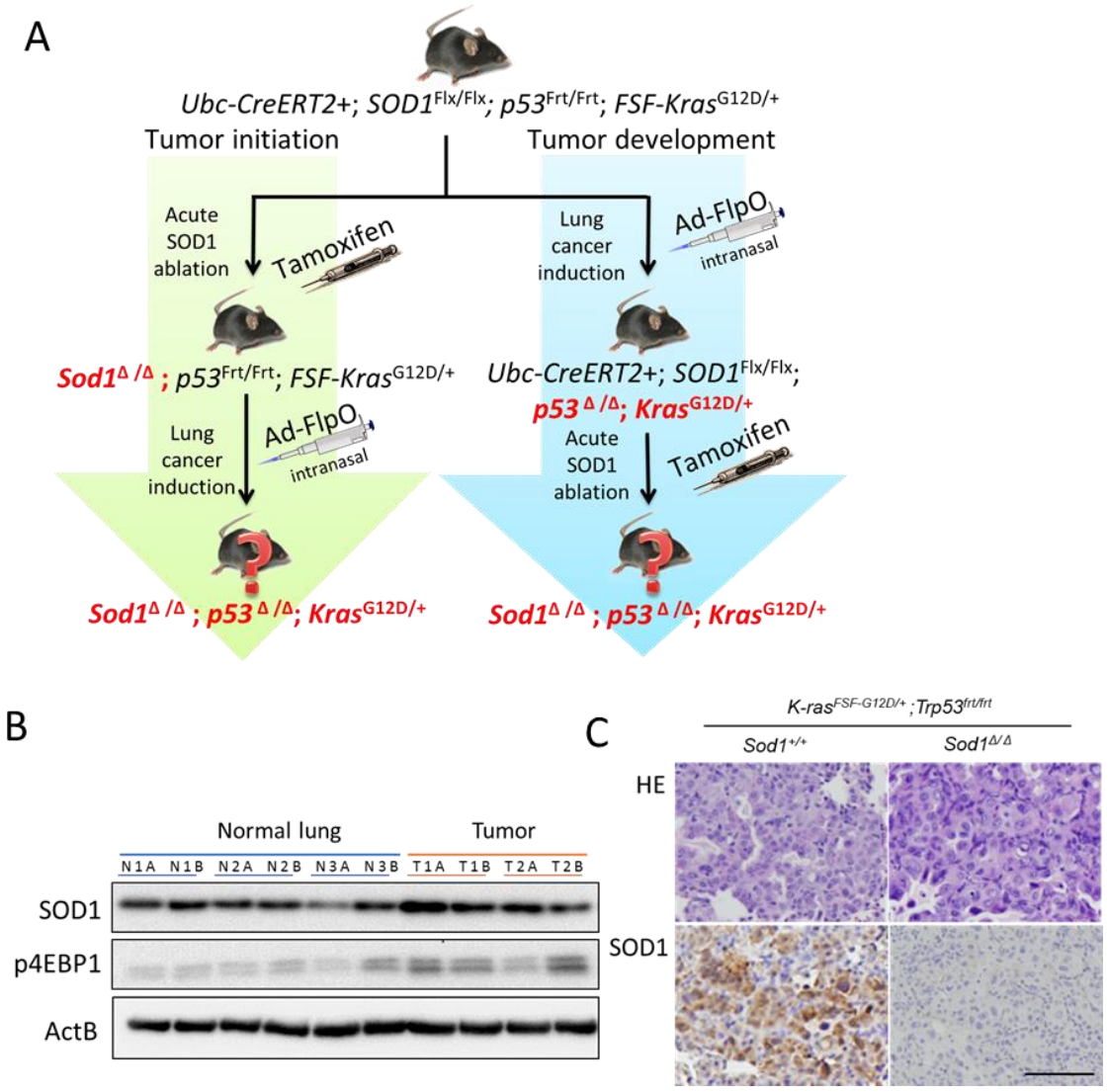

Figure 2.3.1 Scheme for creation of an inducible *Sod1* knockout KP lung cancer model.

(A) Tamoxifen induces deletion of *Sod1,* and Ad-FlpO virus inhalation activates *Kras* mutation and *p53* ablation in the mouse. Administering the inducers in a different order results in a model to study the effects of SOD1-knockout on either tumor initiation (left) or tumor development (right). (B) Western blot analysis of SOD1 protein in KP lung tumor tissue and age-matched normal lung tissue. (C) Representative H&E staining and IHC staining for SOD1 in $Sod1^{+/+}$ and $Sod1^{\Delta/\Delta}$ KP tumors. Scale bar: 100 μm.

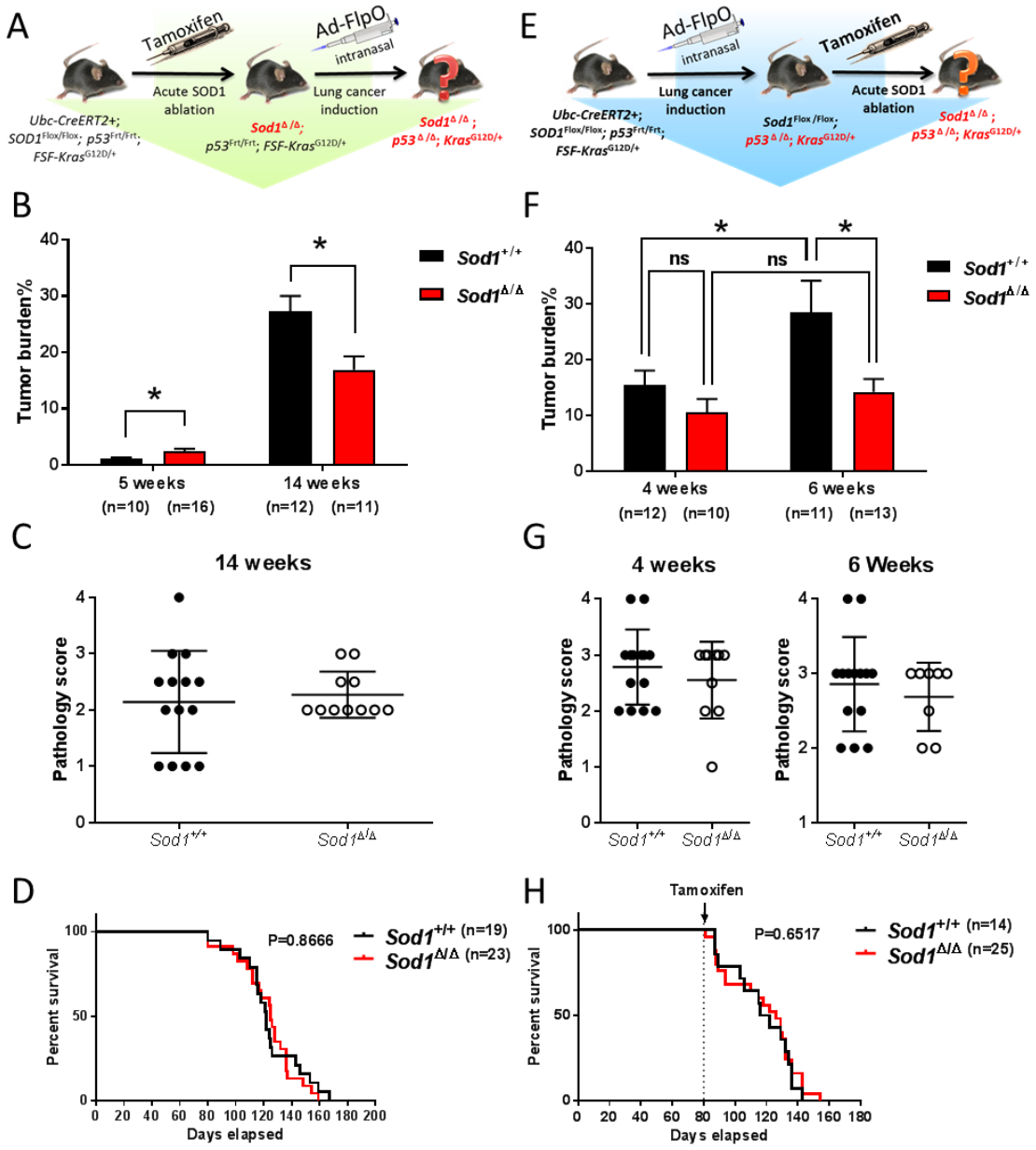

Figure 2.4.1 Acute *Sod1* ablation accelerates KP tumor initiation and suppresses KP tumor maintenance

(A) The scheme for inducing KP lung cancer in SOD1-null mice (from Fig. 2.3.1A; applies to left panel). (B) Quantification of tumor burden in $Sod1^{+/+}$ (n=10 for 5 week, and n=12 for 14-week groups) and $Sod1^{\Delta/\Delta}$ (n=16 for 5 week, and n=11 for 14 week) groups following ad-FlpO administration. Data are shown as mean ± SEM; *p<0.05; ns, not significant. (C) Pathology score

of *Sod1*$^{+/+}$ (n=14) and *Sod1*$^{\Delta/\Delta}$ (n=11) tumors at 14 weeks post tumor induction. (D) Kaplan- Meyer survival analysis of Ad-FlpO-treated *Sod1*$^{+/+}$ or *Sod1*$^{\Delta/\Delta}$ mice (P value calculated by log-rank Mantel–Cox test). (E) The scheme for inducing *Sod*1 knockout in mice bearing KP lung tumors (applies to right panel). (F) Quantification of tumor burden in *Sod1*$^{+/+}$ (n=12 for 4 weeks, n=10 for 6 weeks) and *Sod1*$^{\Delta/\Delta}$ (n=11 for 4 weeks, n=13 for 6 weeks) groups post TMX administration. Data are shown as mean ± SEM; *p<0.05; ns, not significant. (G) Pathology score of *Sod1*$^{+/+}$ (n=14) and *Sod1*$^{\Delta/\Delta}$ (n=10) tumors at 4 weeks after TMX treatment, and *Sod1*$^{+/+}$ (n=14) and *Sod1*$^{\Delta/\Delta}$ (n=8) tumors at 6 weeks after TMX treatment. (H) Kaplan-Meyer survival analysis of TMX-treated *Sod1*$^{+/+}$ or *Sod1*$^{Flox/Flox}$ mice bearing KP lung tumors. (P value calculated by log-rank Mantel–Cox test).

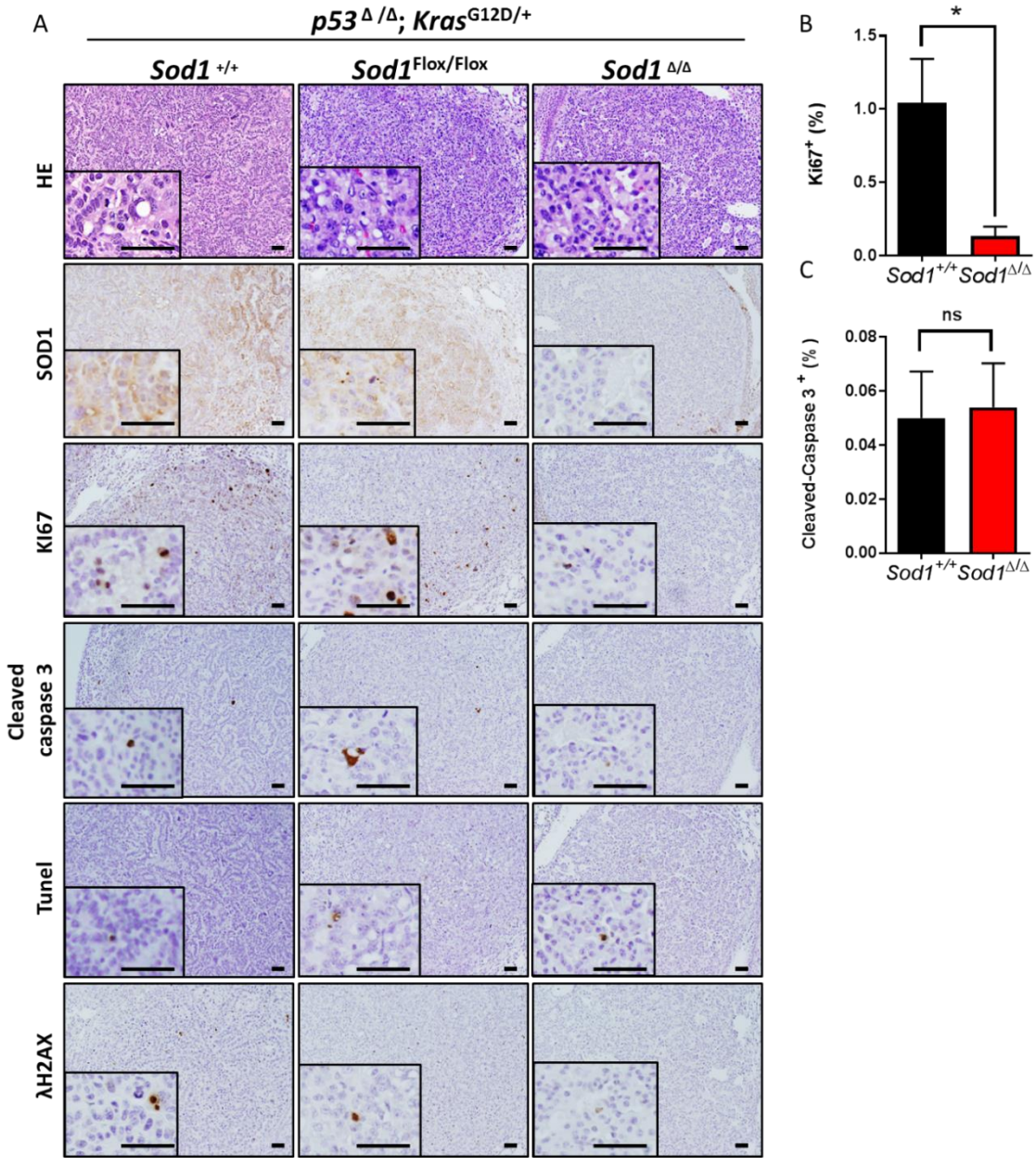

Figure 2.4.2 Loss of SOD1 suppresses KP lung tumor proliferation.

(A) Representative H&E staining and IHC staining for SOD1, Ki67, cleaved caspase 3, TUNEL, and λH2AX in lung tumor sections from TMX-treated *Sod1*$^{+/+}$ or *Sod1*$^{Flox/Flox}$ mice bearing KP tumors. Scale bar, 100 μm. *Sod1*$^{Flox/Flox}$ tumors are those occurring in *Sod1*$^{Flox/Flox}$ mice that have escaped Cre/Loxp recombination. *Sod1*$^{Δ/Δ}$ tumors are those from *Sod1*-knockout mice. (B and C) Quantitative comparison of the percentage cells

expressing Ki67 (B) or cleaved caspase 3 (C) in lung tumors with or without SOD1. *Sod1*$^{Flox/Flox}$ tumors are counted as part of the *Sod1*$^{+/+}$ group. Data shown as mean ± SEM. ns, not significant, *p<0.05.

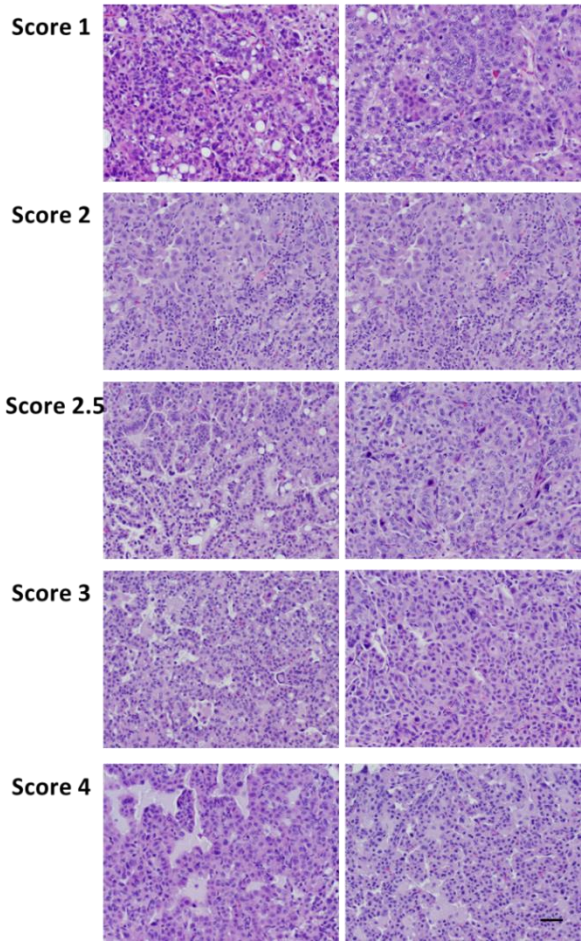

Figure 2.4.3 Examples of pathology scoring.

The numerical pathology scoring of tumor sections stained with H&E is illustrated by two representative examples for each score level. Scale bar: 100 µm.

CHAPTER III SOD1 is required for KP cells proliferation and survival *in vitro*

MATERIALS AND METHODS

Mouse lung tumor cell line derivation

Ubc-CreERT2+; *Sod1*$^{+/+}$; *FSF-Kras*$^{G12D/+}$; *Tp53*$^{Frt/Frt}$ and *Ubc-CreERT2+*; *Sod1*$^{Flox/Flox}$; *FSF-Kras*$^{G12D/+}$; *Tp53*$^{Frt/Frt}$ mice were sacrificed 14 weeks after FLPo adenovirus administration. Lung tumors were dissected, and individual tumors were minced into single cell suspension. Erythrocytes were removed by RBC lysis buffer (155 mM NH_4Cl, 12 mM $NaHCO_3$, 0.1 mM EDTA). Cells were washed with PBS and then placed in culture in RPMI Media 1640 medium (Thermo Fisher Scientific, #72400) supplemented with 10% Fetal bovine serum and 1% Penicillin-Streptomycin solution (Thermo Fisher Scientific, #15140).

4-Hydroxytamoxifen (4HT) treatment

(Z)-4-Hydroxytamoxifen (4HT or 4OH-Tam; Thermo Fisher Scientific, H7904) was dissolved in tetrahydrofuran (Sigma, 360589) at a concentration of 10 mM, then diluted to a final concentration of 75 nM with medium. Tetrahydrofuran was diluted to the same extent to serve as a vehicle control. Following overnight 4HT incubation, cells were either washed with PBS then replenished with fresh medium or were trypsinized and reseeded.

Cell Lysis

Cell were lysed with a lysis buffer comprised of 20 mM Tris-HCl (pH 7.5), 150 mM NaCl, 1 mM Na_2EDTA, 1 mM EGTA, 1% NP-40, 1% sodium deoxycholate, and 1mM PMSF. PhosSTOP (Sigma, 4906845001) and cOmplete™ Protease Inhibitor Cocktail (Sigma, 11697498001) were added, according to the application notes.

Cell Growth Assay

Cell growth was measured by a sulforhodamine B (SRB) colorimetric assay [259]. Cells were seeded in triplicate at a predetermined density (500 - 2000 cells per well) in 96-well plates. At the end of the experiment, the culture medium was aspirated, and cells were fixed in place with 100 µl 10% trichloroacetic acid (Sigma, T6399) at 4 ℃ for 1 h. The fixed cells were then washed four times with water and allowed to air dry. Cells were then stained with 50 µl of 0.057% (wt/vol) sulforhodamine B (Sigma, S1402) (dissolved in 1% acetic acid) for 30 min. The unbound dye was washed once in water and 3 times in 1% acetic acid. The cells were allowed to air dry before the dye was solubilized by adding 200 µl of 10 mM Tris base solution (pH 10.5). Conversion of the colored end product was measured by OD at 510 nm in a TECAN Infinite M200PRO plate reader.

Crystal violet colony staining

Cells adherent to 96-well plates were washed once with PBS, and then stained with 0.5% crystal violet staining solution in 20% methanol for 20 min. with agitation. Unbound dye was washed away 10 times with water, and cells were allowed to air dry.

Annexin V staining apoptosis assay

Cell apoptosis was detected using the PE Annexin V Apoptosis Detection Kit I (BD Pharmingen, Cat# 559763), according to the manufacturer's instructions. Cells were seeded the day before the assay. Viable cells are defined as annexin V and 7-AAD double negative, early-apoptosis is defined as annexin V positive and 7-AAD negative, and late apoptotic or necrotic cells are annexin V and 7-AAD double positive.

Cell cycle analysis

Cell cycle was examined by total DNA content staining. Cells were collected by trypsin digestion and washed in PBS. Cells were then fixed by adding cold 70% ethanol drop-wise to the pellet while vortexing. Cells were fixed at -20 °C overnight. Fixed cells were washed twice in PBS, and 50 µl of 100 µg/ml Rnase A was added. Cells were then stained with 50 µg/ml propidium iodide, and total DNA content was determined by flow cytometry. Cell cycle profiles were analyzed using FlowJo software (FlowJo, LLC).

Senescence β-Galactosidase Staining

Cell senescence was determined by detecting β-galactosidase activity at pH 6, using the Senescence β-Galactosidase Staining Kit (Cell Signaling, Cat#9860). Staining was performed following instruction provided by the kit.

ROS measurement

Intracellular superoxide was measured using dihydroethidium (DHE) (Thermo Fisher Scientific, D1168). Cells ($1x10^5$/well) were seeded into black-walled clear-bottomed 96-well plates (Costar, 3603). Cells were incubated in RPMI 1640 medium without phenol red or serum, with 5mM DHE for 10 minutes before reading on a TECAN infinite M200PRO plate reader at excitation and emission wavelengths of 500/580 nm, respectively. Total ROS was determined using CM-H_2DCFDA (Thermo Fisher Scientific, C6827). Cells ($1x10^5$/well) were seeded into black-walled clear-bottomed 96-well plates (Costar, 3603). Cells were incubated in RPMI 1640 medium without phenol red or serum, with 5mM CMH2-DCFDA for 45 minutes before reading at excitation and emission wavelengths of 495/529 nm, respectively. Fluorescence readings were normalized to total cell number, as measured by the SRB assay[259].

RNA extraction and quantitation using RT-qPCR

Messenger RNA extraction was performed using RNeasy Mini Kit (Qiagen, cat 74104), following the kit manual. Reverse transcription of mRNA was done with the High-Capacity cDNA Reverse Transcription Kit (ThermoFisher, Cat# 4368813). The Sybr Green method was used for mRNA quantitation. PCR reactions were carried out using PowerUp™ SYBR™ Green Master Mix (ThermoFisher, Cat# A25742). The primers used for qPCR are shown below.

Primers for qPCR

Gene	Sense	Antisense
SOD1	GGGTTCCACGTCCATCAGTAT	ACACATTGGCCACACCGTC
ACTB	TGAGCGCAAGTACTCTGTGTGGAT	ACTCATCGTACTCCTGCTTGCTGA
NQO1	TTCTCTGGCCGATTCAGAGT	GGCTGCTTGGAGCAAAATAG
MMP13	GGAGCCCTGATGTTTCCCAT	GTCTTCATCGCCTGGACCATA
PRODH	AGGACCCCATCAACCCTACA	CCTTCATCCTGCACAACGTG
ARG2	CTTGCGTCCTGACGAGATCC	GTGGCATCCCAACCTGGAG
FOSB	CGACTTCAGGCGGAAACTGA	TTCGTAGGGGATCTTGCAGC
PTGS2	GTTCATCCCTGACCCCCAAG	TTTAAGTCCACTCCATGGCCC
CSF2	CGTTGAATGAAGAGGTAGAAGTCG	ACTTGTGTTTCACAGTCCGT

Plasmids

Human *SOD1* was cloned into the lentiviral vector, pInducer20 (Addgene #44012). All pInducer20-SOD1 mutations were generated through site-directed mutagenesis, which was performed according to the QuikChange protocol (Agilent Technologies). The sequences used are shown below.

hSOD1 C58S F ATAATACAGCAGGCAGTACCAGTGCAGG; C58S R CCTGCACTGGTACTGCCTGCTGTATTAT;

hSOD1 C147S F AAGTCGTTTGGCTAGTGGTGTAATTGG; C147S R CCAATTACACCACTAGCCAAACGACTT;

hSOD1 H46R F CATGGATTCCGGGTTCATGAGTTTGG; H46R R CCAAACTCATGAACCCGGAATCCATG;

hSOD1 H48Q F ATGGATTCCATGTTCAGGAGTTTGGAG; H48Q R CTCCAAACTCCTGAACATGGAATCCAT;

hSOD1 G37R F GAAGCATTAAAAGACTGACTGAAGG; G37R R CCTTCAGTCAGTCTTTTAATGCTTC;

hSOD1 G85R F GGAGACTTGCGCAATGTGAC; G85R R GTCACATTGCGCAAGTCTCC;

hSOD1 G93A F ACAAAGATGCTGTGGCCGATGTG; G93A R CACATCGGCCACAGCATCTTTGT;

hSOD1 NES PF CCCATATCCTGGTCCTGCATTACGGTCTCTAAGATATCTAGACCCAGCTTTCTTG;

hSOD1 NES PR CAGGATATGGGTCAATGCCAGACGCGTTTGGGCGATCCCAATTACACC;

hSOD1 NLS PF CCAAAAAAGAAGAGAAAGGTACTCTAAGATATCTAGACCCAG;

hSOD1 NLS PR CCTTTCTCTTCTTTTTTGGACGCGTTTGGGCGATCCCAATTAC;

Establishment of stable Tet-on cells

For lentiviral infections the constructs were transfected along with packaging plasmids psPAX2 (addgene #12260), and pMD2.G(addgene #12259)) into HEK293T cells using Fugene 6 (Promega, cat# E2691). Viral supernatant was collected at 48 and 72 hours after transfection and target cells were transiently infected twice in the presence of 8 μg/ml polybrene (Sigma). Transfected cells were selected with 50 μg/ml G418 (ThermoFisher Scientific, Cat#10131035) at 48 hours after viral infection for 2 weeks.

SOD1 in-gel activity assay

SOD1 activity was measured by the activity gel method described in Weydert et al.[260] Briefly, cells were lysed by sonication and separated by native-PAGE gel at 4 °C. After electrophoresis separation, the gel was stained with nitroblue tetrazolium (NBT). Achromatic bands represent SOD activity.

RNA-sequencing

Library preparation and sequencing

Sequencing service was provided by the Center for Medical Genomics (CMG) at Indiana University School of Medicine, a sequencing core facility of the Indiana CTSI. The concentration and quality of total RNA samples was first assessed using the Agilent 2100 Bioanalyzer. A RIN (RNA Integrity Number) of five or higher was required to pass the quality control. All samples used had RIN values greater than 9.2. Then 400 ng of RNA per sample was used to prepare a dual-indexed strand-specific cDNA library using the TruSeq RNA Access Library Prep Kit (Illumina). The resulting libraries were assessed for quantity and size distribution using Qubit and the Agilent 2100 Bioanalyzer. Pooled libraries (200 pM) were utilized per flowcell for clustering amplification on cBot using HiSeq 3000/4000 PE Cluster Kit and sequenced with 2×75bp paired-end configuration on HiSeq4000 (Illumina) using HiSeq 3000/4000 PE SBS Kit. A Phred quality score (Q score) was used to measure the quality of sequencing. More than 90% of the sequencing reads reached Q30 (99.9% base call accuracy).

Sequence alignment and gene counts

The sequencing data were first assessed using FastQC (Babraham Bioinformatics, Cambridge, UK) for quality control. Then all sequenced libraries were mapped to the mouse genome (UCSC mm10) using STAR RNAseq aligner[261] with the following parameter: "--outSAMmapqUnique 60". The reads distribution across the genome was assessed using bamutils (from ngsutils).[262] Uniquely mapped sequencing reads were assigned to mm10 refGene genes using featureCounts (from subread)[263] with the following parameters: "-s 2 –p –Q 10". Quality control of sequencing and mapping results was summarized using MultiQC[264]. Genes with read count per million (CPM) > 0.5 in more than 3 of the samples were kept. The data was normalized using TMM (trimmed mean of

M values) method. Differential expression analysis was performed using edgeR[264,265]. False discovery rate (FDR) was computed from p-values using the Benjamini-Hochberg procedure.

Bioinformatics Analysis

Multidimensional scaling (MDS) plots was generated in R using the plotMDS function based on gene expression levels. A heatmap of the differentiated genes was generated in R by the function heatmap.2, based on their expression levels.

Metabolomics study

24 hours prior to metabolite collection, cells in culture had their medium switched to fresh DMEM (ThermoFisher, #10566) with 10% Fetal bovine serum and 1% Penicillin Streptomycin (Thermo Fisher Scientific, #15140). Then, 1 hour prior to metabolite collection, the medium was replaced with fresh medium. For metabolite extraction, immediately after medium aspiration, 1 mL 40:40:20 methanol: acetonitrile: water with 0.5% formic acid (ice cold) was added to the cells on ice. Cells were scraped from the plates after adding 50 µl 15% NH_4HCO_3. The cell lysate and methanol mixture were then transferred to 1.5 mL tubes on ice and centrifuged at 15,000xg for 10 minutes at 4 °C. The supernatant (700 µl) was transferred to 1.5 mL tubes on ice and proceeded to LC-MS analysis.

EXPERIMENTAL RESULTS

3.1 Loss of SOD1 suppresses KP Cell Proliferation

Tumor-derived cell lines (TDCLs) were generated from either *Sod1*$^{+/+}$ or *Sod1*$^{Flox/Flox}$ KP mice infected with FLPo (Figure 3.1.1A). 4-OH-Tamoxifen (4HT) was used to activate ERT2-Cre and induce *Sod1* knockout *in vitro*. 4OHTam dosage was titrated to determine the minimal concentration needed to achieve complete DNA recombination. As low as 50 nM 4OHTam achieved near complete recombination following overnight treatment, as evaluated by genotyping PCR primer set #1 (Figure 3.1.1B). However, mild growth inhibition was observed for *Sod1*$^{+/+}$ KP cells treated with 4OHTam at the effective dosage for ERT2-Cre activation (Figure 3.1.1C). This indicates that 4OHTam poses anti-estrogen-related toxicity towards KP cells. Therefore, *Sod1*$^{+/+}$ KP cells were included in all assays to control for any effects of 4OHTam. Cells were treated with 50 to 150 nM 4OHTam overnight, then washed with fresh medium. Western blotting analysis showed that SOD1 protein required 3 days to be completely depleted after overnight 4OHTam treatment, a consequence of the slow turnover rate of SOD1 protein. SOD1 is a stable protein with long half-life of 30 hours, and therefore can persist for several days in the absence of new transription.[248] The proliferation of KP cells was significantly suppressed by 4OHTam-induced SOD1 knockout, compared with that for the *Sod1*$^{+/+}$ KP cells (Figures 3.1.1E and F).

Loss of SOD1 was also found to enhance apoptosis in KP cells, as revealed by flow cytometry of cells stained with annexin V and 7-AAD (Figure 3.1.2, Table 3.1.1). Interestingly, the observed effect is latent, which is likely an indirect result of proliferation inhibition. Following SOD1 protein depletion 3 days after 4OHTam treatment, minimal induction of apoptosis was observed for *Sod1*$^{Flox/Flox}$ KP cells on day 4. By day 5, however, a significant increase in early apoptotic cells was

detected in *Sod1*$^{Flox/Flox}$ KP cells, and the apoptosis rate peaked on day 6. Cell cycle analysis revealed that 4OHTam causes KP cells to arrest at the G2/M phase independent of SOD1 status, despite some clonal variation (Figures 3.1.3 A and B, Tables 3.1.2 and 3.1.3). Loss of SOD1 in KP cells was not observed to induce senescence. To determine if KP cells underwent senescence, cells were stained for senescence-associated β-galactosidase (SA-β-gal) activity at 5 days post 4OHTam treatment. As a positive control for SA-β-gal activity staining, senescence was induced in 3T3 cells by mitomycin C at various doses (Figure 3.1.4B). KP cells exhibited weak SA-β-gal levels, and 4OHTam treatment did not change the staining intensity or the percentage of positively stained cells (Figure 3.1.4A).

3.2 Loss of SOD1 does not increase basal ROS in KP TDCLs but potentiate the cells to oxidative stress.

Considering the linchpin position of SOD1 in cellular redox homeostasis, I asked whether the loss of SOD1 in KP cells enhances cellular ROS levels and contributes to the inhibition of cell proliferation and induction of apoptosis. Unexpectedly, loss of SOD1 did not increase superoxide levels in KP cells at the basal condition, as detected by dihydroethidium (DHE) (Figure 3.5A), This was surprising since SOD1 does protect KP cells from superoxide insult, as demonstrated by the significantly increased superoxide levels when KP *Sod1* knockout cells were treated with paraquat. (Figure 3.2.1A) These results again suggest that the antioxidant effect of SOD1 may be redundant under normal condition. However, they suggest that under normal conditions, KP cells do not suffer from a high level of superoxide insult, when SOD1 is dispensable for maintaining global superoxide homeostasis. Similarly, loss of SOD1 only marginally increases general ROS level in KP cells, as measured by CM-H_2DCFDA under basal conditions. (Figure 3.2.1B) In contrast, H_2O_2

increased general ROS levels regardless of SOD1 status, again demonstrating the specificity of SOD1 for superoxide.

Intriguingly, N-acetyl-l-cysteine (NAC) was effective at lowering the H_2O_2-induced elevation of intracellular ROS (Figure 3.2.1C), but it did not relieve the growth inhibiting effect of SOD1 ablation (Figure 3.2.2A). NAC is a thiol-based antioxidant and derivative of cysteine and precursor of reduced glutathione. A diverse group of antioxidants were then tested in an attempt to rescue *Sod1* knockout KP cell growth: 1. Trolox (6-hydroxy-2,5,7,8-tetramethyl-chromane-2-carboxylic acid) (Figure 3.2.2C), a water-soluble analogue of vitamin E, which is capable of scavenging lipid peroxyl radicals and quenching with singlet oxygen and superoxide anions; 2. glutathione reduced ethyl ester (GSH-MEE) (Figure 3.2.2D), a membrane/lipid permeable derivative of GSH; 3. Tempol (Figure 3.2.2E), a membrane-permeable aminoxyl-type free radical scavenger that exhibits a superoxide dismutase mimetic ability to degrade superoxide radical; and, 4. MnTBAP (Figure 3.2.2F), a cell-permeable superoxide dismutase (SOD) mimetic and peroxynitrite scavenger. None of these widely-used antioxidants were able to rescue the growth disadvantage caused by loss of SOD1.

Nrf2 is activated in cells in response to oxidative stress, inducing Nrf2 target genes, such as Nqo1[266,267]. A lack of induction of Nqo1 transcription indicates that the loss of SOD1 does not result in activation of the Nrf2-mediated oxidative stress pathway as a compensatory mechanism (Figures 3.2.3 A and B). In a study that used a copper chelator ATN-224 to examine the anticancer effect of SOD1 inhibition in the KP lung cancer model[199]. ATN-224 increased the intracellular H_2O_2 level and led to activation of the p38 MAPK pathway and apoptosis in lung cancer cells, effects that were relieved by antioxidants. In KP TDCLs, *Sod1* knockout did not lead to significant increases in, ROS and no antioxidants could rescue the cell death. Accordingly, loss of SOD1 did not activate

p38 in KP TDCLs (Figure 3.2.3 C). It was suggested that when endothelial cells and tumor cells are treated with ATN-224 to inhibit SOD1 activity, H_2O_2 is prevented from attaining physiological levels sufficiently high to sustain tyrosine phosphatase activity, resulting in attenuated growth factor activation[98]. Yet, when stimulated with EGF, *Sod1*-knockout KP cells expressed similar levels of activated EGFR, compared to controls (Figure 3.2.3 D). These discrepancies suggest that ATN-224 and *Sod1* knockout confer distinct cellular effects. It is reasonable to assume that ATN-224 exerts a pleiotropic effect in the cell, as it is likely to target other copper-containing enzymes. In fact, *Sod1* knockout cells showed significantly increased sensitivity towards ATN-224, indicating that non-specific targets of ATN-224 must contribute to its anticancer effect (Figure 3.2.3 E). It is possible that ATN-224 triggers superoxide production independent of SOD1 inhibition, and that this is detrimental for *Sod1* null cells which are incapable of detoxifying intracellular superoxide as shown in Figure 3.2.1 A. Loss of SOD1 also renders the cells more sensitive to buthionine sulphoximine (BSO), which depletes cellular GSH by inhibiting γ-glutamylcysteine synthetase, an enzyme essential for the synthesis of GSH.

3.3 Dismutase activity is required for SOD1 to sustain KP cell proliferation.

To determine whether its dismutase activity is required for SOD1-dependent KP cell proliferation, SOD1 enzymatically dead mutants were expressed and tested for their ability to rescue KP *Sod1* knockout cell proliferation. In the SOD1 molecule, cys58 and cys147 form an intramolecular disulfide bond that is critical for SOD1 dimerization as well as catalytic activity. Thus, dismutase activity is lost in C58S and C147S SOD1 mutants. The copper ion at the catalytic center of SOD1 is ligated to histidyl side chains of His46, His48, and His120. Thus, these residues are critical to its normal function. Indeed, H46R and H48Q are two loss-of-function mutations that cause ALS (Figure 3.3A). To determine if these molecular properties are required for SOD1 to support KP cell

proliferation, wild type SOD1 as well as C58S, C147S, H46R and H48Q mutants were constructed in a pInducer20 doxycycline (dox)-inducible expression vector, and stably transfected into *Sod1*$^{Flox/Flox}$ KP cells. When these dox-induced SOD1 proteins were expressed in KP knockout cells, only the wild type version was able to rescue proliferation (Figures 3.3B and C). This demonstrates that the intramolecular disulfide bonds, as well as binding of the copper ion, are critical for SOD1-dependent KP cells proliferation.

Several known ALS-associated SOD1 mutations still retain full dismutase activity[268]. When such mutants G37R, G93A[248,269] and G85R[270] were similarly tested for their ability to rescue SOD1-null KP cell proliferation, all of these enzymatically-active SOD1 mutants except G85R were able to restore normal proliferation (Figures 3.3 D, E and F). The G85R mutant was reported to show activity in solution assays of yeast extracts, but not in non-denaturing assay gels[269]. A possible explanation is that G85R has a weaker binding affinity for Cu^{2+}, and so, during electrophoresis, Cu^{2+} is extracted from the protein and migrates in the opposite direction of the polypeptides, stripping the SOD1 of its essential copper ion. Taken together, these results indicate that its dismutase activity is required for SOD1 to sustain the proliferation KP cells proliferation.

3.4 Nuclear SOD1, rather than cytosolic SOD1, is important for KP cell proliferation

SOD1 is normally localized to both the cytoplasm and the nucleus[271]. When flag-tagged SOD1 was expressed in KP TCDLs, prominent nuclear localization was observed (Figure 3.4 A). Previously, our lab has shown that SOD1 translocates to the nucleus in response to ROS, where it regulates gene expression at the transcriptional level, serving an important role in maintaining genomic stability[272]. To determine the functional importance of nuclear SOD1 in KP TCDLs, SOD1 protein was tagged with either a nuclear localization sequence (NLS, “PKKKRKV”) or nuclear export sequence (NES, “LALTHILVLHYGL”) in a tet-on inducible SOD1 construct, and stably transfected

into *Sod1*$^{Flox/Flox}$ KP cells. Following 4OHTam induction of SOD1 knockout, doxycycline was added to induce the expression of SOD1 as wild type, SOD1-NLS or SOD1-NES. Importantly, dox-induced SOD1-NLS was found to fully rescue KP cell proliferation in SOD1-knockouts, restoring it to the same extent as SOD1 wild type protein (Figures 3.4 B and C). In contrast, Dox-induced SOD1-NES had little effect. The same phenomenon was observed when SOD1 wild type, SOD1-NLS and SOD1-NES protein were transiently expressed (Figures 3.4 D, E, F and G). The loss of SOD1 in KP cells was found to induce caspase 3-mediated apoptosis without causing increased DNA damage, as measured by λH2AX level (Figure 3.4 F). Interestingly, loss of SOD1 is accompanied by increased phosphorylation of KAP1 (also known as TRIM28). KAP1 is well-known for being phosphorylated by ATM in response to genotoxic stress[273]. However, in S*od1* knockout KP cells, KAP1 phosphorylation did not correlate with phosphorylated ATM. Taken together, these results demonstrate that SOD1 function in the nucleus is critical to sustain KP cell survival, but it is likely to occur through a mechanism other than the DNA damage response-related pathways.

3.5 Analysis of transcriptome alteration in Sod1 knockout KP TDCLs

To explore the function of nuclear-localized SOD1 in KP TDCLs, mRNA transcripts from *Sod1*$^{+/+}$ and *Sod1*$^{Flox/Flox}$ KP cells were sequenced (RNA-seq). One *Sod1*$^{+/+}$ clone and two *Sod1*$^{Flox/Flox}$ clones of KP cells were treated with 4OHTam or vehicle control, RNA was extracted after 4.5 days, and mRNA was sequenced. Global transcriptome analysis revealed minor changes induced by 4OHTam treatment in both *Sod1*$^{+/+}$ and *Sod1*$^{Flox/Flox}$ KP cells, as the 4OHTam-treated and vehicle control samples of each clone clustered closer than the two 4OHTam-treated *Sod1*$^{Flox/Flox}$ clones (Figures 3.5 B and C). Differential expression analysis was preformed to identify genes whose transcriptional levels were altered specifically by 4OHTam-induced *Sod1* knockout. Using the criteria “absolute fold change >2; value of $P < 0.05$; fold change for *Sod1*$^{Flox/Flox}$ versus *Sod1*$^{+/+}$ cells

is greater than 1.5 or opposite effect", the analysis identified 203 upregulated genes and 61 downregulated genes in 4OHTam-treated *Sod1*$^{Flox/Flox}$ KP cells compared with vehicle control cells. These genes are therefore considered SOD1-dependent genes (Figures 3.5 D and E). Ingenuity pathway analysis was employed to determine pathways that are enriched in these SOD1-dependent genes. Significantly enriched pathways by Ingenuity canonical pathway analysis ($p < 0.05$) are listed in Figure 3.5 F. A few genes in the enriched pathways were verified by qPCR analysis. The qPCR analysis confirmed the alteration discovered by RNA-seq (Figure 3.5 G upper panel). The same genes were analyzed again after 4OHTAM-treatment and a different clone for each genotype was included. The result was consistent and a greater difference was observed (Figure 3.5 G bottom panel).

3.6 Analysis of the metabolomics alteration in Sod1 knockout KP TDCLs

To determine the effects of SOD1 ablation on the metabolism and cellular composition of KP TDCLs, a metabolomics approach was employed to measure the pool size of a subset of metabolites in the central carbon, amino acid, and nucleotide metabolism pathways. Six different clones of *Sod1*$^{+/+}$ and 5 *Sod1*$^{Flox/Flox}$ KP cells were treated with 4OHTAM in triplicate and metabolites were analyzed after 5 days. The 101 distinct metabolites identified by LC-MS and their relative values are depicted in a heat map in Figure 3.6 A. Few differences were found after SOD1-knockout. The overall metabolite profile showed significant heterogeneity among clones, which may obscure any differences between cells with or without SOD1. Intriguingly, and consistent with previous results, loss of SOD1 did not alter the levels of redox metabolites, such as NAD+, NADH, NADP+, NADPH, glutathione, and glutathione disulfide. Despite the lack of alteration in the global metabolite profile, certain metabolites such as 2-hydroxyglutarate, N-acetyl-glutamate, and thymidine were significantly increased in 4OHTAM-induced SOD1-knockout KP clones.

DISCUSSION

Consistent with finding *in vivo* that deletion of SOD1 results in reduced KP lung tumor burdens, ablation of SOD1 in mouse KP lung tumors derived cell lines was found to retard cell growth and induce apoptosis. Mutational analysis proved that the dismutase activity of SOD1 is critical for maintaining KP cell survival, although superoxide and general ROS levels were not significantly elevated in these cells, and a diverse group of antioxidants failed to rescue *Sod1*-null KP cells from cell death. In addition, nuclear-localized SOD1 was found to be indispensable for KP cell survival, and when SOD1 is exported out of the nucleus, it can no longer sustain KP cell survival.

Sod1 knockout in mouse embryonic fibroblasts (MEFs) exhibit cell cycle arrest, increased aneuploidy, and senescence accompanied by p53 activation[274]. In KP TDCLs, SOD1 ablation induced increased apoptosis without causing cell cycle arrest or senescence. In this context, p53 is a crucial tumor suppressor that responds to diverse stress signals and orchestrates cellular processes such as cell cycle arrest, cellular senescence, and apoptosis[275-277]. Since KP cells lack p53, they are more resistant to harsh cellular stress, which may explain the lack of cell cycle arrest and senescence in growth-retarded KP TDCLs.

The SOD enzymes are professional scavengers of superoxide in the cell. Therefore, it was an unexpected finding that KP cells without SOD1 do not exhibit elevated levels of superoxide. This is not due to rapid conversion of superoxide into other types of ROS, since no significant increases were detected in non-superoxide ROS such as H_2O_2, HO•, ROO•, and $ONOO^-$. Mitochondria are the major cellular source of superoxide. It is generally believed that superoxide cannot pass through cellular membranes. Superoxide is generated mainly by complexes I and III into the mitochondrial matrix, where it can be removed by SOD2[51,52]. Complex III can also release superoxide into the inter-membrane (IMS) space of mitochondria[278]. Hence, loss of SOD1 would be expected increase superoxide levels in the IMS. However, *in vitro* studies have shown that

increased SOD1 activity paradoxically boosts production of ROS in the IMS[279]. Other studies revealed that SOD1 importation into the IMS is an oxygen-dependent process[280-282]. It may be inferred that SOD1 is imported into IMS only when excessive superoxide is generated in the IMS and therefore a surge in dismutase activity is needed. In addition, there is evidence suggesting that mitochondrial ROS is required for Kras-driven tumorigenesis[111]. Taken together, these results indicate that it is unlikely that loss of SOD1 confers an anticancer effect by altering mitochondrial ROS levels.

Cancer cells often evolve distinct signaling pathways and reprogram energy and nutrient metabolism to support their elevated proliferative state[283]. Oncogenic RAS has been shown to facilitate metabolic reprogramming, particularly in the maintenance of redox homeostasis. Oncogenic Kras upregulates Nrf2 to promote ROS detoxification in lung and pancreatic cancer[118]. Oncogenic Kras has also been implicated in the reprogramming of glutamine metabolism to enhance NADPH production and thus maintain redox balance in pancreatic ductal adenocarcinoma cells[284]. On these grounds, it is unlikely that KP tumor cells suffer from excessive oxidative stress under basal conditions. SOD1 dismutase activity is only required during oxidative insult. Evidently, paraquat treatment significantly increases superoxide levels in *Sod1*-knockout KP TDCLs, while this oxidative insult is well managed by SOD1 in *Sod1* wild type cells (Figure 3.2.1 A). Knockout of *Sod1* also sensitizes KP TDCLs towards BSO-induced GSH depletion. This demonstrates that the loss of *Sod1* does impair the preserved antioxidant potential. Under basal conditions, however, the antioxidant function of SOD1 may be redundant for KP cells survival.

If SOD1 is dispensable for the maintenance of basal cellular redox balance in KP TDCLs, it may be hypothesized that the dismutase activity of SOD1 is dispensable for maintaining their growth. Intriguingly, SOD1 mutants with abrogated dismutase activity could not rescue the KP cells from

SOD1 ablation, while wild type SOD1 or ALS-associated SOD1 mutants that retain full or partial dismutase activity were able to fully rescue KP TDCLs from the loss of endogenous SOD1.

The finding that the dismutase activity of SOD1 is required to maintain the growth KP TDCLs may seem contradictory to the fact that loss of SOD1 does not readily increase apparent ROS levels. However, this may be explained by the possibility that SOD1 loss may alter localized ROS concentrations without affecting global ROS levels. It has been suggested that the change in H_2O_2 required for redox signaling does not cause a significant change in the intracellular redox state, as assessed by the ratio of oxidized glutathione (GSSG)/GSH or NADPH/NADP$^+$[285]. Further speculation can be made that SOD1 may modulate localized and transient redox signaling through its dismutase activity to support KP TDCLs growth.

Cellular distribution is a significant determinant of protein function. Analysis of the localization of SOD1 in rat liver by electron microscope immunocytochemistry revealed that SOD1 is present at different levels in the cytoplasmic matrix (73.1%) and nucleus (11.9%)[286]. Similarly, in hepatocellular carcinoma cells HepG2, SOD1 staining is distributed in the cytosol, peroxisome, and nucleus[271]. Immunolocalization studies of antioxidant genes in rat lung showed that SOD1 expression was present in the cytoplasm and nucleus of all lung cell types[245]. Prominent nuclear localization was observed in KP tumors (Figures 2.3 C and 2.4.2 A) and KP TCDLs (Figure 3.4 A). These findings suggest that SOD1 may be functionally important in the KP cell nucleus. Indeed, this study found that nuclear-targeted SOD1, but not cytoplasmic-targeted SOD1, was able to rescue KP cell growth from the loss of endogenous SOD1, clearly demonstrating that SOD1 exerts its tumor-supporting function in the nucleus of KP TDCLs.

TRIM28/KAP1 is an E3-ubiquitin ligase with diverse functions. It is also a transcription co-repressor. Through its interaction with various DNA binding proteins, KAP1 can repress gene transcription and modify the configuration of chromatin structure. KAP1 cellular functions have

been implicated in the regulation of stem cell differentiation, host defense, DNA damage response, and reactivation of transposable elements[287-289]. KAP1 can be phosphorylated by ATM and induce chromatin relaxation in response to genotoxic stress[273]. KAP1 phosphorylation can also be upregulated by inhibition of phosphatase[288,290]. SOD1 has been shown to modulate membrane-associated phosphatase oxidation and regulate growth factor signals[98]. KAP1 phosphorylation could be enhanced by SOD1-mediated phosphatase inhibition, or by other upstream regulation in the aftermath of the loss of SOD1. Nonetheless, phosphorylated KAP1 may contribute to KP tumor inhibition that follows loss of SOD1.

It was theoretically proposed that increased superoxide levels (resulting from either increased production or decreased SOD activity), would lead to: 1. a decline in the activity of Fe-S containing enzymes; 2. increased levels of free iron; 3. increased levels of H_2O_2; and, 4. a decrease in the reservoir of intracellular reductants, such as GSH and NAD(P)H[154]. Several of these predicted phenomena have been proved by experiments in yeast and mammalian studies. In Sod1p-null yeast cells, superoxide inhibits 4Fe-4S cluster enzymes involved in amino acid biosynthesis and leads to auxotrophy for leucine and lysine[291]. Yeast cells lacking either sod1 or sod2, or both, resulted in elevated free iron levels[292]. Furthermore, elevated levels of superoxide increases the labile iron pool in cancer cells[121].

Surveying the nuclear Fe-S containing proteins in mouse yielded a list of genes whose function can be categorized as either classes: DNA metabolism (DNA replication and DNA repair) or Fe-S cluster biogenesis (Table 2). Assuming that the Fe-S cluster biogenesis genes serve to generate and maintain Fe-S clusters, DNA metabolism is likely to be the core function of nuclear Fe-S proteins. The molecular roles of Fe-S clusters in DNA metabolic enzymes are still not clear. It has been proposed that these Fe-S clusters play a non-catalytic role in stabilizing the structure of the protein[293]. For instance, the Fe-S cluster in DNA polymerases it thought to be essential in

stabilizing polymerase complex. Oxidative damage to the cluster may lead to an attenuated rate of DNA replication[294]. However, locating these highly redox-sensitive Fe-S clusters in close proximity to DNA is believed to be dangerous since it puts genome integrity at risk. Another more attractive model proposes that the redox-active Fe-S clusters are employed to scan the genome for DNA damage[295,296]. Electron transport can occur over long molecular distances along the DNA helix but can be exquisitely sensitive to perturbation in the π-stacked base pairs[297-299]. Thus, genomic loci where electron charge transport is interrupted by DNA damage can be detected by Fe-S cluster containing enzymes such as DNA repair glycosylases[296,300].

Nox4 is upregulated by oncogenic Ras and increases nuclear H_2O_2[301]. It is reasonable to speculate that, in *Sod1* null *Kras* mutant cells, elevated nuclear H_2O_2 may cause the release of Fe^{2+} from Fe-S clusters, which in turn leads to accumulation of superoxide and eventually disrupts Fe-S cluster-containing proteins. The consequences may include: 1. inhibition of Fe-S biogenesis enzymes, which can lead to partial or complete inactivation of DNA metabolic enzymes; or 2. attenuation of DNA replication and suspended or neglected DNA repair. It is also possible that SOD1 may modulate DNA metabolic enzymes by generating local and transient H_2O_2.

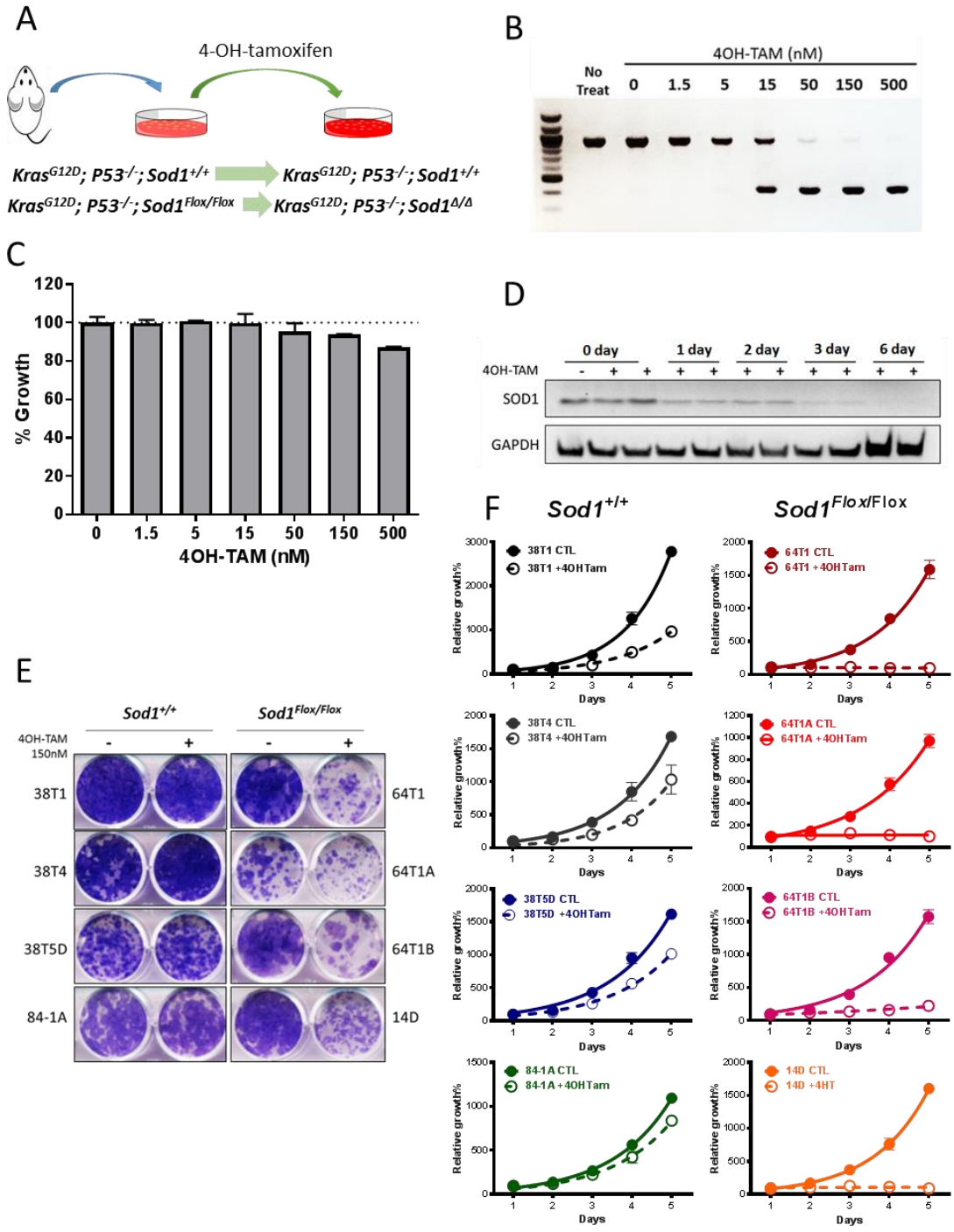

Figure 3.1.1 Loss of SOD1 suppresses KP Cell Proliferation *in vitro*.

(A) Scheme of method used for deletion *in vitro* of *Sod1* in KP TDCLs by 4-OH-Tamoxifen. (B) Genotyping PCR on genomic DNA of TDCLs following treatment with graded doses of 4OH-TAM. (C) Quantitative comparison of western blot analysis of SOD1 protein levels following treatment

with graded doses of 4OH-TAM. Data shown are means ± SD of three independent experiments. (D) Western blot analysis of SOD1 protein level in *Sod1*$^{Flox/Flox}$ TDCLs treated with or without 4OH-TAM for the indicated days. (E) To measure the effects on cell proliferation, *Sod1*$^{+/+}$ or *Sod1*$^{Flox/Flox}$ TDCLs were treated with 150nM 4OH-TAM overnight, cultured for 7 days, and then stained with crystal violet. (F) To generate growth curves, *Sod1*$^{+/+}$ (left panel) and *Sod1*$^{Flox/Flox}$ (right panel) TDCLs were treated with 4OH-TAM overnight, then cultured for the indicated number of days. Cell growth was measured using the SRB assay. Tetrahydrofuran was used as a vehicle control (CTL). Data represent means ± SD of three independent experiments.

Sod1 genotype		*Sod1*$^{+/+}$				*Sod1*$^{Flox/Flox}$			
Clone#		38T1		38T4		64T1		64T1A	
Day# post treat-ment	Treat / Cell%	Control	4OH-Tam	Control	4OH-Tam	Control	4OH-Tam	Control	4OH-Tam
Day 4	Viable	86.9	77.5	91.2	82.3	92.7	86.1	88.6	70.6
	Early Apoptosis	4.18	9.99	1.92	7.50	2.09	5.05	3.46	13.2
	Apoptosis	8.23	11.9	6.62	9.33	4.90	8.30	7.24	14.8
Day 5	Viable	90.8	79.9	95.1	90.4	90.4	64.8	87.8	70.7
	Early Apoptosis	2.07	6.16	1.32	3.39	2.91	16.5	3.30	12.4
	Apoptosis	6.30	11.8	3.44	5.61	6.10	13.4	7.96	13.7
Day 6	Viable	88.4	80.7	78.4	74.9	89.3	46.8	85.6	47.1
	Early Apoptosis	3.37	6.11	3.96	9.72	3.52	30.8	5.63	29.8
	Apoptosis	6.62	10.9	16.7	14.1	6.45	19.3	8.01	16.6

Table 3.1.1 Summary of apoptosis in data from Figure 3.1.2

The extent of apoptosis in Sod1$^{+/+}$ or Sod1$^{Flox/Flox}$ TDCLs is expressed as percentages of cells classified as viable, early apoptotic, or late apoptotic, based on their staining pattern with annexin V and 7-AAD.

Sod1 genotype		*Sod1*$^{+/+}$				*Sod1*$^{Flox/Flox}$			
Clone#		38T1		38T4		64T1		64T1A	
Day# post treat-ment	Treat / Cell%	Control	4OH-Tam	Control	4OH-Tam	Control	4OH-Tam	Control	4OH-Tam
Day 4	G1	23.5	12.0	38.7	26.8	32.2	29.2	29.9	29.4
	S	40.7	5.41	10.6	2.46	27.8	1.73	28.8	10.6
	G2/M	29.2	79.0	48.2	70.8	35.1	63.2	33.7	56.7

Table 3.1.2 Summary of cell cycle data from in Figure 3.1.3.

Day 4, expressed as percentage of cells classified as being in the G1, S or G2/M phases, according to total DNA content staining.

Sod1 genotype		*Sod1*$^{+/+}$				*Sod1*$^{Flox/Flox}$			
Clone#		38T1		84-1A		64T1		14D	
Day# post treat-ment	Treat / Cell%	Control	4OH-Tam	Control	4OH-Tam	Control	4OH-Tam	Control	4OH-Tam
Day 6	G1	21.6	7.90	34.1	23.5	25.7	22	31.3	20.3
	S	40	4.38	31.2	37.9	21.8	14.5	29.8	31.4
	G2/M	27.3	87.6	24.6	26.5	47.1	59.9	25.4	35.8

Table 3.1.3 Summary of cell cycle data from Figure 3.1.3

Day 6, expressed as percentage of cells classified as being in the G1, S or G2/M phases.

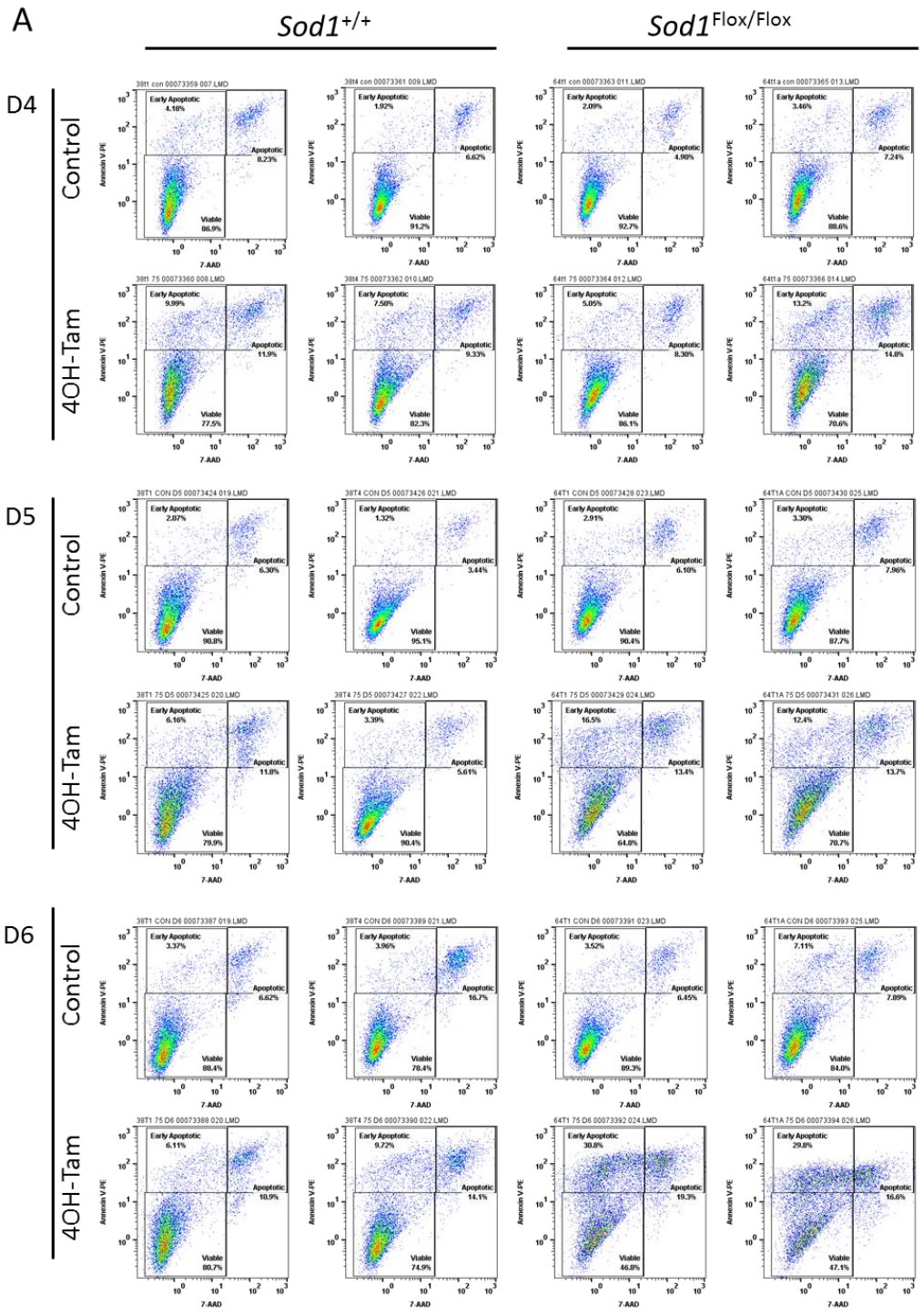

Figure 3.1.2 Loss of SOD1 induces apoptosis in KP TDCLs.

Two clones each of *Sod1*$^{+/+}$ (left panel) or *Sod1*$^{Flox/Flox}$ (right panel) TDCLs were treated overnight with 4OHTAM or vehicle control. To determine the effects on apoptosis, cells were collected on

the indicated days post treatment (day 4, 5, and 6), stained with annexin V-PE and 7-AAD, and analyzed by flow cytometry.

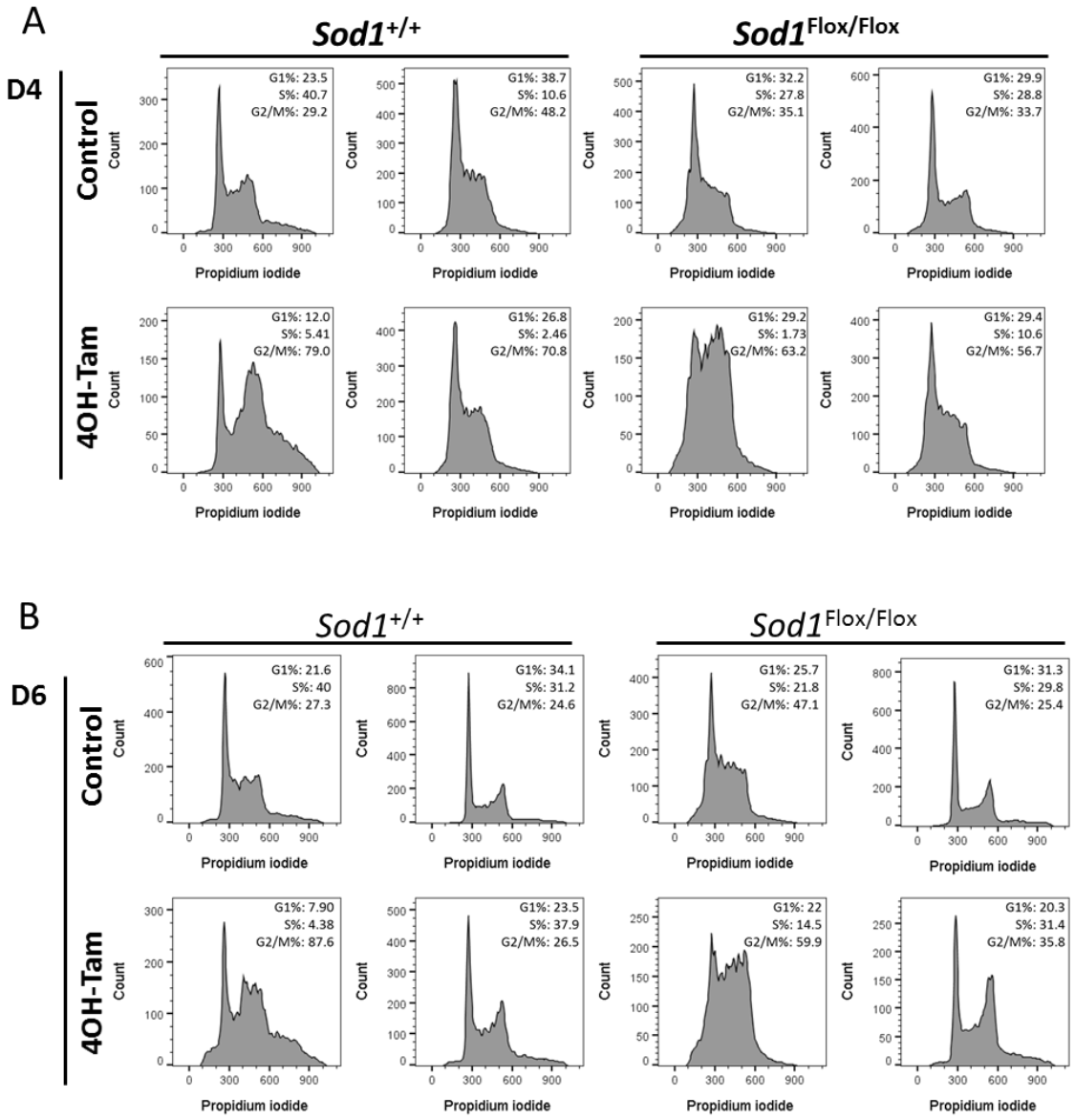

Figure 3.1.3 4OH-Tam causes KP TDCLs to arrest at G2/M independent of SOD1 status.

Two clones each of *Sod1*$^{+/+}$ and *Sod1*$^{Flox/Flox}$ TDCLs were treated overnight with or 4OHTAM or vehicle control and cell cycle status determined by DNA content profile on day 4 (A) and day 6 (B) post treatment. The percentages of cells in each phase of the cell cycle are given. Dead cells (Sub G1) were excluded from the analysis.

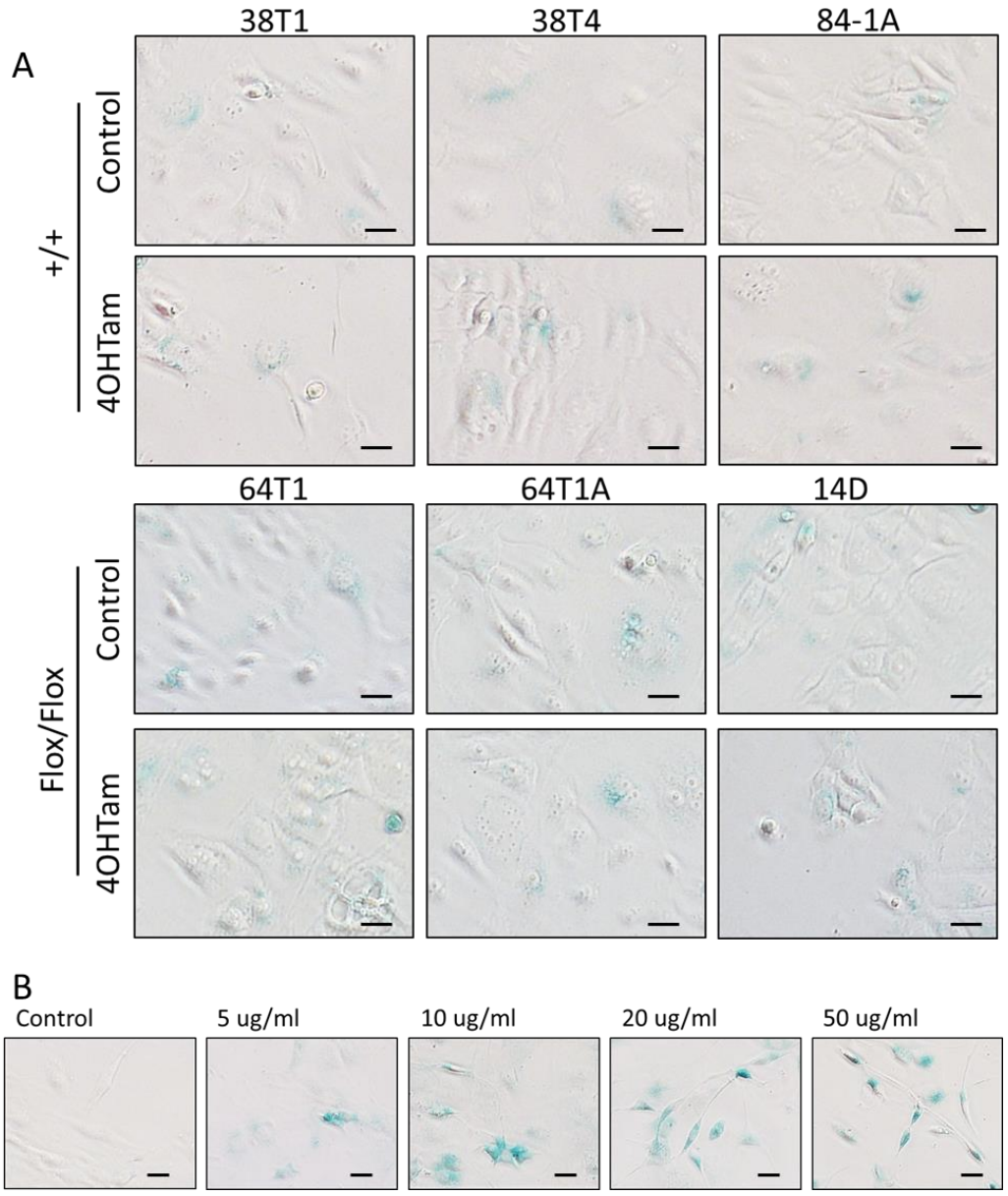

Figure 3.1.4 Loss of SOD1 does not induce senescence in KP TDCLs.

(A) Three clones each of *Sod1*$^{+/+}$ (top panel) and *Sod1*$^{Flox/Flox}$ (bottom panel) TDCLs were treated overnight with 4OHTAM or vehicle control and stained for β-galactosidase activity on day 5 post treatment. (B) As a positive control, 3T3 cells were treated with mitomycin C at the indicated concentrations for 2 hours, allowed to recover for 6 days, then stained for β-galactosidase. Scale bar, 10 μm.

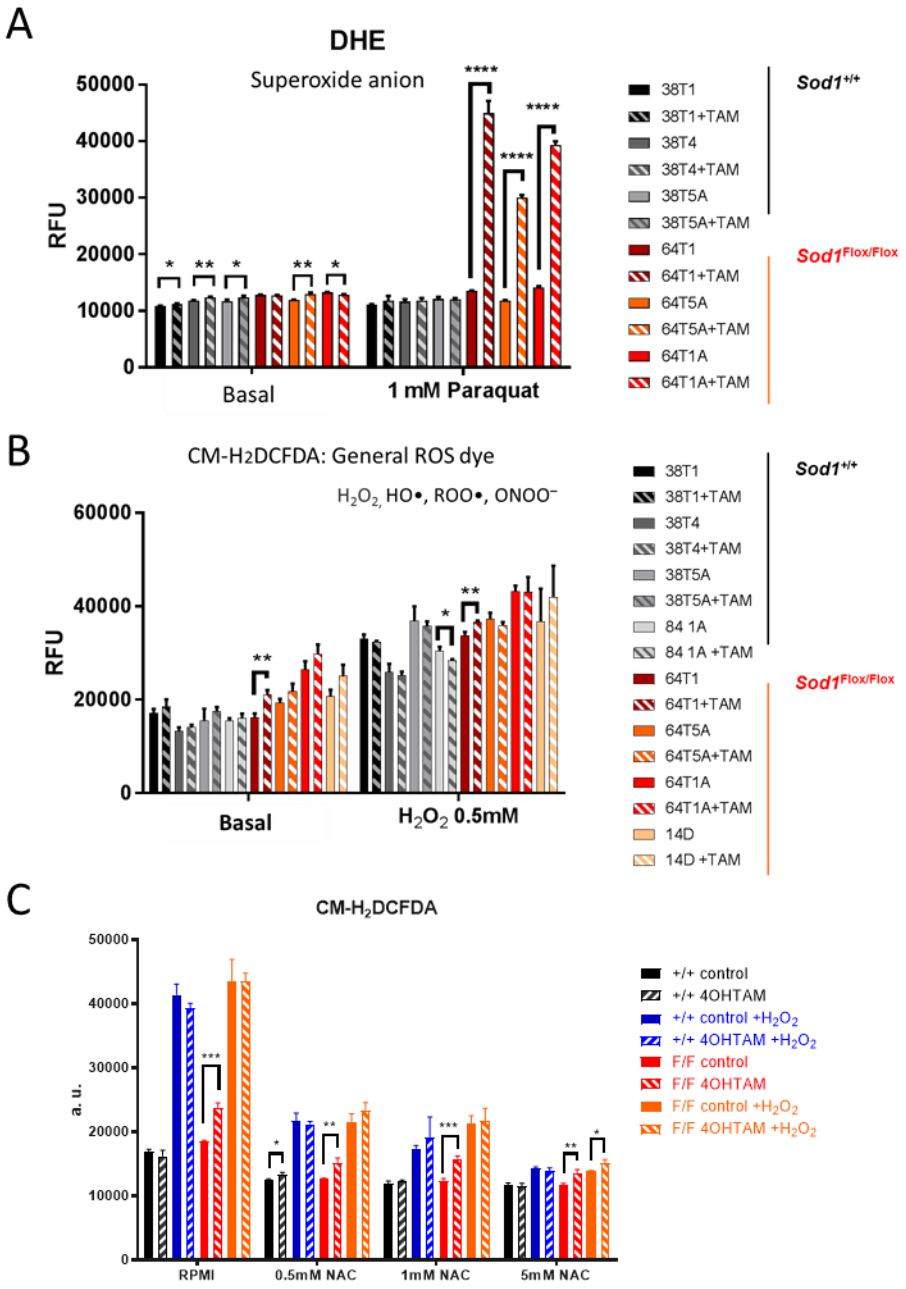

Figure 3.2.1 Loss of SOD1 does not increase ROS level in KP cells.

(A) Effects on superoxide levels: 6 days after 4HTam treatment, 3 clones each of *Sod1*$^{+/+}$ and *Sod1*$^{Flox/Flox}$ TDCLs were stained with DHE (5 µM for 5 min) following treatment with or without paraquat (1 mM, for 1 hour). (B) Effects on general ROS levels: 6 days after 4HT treatment, 4 clones each of SOD1$^{+/+}$ and SOD1$^{Flox/Flox}$ TDCLs were stained with CM-H_2DCFDA (5 µM, for 45 min) following treatment with or without paraquat (0.5 mM for 15 min). (C) Effects of N-acetylcysteine

(NAC) on general ROS levels: 4HT or vehicle treated *Sod1*$^{+/+}$ and S*od1*$^{Flox/Flox}$ TDCLs were treated with or without 0.5 mM H_2O_2 in the presence of graded concentrations of NAC, and general ROS levels were measured using CM-H_2DCFDA, as in B. Data represent means ± SD of three independent experiments. *p<0.05, **p<0.01, ***p<0.001.

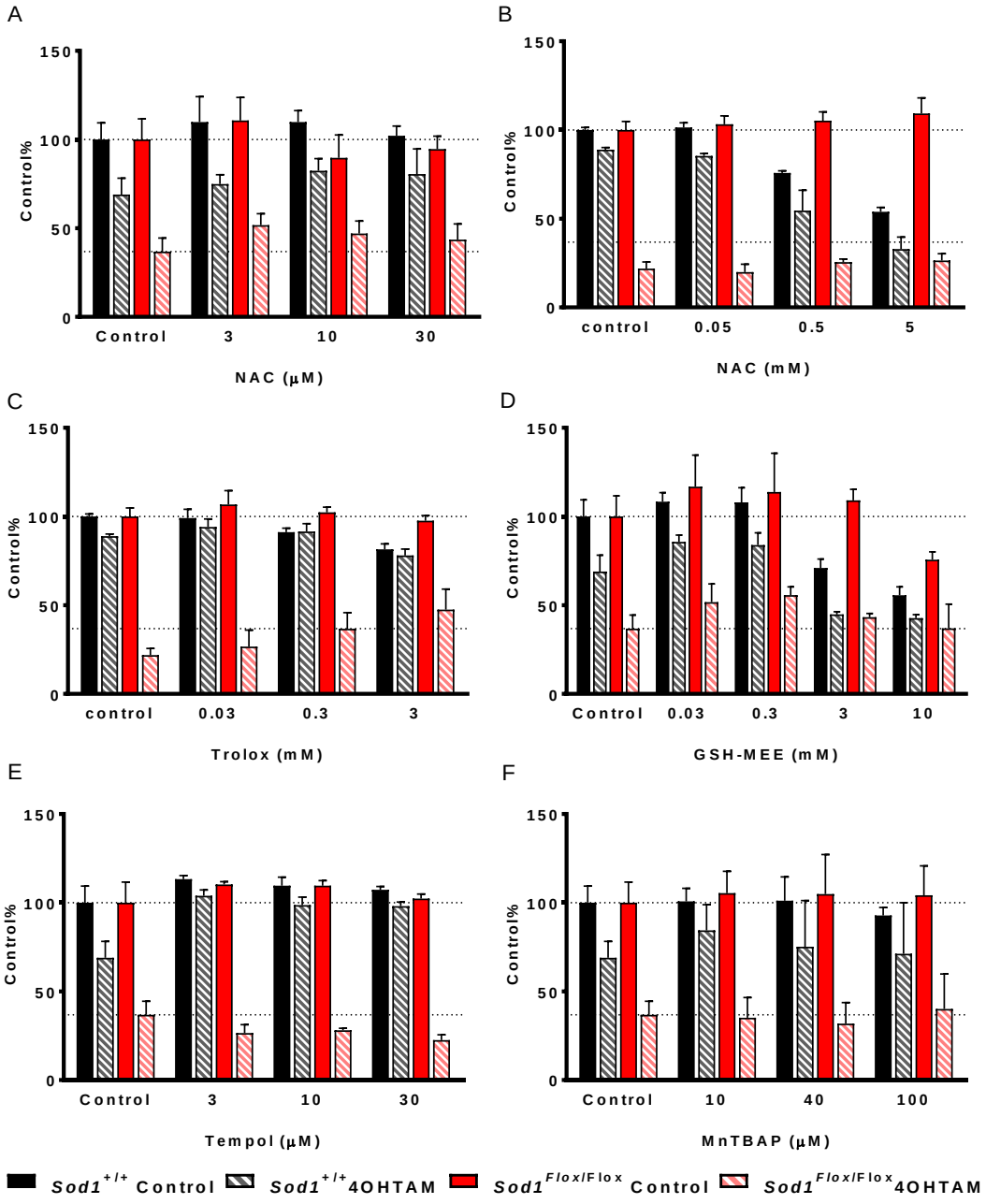

Figure 3.2.2 Antioxidants do not rescue KP proliferation from loss of SOD1.

(A) 4HT or vehicle treated *Sod1*$^{+/+}$ or *Sod1*$^{Flox/Flox}$ TDCLs were seeded into 96-well plates and cultured with graded concentrations of the following antioxidants: N-acetylcysteine (NAC) (A and B), Trolox (C), GSH-MEE (D), Tempol (E), or MnTBAP (F). Cell growth after 7 days was measured using the SRB assay. Data represent means ± SD of three independent experiments.

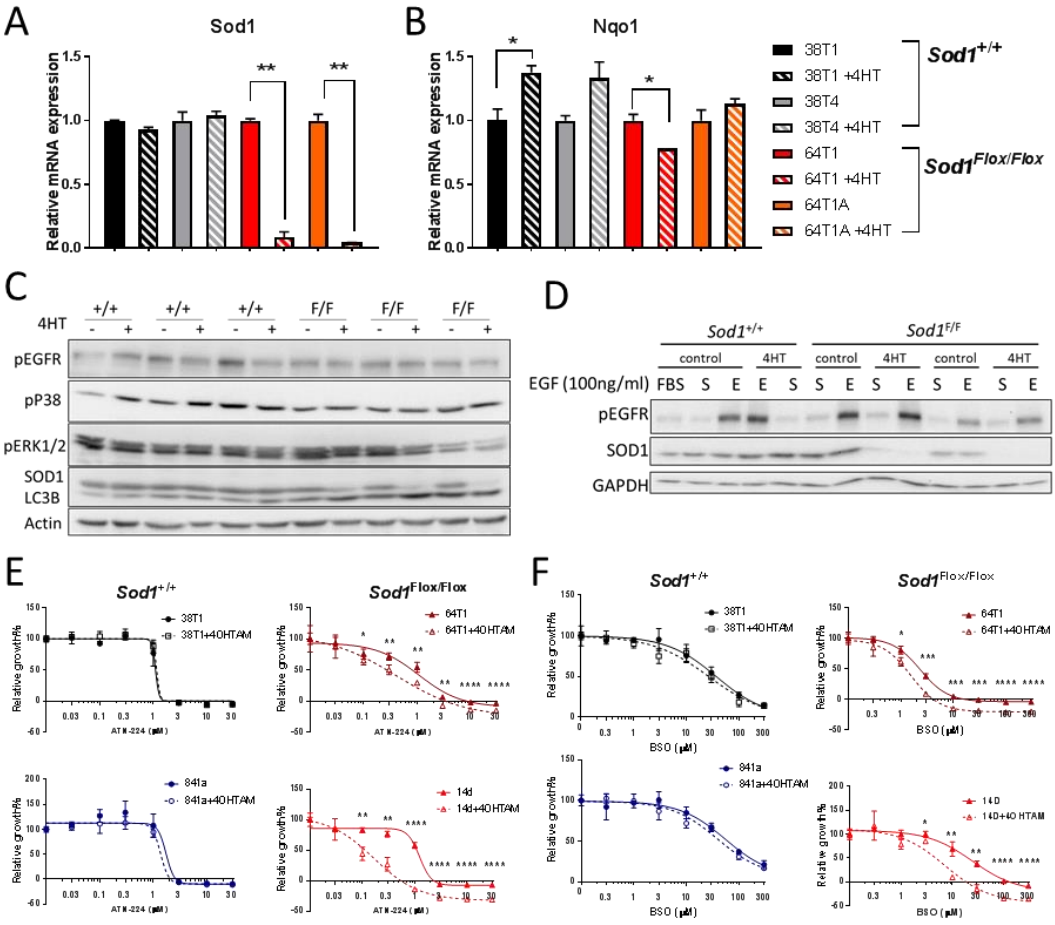

Figure 3.2.3 Loss of SOD1 in KP TDCLs does not alter the MAP kinase pathway.

(A and B) Quantification of Sod1 and Nqo1 mRNA levels in 4HT- or vehicle-treated *Sod1*$^{+/+}$ or *Sod1*$^{Flox/Flox}$ TDCLs. Data shown as mean ± SD of three independent experiments. *p<0.05, **p<0.01, ****p<0.0001. (C) Western blot analysis of phospho-EGFR, phospho-p38, phospho-ERK1/2, SOD1, LC3B and actin levels in *Sod1*$^{+/+}$ or *Sod1*$^{Flox/Flox}$ TDCLs treated with 4OH-TAM or vehicle. (D) Western blot analysis of phospho-EGFR, SOD1 and GAPDH protein levels in *Sod1*$^{+/+}$ and *Sod1*$^{Flox/Flox}$ TDCLs treated with 4OH-TAM or vehicle and cultured in full medium (containing fetal bovine serum, FBS), serum starvation conditions (S), or with EGF stimulation (100ng/ml for 10 min). (E, F) Cell growth by *Sod1*$^{+/+}$ or *Sod1*$^{Flox/Flox}$ TDCLs treated with 4OH-TAM or vehicle, and graded concentrations of ATN-224 (E) or BSO (F) for 2 days, as measured by SRB assay. Data represent means ± SD of three independent experiments.

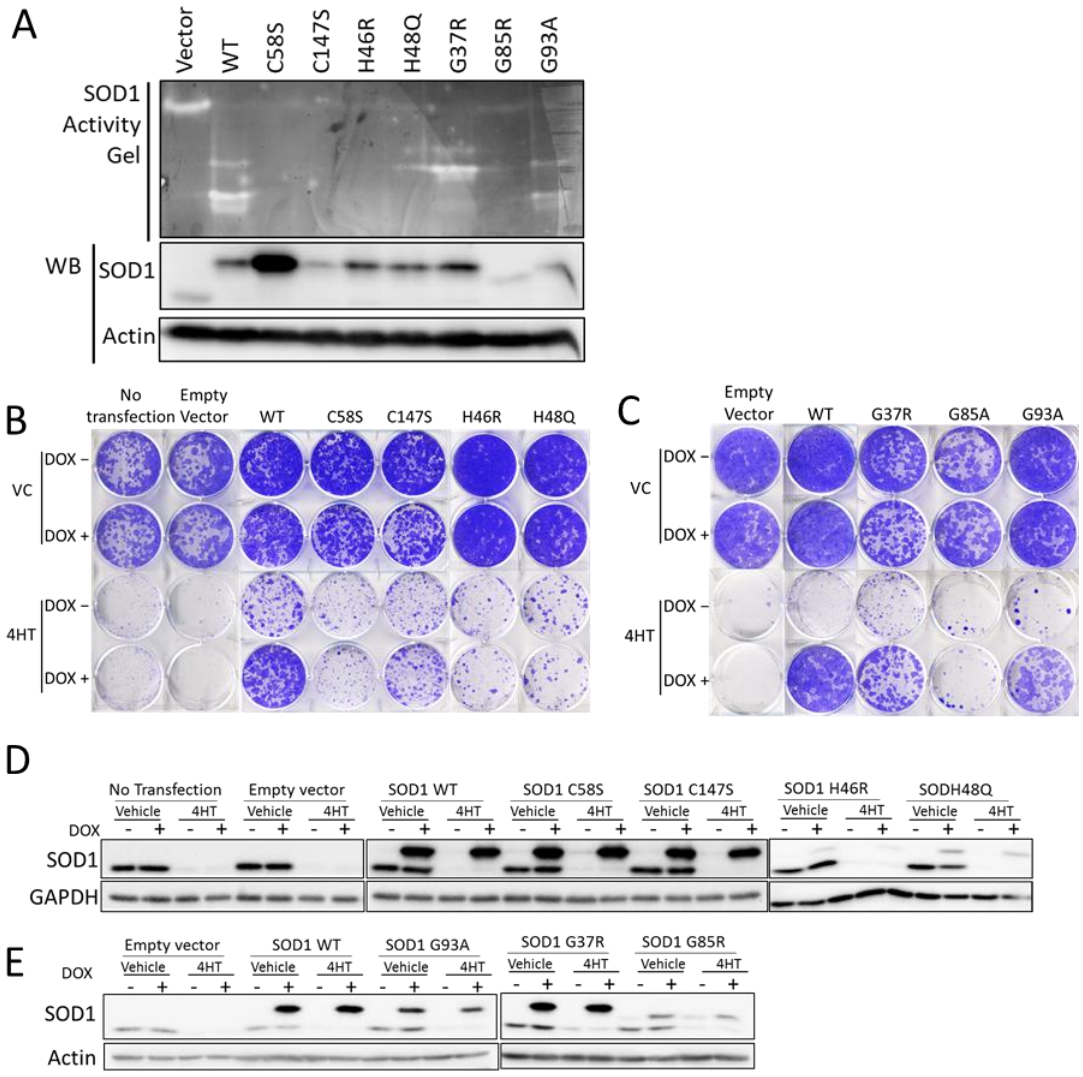

Figure 3.3 Dismutase activity is required for SOD1 to sustain KP cells proliferation.

(A) SOD1 activity was analyzed in gel for pInducer20 (vector only), pInducer20-SOD1 wild type, C58S, C147S, H46R, H48Q, G37R, G85R, or G93A stable transfectants of *Sod1*$^{Flox/Flox}$ KP cells, after treatment with 4OH-TAM (except vector control) and doxycycline (Dox; 500 ng/ml). (B, C) Clonogenic proliferation assay of pInducer20, pInducer20-flag-SOD1 wild type, C58S, C147S, H46R, H48Q (B) and G37R, G85R, and G93A (C) stable transfectants of *Sod1*$^{Flox/Flox}$ KP cells. Cells were treated with 4OH-TAM (4HT) overnight, then Dox (500 ng/ml) was added and the cells were cultured for 7 days. (D, E) Western blotting analysis of the cells treated as in B and C, at 4 days after 4HT treatment.

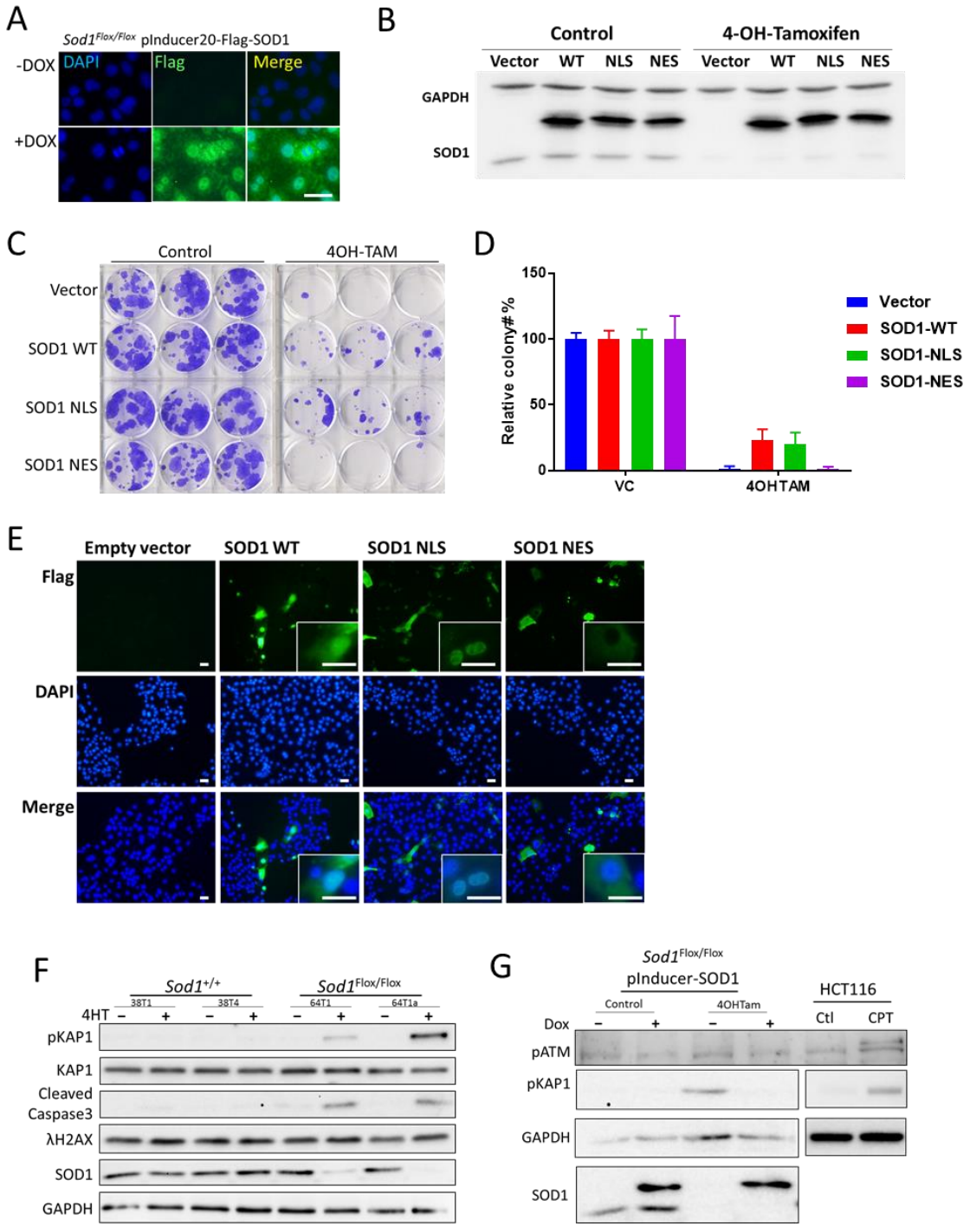

Figure 3.4 Nuclear SOD1 is important for KP cell proliferation.

(A) Immunofluorescence staining for flag in pInducer20-Flag-SOD1 stable transfectants of *Sod1*$^{Flox/Flox}$ KP cells. (Scale bar, 25 μm). (B) Western blot analysis of pInducer20, pInducer20-SOD1 wild type, NLS, and NES stable transfectants of *Sod1*$^{Flox/Flox}$ KP cells. Cells were treated with 4OH-

TAM (4HT) overnight, then doxycycline (Dox; 50 ng/ml) was added, and cells were collected on day 4 post 4HT treatment. (C) Clonogenic proliferation assay of pInducer20, pInducer20-SOD1 wild type, NLS, and NES stable transfectants of *Sod1*$^{Flox/Flox}$ KP cells. Cells were treated with 4OH-TAM (4HT) overnight, then Dox (50 ng/ml) was added, and the cells were grown for 7 days. (D) Quantification of colony formation of the cultures in C. Data represent means ± SD of three independent experiments. (E) Immunofluorescence staining for SOD1 in cultures from C (above) on the day of the clonogenic assay. (Scale bar, 25 μm). (F) Western blot analysis for phospho-KAP1, KAP1, cleaved caspase 2, λH2AX, SOD1 and GAPDH in *Sod1*$^{+/+}$ or *Sod1*$^{Flox/Flox}$ KP cells treated with 4-OH-TMX. (G) Western blot analysis for phospho-ATM, phospho-KAP1, GAPDH, and SOD1 in *Sod1*$^{Flox/Flox}$ pInducer20-SOD1-WT cells treated 4OH-TMX, with or without doxycycline for 4 days. HCT116 cells were treated with camptothecin (CPT; 1μM) for 4 hours.

A

	Sample	Clone	Treatment	SOD1 status
1	WT_control	SOD1 WT	Control	SOD1 +/+
2	WT_TAM	SOD1 WT	4OH-Tam	SOD1 +/+
3	Flox1_control	SOD1 Floxed 1	Control	SOD1 Flox/Flox
4	Flox1_TAM	SOD1 Floxed 1	4OH-Tam	SOD1 Δ/ Δ
5	Flox2_control	SOD1 Floxed 2	Control	SOD1 Flox/Flox
6	Flox2_Tam	SOD1 Floxed 2	4OH-Tam	SOD1 Δ/ Δ

B

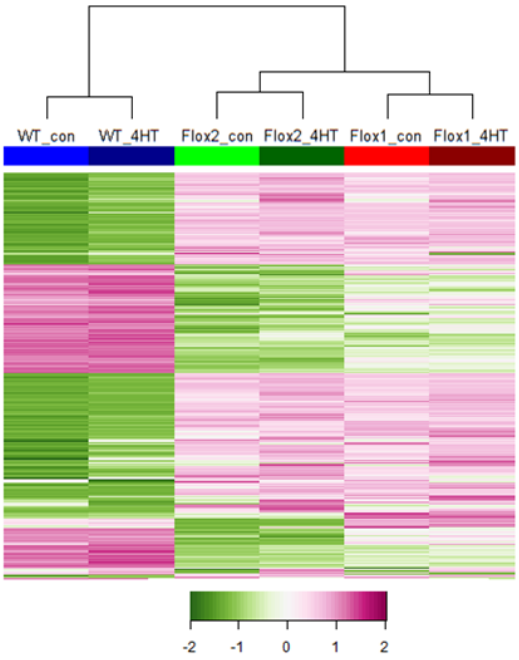

C

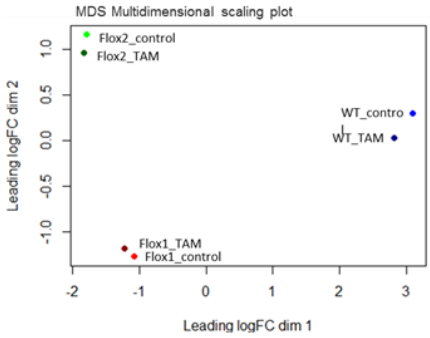

D

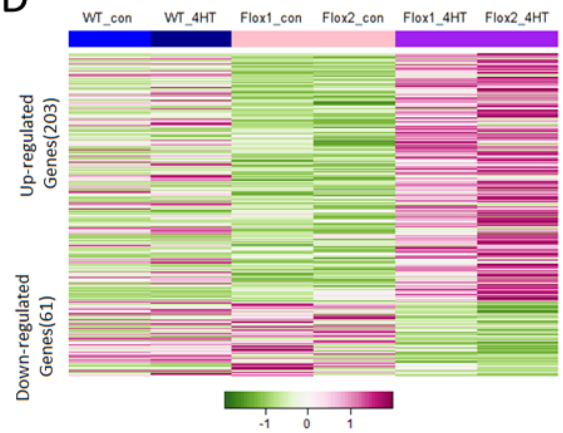

E

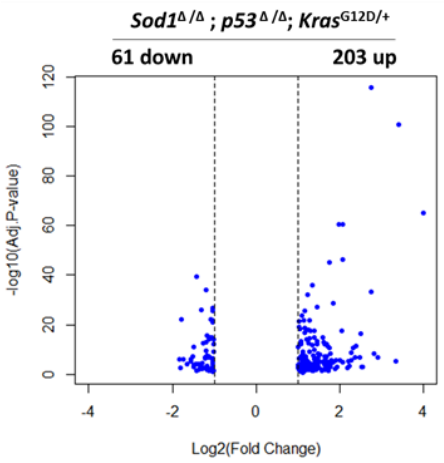

F

Ingenuity Canonical Pathways	-log(p-value)	Ratio	Molecules
Unfolded protein response	3.88	0.0909	CEBPD,PPP1R15A,DDIT3,PDIA2,DNAJB9
Intrinsic Prothrombin Activation Pathway	3.28	0.0952	KLK6,KLK10,F13A1,COL18A1
Prostanoid Biosynthesis	2.56	0.222	PTGS2,HPGDS
Citrulline Biosynthesis	2.56	0.222	ARG2,LOC102724788/PRODH
VDR/RXR Activation	2.28	0.0513	CSF2,KLK6,CYP27B1,TGFB2
Granulocyte Adhesion and Diapedesis	2.24	0.0331	HRH1,CLDN15,ITGB2,MMP13,CLDN1,CXCL2
Superpathway of Citrulline Metabolism	2.11	0.133	ARG2,LOC102724788/PRODH
Agranulocyte Adhesion and Diapedesis	2.1	0.0311	HRH1,CLDN15,ITGB2,MMP13,CLDN1,CXCL2
Role of IL-17F in Allergic Inflammatory Airway Diseases	2.1	0.0652	CSF2,MMP13,RPS6KA6
Role of Macrophages, Fibroblasts and Endothelial Cells in Rheumatoid Arthritis	1.64	0.0224	CAMK2B,ADAMTS4,CSF2,CEBPD,PDGFD,TRAF1,MMP13
Role of Tissue Factor in Cancer	1.6	0.0323	CSF2,PDIA2,MMP13,RPS6KA6
Hepatic Fibrosis / Hepatic Stellate Cell Activation	1.58	0.0267	LY96,PDGFD,TGFB2,MMP13,COL18A1
Proline Degradation	1.58	0.333	LOC102724788/PRODH
1,25-dihydroxyvitamin D3 Biosynthesis	1.58	0.333	CYP27B1
MSP-RON Signaling Pathway	1.57	0.0417	KLK6,KLK10,ITGB2
Atherosclerosis Signaling	1.56	0.0315	PDGFD,ITGB2,MMP13,COL18A1
Arginine Degradation I (Arginase Pathway)	1.45	0.25	ARG2
Coagulation System	1.41	0.0571	F13A1,BDKRB2
MIF-mediated Glucocorticoid Regulation	1.41	0.0571	LY96,PTGS2
Osteoarthritis Pathway	1.38	0.0236	ADAMTS4,PTGS2,C1QTNF4,MMP13,CASP4
Myo-inositol Biosynthesis	1.36	0.2	IMPA2

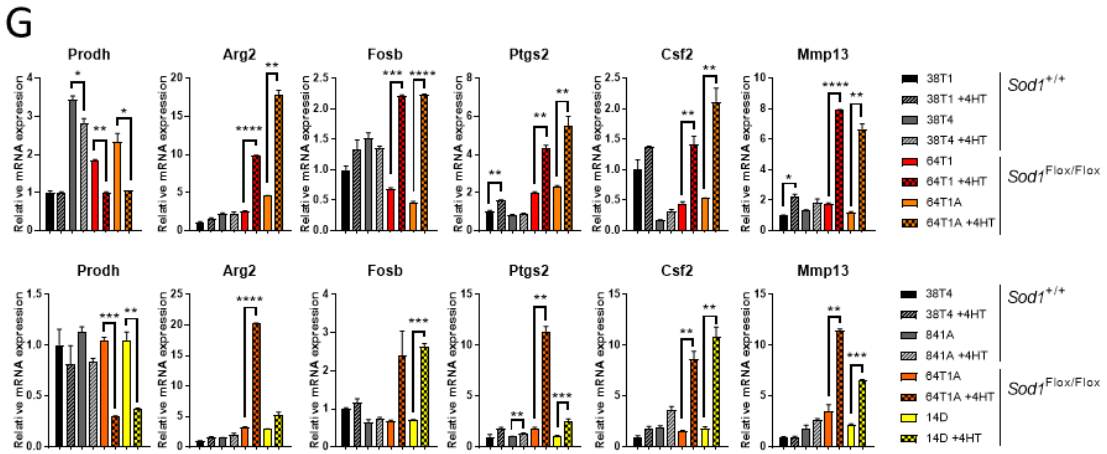

Figure 3.5 Changes in KP TDCLs transcriptome following loss of SOD1.

(A) List of KP TDCL clones and treatments for mRNA sequencing. (B) Heatmap depicting differential expression of top 500 viable genes in *Sod1*$^{+/+}$ and *Sod1*$^{Flox/Flox}$ KP TDCLs treated with or without 4-OH-tamoxifen as determined by RNA-seq. Pink indicates upregulation, and green indicates downregulation. (C) Multidimensional scaling (MDS) plot depicting global transcriptome differences among *Sod1*$^{+/+}$ and *Sod1*$^{Flox/Flox}$ KP TDCLs treated with or without 4-OH-tamoxifen. (D) Heatmap of differential gene expression after *Sod1* knockout in *Sod1*$^{Flox/Flox}$ KP TDCLs treated with or without 4-OH-tamoxifen. (E) Fold change and adjusted p values of differentially expressed genes of cells in D, above. (F) Top pathways enriched in *Sod1* knockout-dependent genes analyzed by Ingenuity canonical pathway analysis. Ratio indicates the percentage of identified genes (Molecules) in total genes listed in the corresponding pathway. (G) qPCR analysis for Prodh, Arg2, Fosb, Prgs2, Csf2 and Mmp13 mRNA levels in *Sod1*$^{+/+}$ and *Sod1*$^{Flox/Flox}$ KP TDCLs treated with or without 4-OH-tamoxifen, for 4 days (upper panel) or 5 days (lower panel). Data represent means ± SD of three independent experiments. *p<0.05, **p<0.01, ***p<0.001, ****p<0.0001.

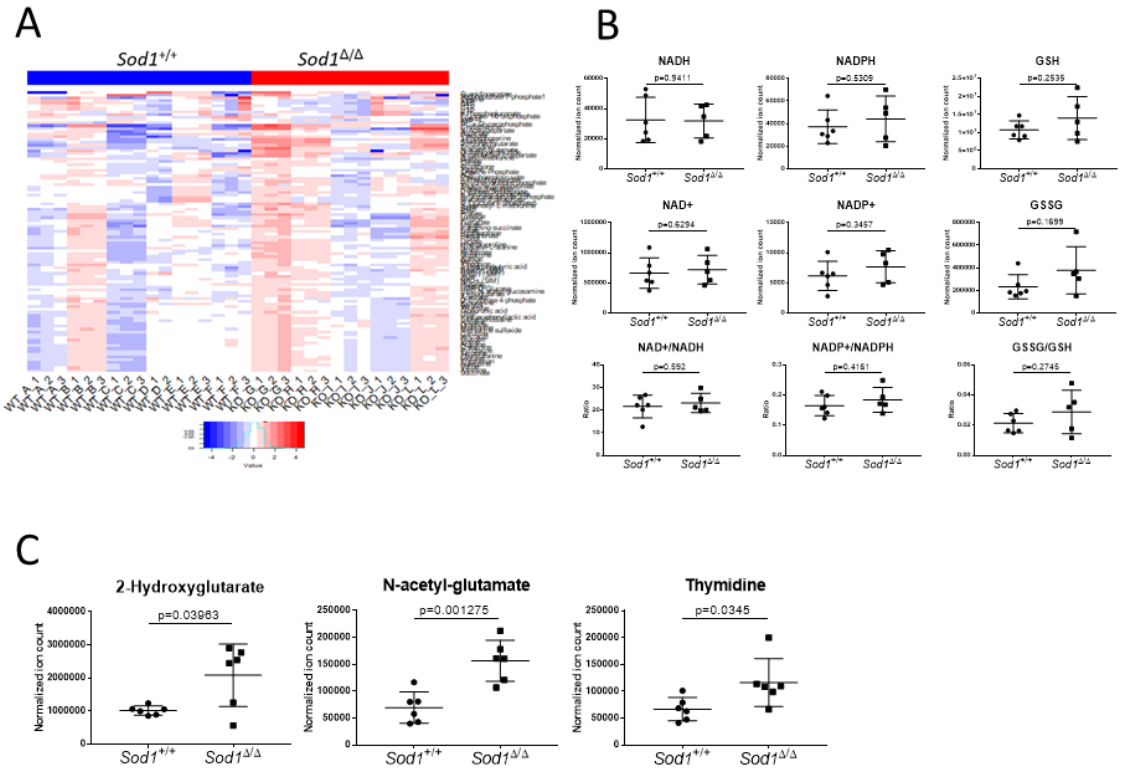

Figure 3.6 Metabolomics analysis of KP TDCLs after loss of SOD1.

(A) Heatmap depicting pool size levels of 101 metabolites in *Sod1*$^{+/+}$ and *Sod1*$^{Flox/Flox}$ KP TDCLs treated with 4-OH-tamoxifen, as determined by LC-MS. Data was log2-transformed and metabolite levels were normalized to the average for all samples. (B) Comparison of levels of NAD+, NADH, NAD+/NADH, NADP+, NADPH, NADP+/NADPH, GSSG, GSH, GSSG/GSH in *Sod1*$^{+/+}$ and *Sod1*$^{Flox/Flox}$ KP TDCLs treated with 4-OH-tamoxifen as determined by LC-MS. (C) Comparison of levels of 2-hydroxyglutarate, N-acetyl-glutamate, and thymidine in cells treated as in B, above.

Table 4 Nuclear Fe-S cluster containing genes in mouse.

DNA metabolism		
Gene ID	Gene name	Function
Rev3l	REV3 like, DNA directed polymerase zeta catalytic subunit	Catalytic subunit of DNA Polymerase ζ , translesion DNA synthesis
Pola1	Polymerase (DNA directed), alpha 1	Catalytic subunit of polymerase α, DNA replication
Pold1	Polymerase (DNA directed), delta 1, catalytic subunit	Catalytic subunit of polymerase δ, DNA replication
Pole	Polymerase (DNA directed), epsilon	Catalytic subunit of polymerase ε, DNA replication
Brip1	BRCA1 interacting protein C-terminal helicase 1	Helicase, repair of DNA interstrand crosslinks
Dna2	DNA replication helicase/nuclease 2	Helicase/nuclease, DNA repair, Okazaki fragment maturation, telomere maintenance
Rtel1	Regulator of telomere elongation helicase 1	Helicase, regulation of telomere length, anti-recombinase
Ercc2	Excision repair cross-complementing rodent repair deficiency, complementation group 2	Helicase, nucleotide excision repair
Ddx11	DEAD/H (Asp-Glu-Ala-Asp/His) box helicase 11	Helicase, sister chromatid cohesion, heterochromatin organization
Exo5	Exonuclease 5	Exonuclease, genome stability
Prim2	DNA primase, p58 subunit	Subunit of DNA Primase, DNA synthesis and double-strand break repair
Mutyh	mutY DNA glycosylase	DNA glycosylase, base excision repair
Nthl1	nth (endonuclease III)-like 1 (E.coli)	DNA glycosylase, base excision repair
Fe-S cluster biogenesis		
Gene ID	Gene name	Function
Nfu1	NFU1 iron-sulfur cluster scaffold	Fe-S cluster insertion
Nubp1	Nucleotide binding protein 1	Component of the cytosolic iron-sulfur (Fe-S) protein assembly (CIA) machinery
Nubp2	Nucleotide binding protein 2	Component of the cytosolic iron-sulfur (Fe-S) protein assembly (CIA) machinery
Ciapin1	Cytokine induced apoptosis inhibitor 1	Component of the cytosolic iron-sulfur (Fe-S) protein assembly (CIA) machinery
Glrx5	Glutaredoxin 5	Intermediate carrier involved in the transfer of Fe-S clusters
Glrx2	Glutaredoxin 2 (thioltransferase)	Promote Fe-S cluster biosynthesis.

OVERALL CONCLUSION AND FUTURE DIRECTIONS

A physiologically-relevant, non-small cell lung cancer (NSCLC) mouse model was established to study the role of SOD1 in the context of $Kras^{G12D}$, p53-loss lung cancer. Using this model, the anticancer function of SOD1 was demonstrated for the first time using specific gene knockout techniques; SOD1 is required for the maintenance of KP lung cancer *in vivo*. At the same time, due to their pleiotropic effects, the copper chelators used in studying SOD1 function must be carefully interpreted. In dissecting the mechanism of SOD1-dependent tumor growth, I demonstrated that the dismutase activity of SOD1 is critically required for the growth of KP TDCLs. Furthermore, only nuclear-localized SOD1 was found to support the maintenance of KP TDCLs. To summarize, SOD1 functions essentially in the nucleus through its superoxide dismutase activity to support KP tumor maintenance, and ablation of SOD1 leads to inhibition of KP tumor growth, suggesting that SOD1 may be a potential therapeutic target in the treatment of lung cancer.

It remains unclear what the exact molecular functions of SOD1 are in the nucleus of KP TDCLs, and why SOD1 deletion has an anticancer effect. In this study, SOD1 was successfully targeted to the nucleus by engineered NLS sequences. Furthermore, this nuclear-targeted SOD1 fully replaced the wild type SOD1 in supporting KP cell growth. This provides a feasible tool to study the nuclear function of SOD1. Proteins that specifically bind to nuclear SOD1 could be identified by immunoprecipitation with SOD1 in cells in which endogenous SOD1 has been replaced with SOD1-NLS, followed by mass spectrometry analysis. Chromatin Immunoprecipitation Sequencing (Chip-seq) could then be done in parallel to provide information on both the interactome of SOD1 and potential genomic binding region of SOD1.

The results of this study show that the dismutase activity of SOD1 is critical for its ability to support KP cell growth. Dismutation of superoxide generates O_2 and H_2O_2. H_2O_2-mediated oxidation of redox-sensitive cysteine thiol groups is a major redox signaling mechanism[302-304]. It is

reasonable to speculate that SOD1 may specifically modulate tumor supportive pathways through the oxidation of cysteine thiol groups in certain nuclear enzymes by locally-generated H_2O_2. Many proteomic approaches to identify and quantify cellular redox-sensitive cysteine S-modifications have been developed and these methods are widely applied in biomedical research[305-309]. Analysis of global cysteine proteomics have revealed that Nrf2 deficiency induces preferential cysteine oxidation in the mRNA translation machinery in pancreatic cancer. Importantly, Nrf2 ablation does not cause a widespread change in protein oxidation[117]. Similar proteomics assessments of global cysteine oxidation alteration in tumors with gain-of-function mutant Nrf2 identified an orphan nuclear receptor as a potential target in Nrf2-mutant lung cancers[310]. To identify the specific proteins and pathways that may be regulated by SOD1 in the nucleus of KP cells, a proteomic-based analysis may be employed to compare cysteine thiol group oxidation in *Sod1*-knockout KP TDCLs, with or without the expression of nuclear-localized SOD1-NLS. Such an approach is likely to provide important clues to the molecular function of nuclear SOD1 in KP TDCLs.

REFERENCES

1 Bray, F. *et al.* Global cancer statistics 2018: GLOBOCAN estimates of incidence and mortality worldwide for 36 cancers in 185 countries. *CA Cancer J. Clin.* **0**, doi:10.3322/caac.21492.

2 Alberg, A. J., Brock, M. V., Ford, J. G., Samet, J. M. & Spivack, S. D. Epidemiology of Lung Cancer: Diagnosis and Management of Lung Cancer, 3rd ed: American College of Chest Physicians Evidence-Based Clinical Practice Guidelines. *Chest* **143**, e1S-e29S, doi:10.1378/chest.12-2345 (2013).

3 Gridelli, C. *et al.* Non-small-cell lung cancer. *Nature Reviews Disease Primers* **1**, 15009, doi:10.1038/nrdp.2015.9 (2015).

4 Sun, S., Schiller, J. H. & Gazdar, A. F. Lung cancer in never smokers — a different disease. *Nature Reviews Cancer* **7**, 778, doi:10.1038/nrc2190 (2007).

5 Santos, E. *et al.* Malignant activation of a K-ras oncogene in lung carcinoma but not in normal tissue of the same patient. *Science* **223**, 661-664, doi:10.1126/science.6695174 (1984).

6 Davies, H. *et al.* Mutations of the BRAF gene in human cancer. *Nature* **417**, 949, doi:10.1038/nature00766 (2002).

7 Stephens, P. *et al.* Lung cancer: intragenic ERBB2 kinase mutations in tumours. *Nature* **431**, 525, doi:10.1038/431525b (2004).

8 Lynch, T. J. *et al.* Activating mutations in the epidermal growth factor receptor underlying responsiveness of non–small-cell lung cancer to gefitinib. *N. Engl. J. Med.* **350**, 2129-2139, doi:10.1056/NEJMoa040938 (2004).

9 Paez, J. G. *et al.* EGFR mutations in lung cancer: correlation with clinical response to gefitinib therapy. *Science* **304**, 1497-1500, doi:10.1126/science.1099314 (2004).

10 Engelman, J. A. *et al.* MET amplification leads to gefitinib resistance in lung cancer by activating ERBB3 signaling. *Science* **316**, 1039-1043, doi:10.1126/science.1141478 (2007).

11 Weiss, J. *et al.* Frequent and focal FGFR1 amplification associates with therapeutically tractable FGFR1 dependency in squamous cell lung cancer. *Sci. Transl. Med.* **2**, 62ra93-62ra93, doi:10.1126/scitranslmed.3001451 (2010).

12 Vaishnavi, A. *et al.* Oncogenic and drug-sensitive NTRK1 rearrangements in lung cancer. *Nat. Med.* **19**, 1469, doi:10.1038/nm.3352 (2013).

13 McDermott, U. *et al.* Ligand-dependent platelet-derived growth factor receptor (PDGFR)-α activation sensitizes rare lung cancer and sarcoma cells to PDGFR kinase inhibitors. *Cancer Res.* **69**, 3937-3946, doi:10.1158/0008-5472.CAN-08-4327 (2009).

14 Fernandez-Cuesta, L. *et al.* CD74–NRG1 fusions in lung adenocarcinoma. *Cancer Discov.* **4**, 415-422, doi:10.1158/2159-8290.CD-13-0633 (2014).

15 Kohno, T. *et al.* KIF5B-RET fusions in lung adenocarcinoma. *Nat. Med.* **18**, 375, doi:10.1038/nm.2644 (2012).

16 Soda, M. *et al.* Identification of the transforming EML4–ALK fusion gene in non-small-cell lung cancer. *Nature* **448**, 561, doi:10.1038/nature05945 (2007).

17 Chen, Z., Fillmore, C. M., Hammerman, P. S., Kim, C. F. & Wong, K.-K. Non-small-cell lung cancers: a heterogeneous set of diseases. *Nat. Rev. Cancer* **14**, 535-546, doi:10.1038/nrc3775 (2014).

18 The Cancer Genome Atlas Research, N. *et al.* Comprehensive molecular profiling of lung adenocarcinoma. *Nature* **511**, 543, doi:10.1038/nature13385 (2014).

19 Lee, T. *et al.* Non-small Cell Lung Cancer with Concomitant EGFR, KRAS, and ALK Mutation: Clinicopathologic Features of 12 Cases. *Journal of pathology and translational medicine* **50**, 197-203, doi:10.4132/jptm.2016.03.09 (2016).

20 Liao, B. C., Lin, C. C. & Yang, J. C. Second and third-generation epidermal growth factor receptor tyrosine kinase inhibitors in advanced nonsmall cell lung cancer. *Curr. Opin. Oncol.* **27**, 94-101, doi:10.1097/cco.0000000000000164 (2015).

21 Hallberg, B. & Palmer, R. H. Mechanistic insight into ALK receptor tyrosine kinase in human cancer biology. *Nat. Rev. Cancer* **13**, 685-700, doi:10.1038/nrc3580 (2013).

22 Postow, M. A., Callahan, M. K. & Wolchok, J. D. Immune Checkpoint Blockade in Cancer Therapy. *J. Clin. Oncol.* **33**, 1974-1982, doi:10.1200/JCO.2014.59.4358 (2015).

23 Kosaka, T. *et al.* Mutations of the epidermal growth factor receptor gene in lung cancer: biological and clinical implications. *Cancer Res.* **64**, 8919-8923, doi:10.1158/0008-5472.can-04-2818 (2004).

24 Tam, I. Y. *et al.* Distinct epidermal growth factor receptor and KRAS mutation patterns in non-small cell lung cancer patients with different tobacco exposure and clinicopathologic features. *Clin. Cancer Res.* **12**, 1647-1653, doi:10.1158/1078-0432.ccr-05-1981 (2006).

25 Comprehensive genomic characterization of squamous cell lung cancers. *Nature* **489**, 519-525, doi:10.1038/nature11404 (2012).

26 George, J. *et al.* Comprehensive genomic profiles of small cell lung cancer. *Nature* **524**, 47-53, doi:10.1038/nature14664 (2015).

27 Cox, A. D., Fesik, S. W., Kimmelman, A. C., Luo, J. & Der, C. J. Drugging the undruggable RAS: Mission possible? *Nat. Rev. Drug Discov.* **13**, 828-851, doi:10.1038/nrd4389 (2014).

28 Vigil, D., Cherfils, J., Rossman, K. L. & Der, C. J. Ras superfamily GEFs and GAPs: validated and tractable targets for cancer therapy? *Nat. Rev. Cancer* **10**, 842-857, doi:10.1038/nrc2960 (2010).

29 Baines, A. T., Xu, D. & Der, C. J. Inhibition of Ras for cancer treatment: the search continues. *Future Med. Chem.* **3**, 1787-1808, doi:10.4155/fmc.11.121 (2011).

30 Blasco, R. B. *et al.* c-Raf, but not B-Raf, is essential for development of K-Ras oncogene-driven non-small cell lung carcinoma. *Cancer Cell* **19**, 652-663, doi:10.1016/j.ccr.2011.04.002 (2011).

31 Collisson, E. A. *et al.* A central role for RAF-->MEK-->ERK signaling in the genesis of pancreatic ductal adenocarcinoma. *Cancer Discov.* **2**, 685-693, doi:10.1158/2159-8290.cd-11-0347 (2012).

32 Gupta, S. *et al.* Binding of ras to phosphoinositide 3-kinase p110alpha is required for ras-driven tumorigenesis in mice. *Cell* **129**, 957-968, doi:10.1016/j.cell.2007.03.051 (2007).

33 Lim, K. H. & Counter, C. M. Reduction in the requirement of oncogenic Ras signaling to activation of PI3K/AKT pathway during tumor maintenance. *Cancer Cell* **8**, 381-392, doi:10.1016/j.ccr.2005.10.014 (2005).

34 Papke, B. & Der, C. J. Drugging RAS: Know the enemy. *Science* **355**, 1158-1163, doi:10.1126/science.aam7622 (2017).

35 Janes, M. R. *et al.* Targeting KRAS Mutant Cancers with a Covalent G12C-Specific Inhibitor. *Cell* **172**, 578-589.e517, doi:10.1016/j.cell.2018.01.006 (2018).

36 Ostrem, J. M., Peters, U., Sos, M. L., Wells, J. A. & Shokat, K. M. K-Ras(G12C) inhibitors allosterically control GTP affinity and effector interactions. *Nature* **503**, 548-551, doi:10.1038/nature12796 (2013).

37 Karnoub, A. E. & Weinberg, R. A. Ras oncogenes: split personalities. *Nat. Rev. Mol. Cell Biol.* **9**, 517-531, doi:10.1038/nrm2438 (2008).

38 Schmick, M. *et al.* KRas localizes to the plasma membrane by spatial cycles of solubilization, trapping and vesicular transport. *Cell* **157**, 459-471, doi:10.1016/j.cell.2014.02.051 (2014).

39 Papke, B. *et al.* Identification of pyrazolopyridazinones as PDEdelta inhibitors. *Nature communications* **7**, 11360, doi:10.1038/ncomms11360 (2016).

40 Zimmermann, G. *et al.* Small molecule inhibition of the KRAS-PDEdelta interaction impairs oncogenic KRAS signalling. *Nature* **497**, 638-642, doi:10.1038/nature12205 (2013).

41 Rizvi, N. A. *et al.* Cancer immunology. Mutational landscape determines sensitivity to PD-1 blockade in non-small cell lung cancer. *Science* **348**, 124-128, doi:10.1126/science.aaa1348 (2015).

42 Champiat, S., Ferte, C., Lebel-Binay, S., Eggermont, A. & Soria, J. C. Exomics and immunogenics: Bridging mutational load and immune checkpoints efficacy. *Oncoimmunology* **3**, e27817, doi:10.4161/onci.27817 (2014).

43 Borghaei, H. *et al.* Nivolumab versus Docetaxel in Advanced Nonsquamous Non-Small-Cell Lung Cancer. *N. Engl. J. Med.* **373**, 1627-1639, doi:10.1056/NEJMoa1507643 (2015).

44 Dong, Z. Y. *et al.* Potential Predictive Value of TP53 and KRAS Mutation Status for Response to PD-1 Blockade Immunotherapy in Lung Adenocarcinoma. *Clin. Cancer Res.* **23**, 3012-3024, doi:10.1158/1078-0432.ccr-16-2554 (2017).

45 Lyons, T. W., Reinhard, C. T. & Planavsky, N. J. The rise of oxygen in Earth's early ocean and atmosphere. *Nature* **506**, 307, doi:10.1038/nature13068 (2014).

46 Sheng, Y. *et al.* Superoxide dismutases and superoxide reductases. *Chem. Rev.* **114**, 3854-3918, doi:10.1021/cr4005296 (2014).

47 Bielski, B. H., Cabelli, D. E., Arudi, R. L. & Ross, A. B. Reactivity of HO2/O− 2 radicals in aqueous solution. *J. Phys. Chem. Ref. Data* **14**, 1041-1100, doi:10.1063/1.555739 (1985).

48 Lynch, R. E. & Fridovich, I. Permeation of the erythrocyte stroma by superoxide radical. *J. Biol. Chem.* **253**, 4697-4699 (1978).

49 Bartesaghi, S. & Radi, R. Fundamentals on the biochemistry of peroxynitrite and protein tyrosine nitration. *Redox Biology* **14**, 618-625, doi:10.1016/j.redox.2017.09.009 (2018).

50 Szabo, C., Ischiropoulos, H. & Radi, R. Peroxynitrite: biochemistry, pathophysiology and development of therapeutics. *Nature Reviews Drug Discovery* **6**, 662-680, doi:10.1038/nrd2222 (2007).

51 Handy, D. E. & Loscalzo, J. Redox regulation of mitochondrial function. *Antioxid. Redox Signal.* **16**, 1323-1367, doi:10.1089/ars.2011.4123 (2012).

52 Finkel, T. Signal transduction by mitochondrial oxidants. *J. Biol. Chem.* **287**, 4434-4440, doi:10.1074/jbc.R111.271999 (2012).

53 Turrens, J. F. Mitochondrial formation of reactive oxygen species. *The Journal of Physiology* **552**, 335-344, doi:10.1113/jphysiol.2003.049478 (2003).

54 Nishino, T., Okamoto, K., Eger, B. T., Pai, E. F. & Nishino, T. Mammalian xanthine oxidoreductase - mechanism of transition from xanthine dehydrogenase to xanthine oxidase. *FEBS J.* **275**, 3278-3289, doi:10.1111/j.1742-4658.2008.06489.x (2008).

55 Schrader, M. & Fahimi, H. D. Peroxisomes and oxidative stress. *Biochim. Biophys. Acta* **1763**, 1755-1766, doi:10.1016/j.bbamcr.2006.09.006 (2006).

56 Cao, S. S. & Kaufman, R. J. Endoplasmic reticulum stress and oxidative stress in cell fate decision and human disease. *Antioxid. Redox Signal.* **21**, 396-413, doi:10.1089/ars.2014.5851 (2014).

57 Zangar, R. C., Davydov, D. R. & Verma, S. Mechanisms that regulate production of reactive oxygen species by cytochrome P450. *Toxicol. Appl. Pharmacol.* **199**, 316-331, doi:10.1016/j.taap.2004.01.018 (2004).

58 Schröder, K., Weissmann, N. & Brandes, R. P. Organizers and activators: Cytosolic Nox proteins impacting on vascular function. *Free Radical Biol. Med.* **109**, 22-32, doi:10.1016/j.freeradbiomed.2017.03.017 (2017).

59 Case, A. J. On the Origin of Superoxide Dismutase: An Evolutionary Perspective of Superoxide-Mediated Redox Signaling. *Antioxidants* **6**, 82, doi:10.1021/cr4005296 (2017).

60 D'Autreaux, B. & Toledano, M. B. ROS as signalling molecules: mechanisms that generate specificity in ROS homeostasis. *Nat. Rev. Mol. Cell Biol.* **8**, 813-824, doi:10.1038/nrm2256 (2007).

61 Schieber, M. & Chandel, N. S. ROS function in redox signaling and oxidative stress. *Curr. Biol.* **24**, R453-462, doi:10.1016/j.cub.2014.03.034 (2014).

62 Guo, Z., Kozlov, S., Lavin, M. F., Person, M. D. & Paull, T. T. ATM Activation by Oxidative Stress. *Science* **330**, 517-521, doi:10.1126/science.1192912 (2010).

63 Lee, S.-R. *et al.* Reversible Inactivation of the Tumor Suppressor PTEN by H2O2. *J. Biol. Chem.* **277**, 20336-20342, doi:10.1074/jbc.M111899200 (2002).

64 Anastasiou, D. *et al.* Inhibition of pyruvate kinase M2 by reactive oxygen species contributes to cellular antioxidant responses. *Science* **334**, 1278-1283, doi:10.1126/science.1211485 (2011).

65 Finkel, T. Signal transduction by reactive oxygen species. *The Journal of cell biology* **194**, 7-15, doi:10.1083/jcb.201102095 (2011).

66 Janssen-Heininger, Y. M. *et al.* Redox-based regulation of signal transduction: principles, pitfalls, and promises. *Free Radic. Biol. Med.* **45**, 1-17, doi:10.1016/j.freeradbiomed.2008.03.011 (2008).

67 Hidalgo, E. & Demple, B. An iron-sulfur center essential for transcriptional activation by the redox-sensing SoxR protein. *EMBO J.* **13**, 138-146, doi:10.1002/j.1460-2075.1994.tb06243.x (1994).

68 Choi, H.-J. *et al.* Structural Basis of the Redox Switch in the OxyR Transcription Factor. *Cell* **105**, 103-113, doi:10.1016/S0092-8674(01)00300-2 (2001).

69 Lee, J. W. & Helmann, J. D. The PerR transcription factor senses H2O2 by metal-catalysed histidine oxidation. *Nature* **440**, 363-367, doi:10.1038/nature04537 (2006).

70 Semenza, G. L. Targeting HIF-1 for cancer therapy. *Nat. Rev. Cancer* **3**, 721-732, doi:10.1038/nrc1187 (2003).

71 LaGory, E. L. & Giaccia, A. J. The ever-expanding role of HIF in tumour and stromal biology. *Nat. Cell Biol.* **18**, 356, doi:10.1038/ncb3330 (2016).

72 Ivan, M. *et al.* HIFalpha targeted for VHL-mediated destruction by proline hydroxylation: implications for O2 sensing. *Science* **292**, 464-468, doi:10.1126/science.1059817 (2001).

73 Jaakkola, P. *et al.* Targeting of HIF-alpha to the von Hippel-Lindau ubiquitylation complex by O2-regulated prolyl hydroxylation. *Science* **292**, 468-472, doi:10.1126/science.1059796 (2001).

74 Yu, F., White, S. B., Zhao, Q. & Lee, F. S. HIF-1alpha binding to VHL is regulated by stimulus-sensitive proline hydroxylation. *Proc. Natl. Acad. Sci. U. S. A.* **98**, 9630-9635, doi:10.1073/pnas.181341498 (2001).

75 Coleman, M. L. & Ratcliffe, P. J. Signalling Cross Talk of the HIF System: Involvement of the FIH Protein. *Curr. Pharm. Des.* **15**, 3904-3907, doi:10.2174/138161209789649448 (2009).

76 Malhotra, D. *et al.* Global mapping of binding sites for Nrf2 identifies novel targets in cell survival response through ChIP-Seq profiling and network analysis. *Nucleic Acids Res.* **38**, 5718-5734, doi:10.1093/nar/gkq212 (2010).

77 Murakami, S. & Motohashi, H. Roles of Nrf2 in cell proliferation and differentiation. *Free Radic. Biol. Med.* **88**, 168-178, doi:10.1016/j.freeradbiomed.2015.06.030 (2015).

78 Zhang, D. D., Lo, S. C., Cross, J. V., Templeton, D. J. & Hannink, M. Keap1 is a redox-regulated substrate adaptor protein for a Cul3-dependent ubiquitin ligase complex. *Mol. Cell. Biol.* **24**, 10941-10953, doi:10.1128/mcb.24.24.10941-10953.2004 (2004).

79 Furukawa, M. & Xiong, Y. BTB protein Keap1 targets antioxidant transcription factor Nrf2 for ubiquitination by the Cullin 3-Roc1 ligase. *Mol. Cell. Biol.* **25**, 162-171, doi:10.1128/mcb.25.1.162-171.2005 (2005).

80 Dinkova-Kostova, A. T. *et al.* Direct evidence that sulfhydryl groups of Keap1 are the sensors regulating induction of phase 2 enzymes that protect against carcinogens and oxidants. *Proc. Natl. Acad. Sci. U. S. A.* **99**, 11908-11913, doi:10.1073/pnas.172398899 (2002).

81 Baird, L., Llères, D., Swift, S. & Dinkova-Kostova, A. T. Regulatory flexibility in the Nrf2-mediated stress response is conferred by conformational cycling of the Keap1-Nrf2 protein complex. *Proc. Natl. Acad. Sci. U. S. A.* **110**, 15259-15264, doi:10.1073/pnas.1305687110 (2013).

82 Paull, T. T. Mechanisms of ATM Activation. *Annu. Rev. Biochem* **84**, 711-738, doi:10.1146/annurev-biochem-060614-034335 (2015).

83 Barzilai, A., Rotman, G. & Shiloh, Y. ATM deficiency and oxidative stress: a new dimension of defective response to DNA damage. *DNA Repair (Amst)* **1**, 3-25, doi:10.1016/S1568-7864(01)00007-6 (2002).

84 Kamsler, A. *et al.* Increased oxidative stress in ataxia telangiectasia evidenced by alterations in redox state of brains from Atm-deficient mice. *Cancer Res.* **61**, 1849-1854 (2001).

85 Quick, K. L. & Dugan, L. L. Superoxide stress identifies neurons at risk in a model of ataxia-telangiectasia. *Ann. Neurol.* **49**, 627-635, doi:10.1002/ana.1005 (2001).

86 Guo, Z., Deshpande, R. & Paull, T. T. ATM activation in the presence of oxidative stress. *Cell Cycle* **9**, 4805-4811, doi:10.4161/cc.9.24.14323 (2010).

87 Bae, Y. S. *et al.* Epidermal growth factor (EGF)-induced generation of hydrogen peroxide Role in EGF receptor-mediated tyrosine phosphorylation. *J. Biol. Chem.* **272**, 217-221, doi:10.1074/jbc.272.1.217 (1997).

88 Giannoni, E., Buricchi, F., Raugei, G., Ramponi, G. & Chiarugi, P. Intracellular Reactive Oxygen Species Activate Src Tyrosine Kinase during Cell Adhesion and Anchorage-Dependent Cell Growth. *Mol. Cell. Biol.* **25**, 6391-6403, doi:10.1128/mcb.25.15.6391-6403.2005 (2005).

89 Woo, H. A. *et al.* Inactivation of Peroxiredoxin I by Phosphorylation Allows Localized H2O2 Accumulation for Cell Signaling. *Cell* **140**, 517-528, doi:10.1016/j.cell.2010.01.009 (2010).

90 Sundaresan, M., Yu, Z.-X., Ferrans, V. J., Irani, K. & Finkel, T. Requirement for generation of H2O2 for platelet-derived growth factor signal transduction. *Science* **270**, 296-299, doi:10.1126/science.270.5234.296 (1995).

91 Lee, S. R., Kwon, K. S., Kim, S. R. & Rhee, S. G. Reversible inactivation of protein-tyrosine phosphatase 1B in A431 cells stimulated with epidermal growth factor. *J. Biol. Chem.* **273**, 15366-15372, doi:10.1074/jbc.273.25.15366 (1998).

92 Denu, J. M. & Tanner, K. G. Specific and reversible inactivation of protein tyrosine phosphatases by hydrogen peroxide: evidence for a sulfenic acid intermediate and implications for redox regulation. *Biochemistry* **37**, 5633-5642, doi:10.1021/bi973035t (1998).

93 Meng, T. C., Fukada, T. & Tonks, N. K. Reversible oxidation and inactivation of protein tyrosine phosphatases in vivo. *Mol. Cell* **9**, 387-399, doi:10.1016/S1097-2765(02)00445-8 (2002).

94 Baumer, A. T. *et al.* Phosphatidylinositol 3-kinase-dependent membrane recruitment of Rac-1 and p47phox is critical for alpha-platelet-derived growth factor receptor-induced production of reactive oxygen species. *J. Biol. Chem.* **283**, 7864-7876, doi:10.1074/jbc.M704997200 (2008).

95 Adachi, M. *et al.* Mammalian SH2-containing protein tyrosine phosphatases. *Cell* **85**, 15, doi:10.1016/S0092-8674(00)81077-6 (1996).

96 Worby, C. A. & Dixon, J. E. PTEN. *Annu. Rev. Biochem* **83**, 641-669, doi:10.1146/annurev-biochem-082411-113907 (2014).

97 Kwon, J. *et al.* Reversible oxidation and inactivation of the tumor suppressor PTEN in cells stimulated with peptide growth factors. *Proc. Natl. Acad. Sci. U. S. A.* **101**, 16419-16424, doi:10.1073/pnas.0407396101 (2004).

98 Juarez, J. C. *et al.* Superoxide dismutase 1 (SOD1) is essential for H(2)O(2)-mediated oxidation and inactivation of phosphatases in growth factor signaling. *Proc. Natl. Acad. Sci. U. S. A.* **105**, 7147-7152, doi:10.1073/pnas.0709451105 (2008).

99 Cross, C. E. *et al.* Oxygen radicals and human disease. Davis conference. *Ann. Intern. Med.* **107**, 526-545, doi:10.7326/0003-4819-107-4-526 (1987).

100 Shibutani, S., Takeshita, M. & Grollman, A. P. Insertion of specific bases during DNA synthesis past the oxidation-damaged base 8-oxodG. *Nature* **349**, 431, doi:10.1038/349431a0 (1991).

101 Ogrunc, M. *et al.* Oncogene-induced reactive oxygen species fuel hyperproliferation and DNA damage response activation. *Cell Death Differ.* **21**, 998, doi:10.1038/cdd.2014.16 (2014).

102 Sablina, A. A. *et al.* The antioxidant function of the p53 tumor suppressor. *Nat. Med.* **11**, 1306, doi:10.1038/nm1320 (2005).

103 Li, T. *et al.* Tumor Suppression in the Absence of p53-Mediated Cell-Cycle Arrest, Apoptosis, and Senescence. *Cell* **149**, 1269-1283, doi:10.1016/j.cell.2012.04.026 (2012).

104 Cao, L. *et al.* Absence of full-length Brca1 sensitizes mice to oxidative stress and carcinogen-induced tumorigenesis in the esophagus and forestomach. *Carcinogenesis* **28**, 1401-1407, doi:10.1093/carcin/bgm060 (2007).

105 Iommarini, L., Ghelli, A., Gasparre, G. & Porcelli, A. M. Mitochondrial metabolism and energy sensing in tumor progression. *Biochim. Biophys. Acta* **1858**, 582-590, doi:10.1016/j.bbabio.2017.02.006 (2017).

106 Wallace, D. C. Mitochondria and cancer. *Nat. Rev. Cancer* **12**, 685-698, doi:10.1038/nrc3365 (2012).

107 Funes, J. M. *et al.* Transformation of human mesenchymal stem cells increases their dependency on oxidative phosphorylation for energy production. *Proc. Natl. Acad. Sci. U. S. A.* **104**, 6223-6228, doi:10.1073/pnas.0700690104 (2007).

108 Sabharwal, S. S. & Schumacker, P. T. Mitochondrial ROS in cancer: initiators, amplifiers or an Achilles' heel? *Nat. Rev. Cancer* **14**, 709-721, doi:10.1038/nrc3803 (2014).

109 Safford, S. E., Oberley, T. D., Urano, M. & Clair, D. K. Suppression of Fibrosarcoma Metastasis by Elevated Expression of Manganese Superoxide Dismutase1. *Cancer Res.* **54**, 4261-4265 (1994).

110 K., S. C. D., X., S. W., D., O. T., E., M. K. & H., S. C. W. Suppression of radiation-induced neoplastic transformation by overexpression of mitochondrial superoxide dismutase. *Mol. Carcinog.* **6**, 238-242, doi:10.1002/mc.2940060404 (1992).

111 Weinberg, F. *et al.* Mitochondrial metabolism and ROS generation are essential for Kras-mediated tumorigenicity. *Proc. Natl. Acad. Sci. U. S. A.* **107**, 8788-8793, doi:10.1073/pnas.1003428107 (2010).

112 Trachootham, D. *et al.* Selective killing of oncogenically transformed cells through a ROS-mediated mechanism by β-phenylethyl isothiocyanate. *Cancer Cell* **10**, 241-252, doi:10.1016/j.ccr.2006.08.009 (2006).

113 Gorrini, C., Harris, I. S. & Mak, T. W. Modulation of oxidative stress as an anticancer strategy. *Nat. Rev. Drug Discov.* **12**, 931-947, doi:10.1038/nrd4002 (2013).

114 Shaw, A. T. *et al.* Selective killing of K-ras mutant cancer cells by small molecule inducers of oxidative stress. *Proc. Natl. Acad. Sci. U. S. A.* **108**, 8773-8778, doi:10.1073/pnas.1105941108 (2011).

115 Sayin, V. I. *et al.* Antioxidants Accelerate Lung Cancer Progression in Mice. *Sci. Transl. Med.* **6**, 221ra215, doi:10.1126/scitranslmed.3007653 (2014).

116 Harris, Isaac S. *et al.* Glutathione and Thioredoxin Antioxidant Pathways Synergize to Drive Cancer Initiation and Progression. *Cancer Cell* **27**, 211-222, doi:10.1016/j.ccell.2014.11.019 (2015).

117 Chio, I. I. C. *et al.* NRF2 Promotes Tumor Maintenance by Modulating mRNA Translation in Pancreatic Cancer. *Cell* **166**, 963-976, doi:10.1016/j.cell.2016.06.056 (2016).

118 DeNicola, G. M. *et al.* Oncogene-induced Nrf2 transcription promotes ROS detoxification and tumorigenesis. *Nature* **475**, 106-109, doi:10.1038/nature10189 (2011).

119 Cairns, R. A., Harris, I. S. & Mak, T. W. Regulation of cancer cell metabolism. *Nat. Rev. Cancer* **11**, 85-95, doi:10.1038/nrc2981 (2011).

120 Szatrowski, T. P. & Nathan, C. F. Production of large amounts of hydrogen peroxide by human tumor cells. *Cancer Res.* **51**, 794-798 (1991).

121 Schoenfeld, J. D. *et al.* O2(-) and H2O2-Mediated Disruption of Fe Metabolism Causes the Differential Susceptibility of NSCLC and GBM Cancer Cells to Pharmacological Ascorbate. *Cancer Cell* **31**, 487-500.e488, doi:10.1016/j.ccell.2017.02.018 (2017).

122 Diehn, M. *et al.* Association of reactive oxygen species levels and radioresistance in cancer stem cells. *Nature* **458**, 780-783, doi:10.1038/nature07733 (2009).

123 Talks, K. L. *et al.* The expression and distribution of the hypoxia-inducible factors HIF-1alpha and HIF-2alpha in normal human tissues, cancers, and tumor-associated macrophages. *Am. J. Pathol.* **157**, 411-421, doi:10.1016/S0002-9440(10)64554-3 (2000).

124 Zhong, H. *et al.* Overexpression of hypoxia-inducible factor 1alpha in common human cancers and their metastases. *Cancer Res.* **59**, 5830-5835 (1999).
125 Gao, P. *et al.* HIF-dependent antitumorigenic effect of antioxidants in vivo. *Cancer Cell* **12**, 230-238, doi:10.1016/j.ccr.2007.08.004 (2007).
126 Kaelin, W. G., Jr. The von Hippel-Lindau tumour suppressor protein: O2 sensing and cancer. *Nat. Rev. Cancer* **8**, 865-873, doi:10.1038/nrc2502 (2008).
127 Majmundar, A. J., Wong, W. J. & Simon, M. C. Hypoxia-Inducible Factors and the Response to Hypoxic Stress. *Mol. Cell* **40**, 294-309, doi:10.1016/j.molcel.2010.09.022 (2010).
128 Bertout, J. A., Patel, S. A. & Simon, M. C. The impact of O2 availability on human cancer. *Nature Reviews Cancer* **8**, 967, doi:10.1038/nrc2540 (2008).
129 Semenza, G. L. Evaluation of HIF-1 inhibitors as anticancer agents. *Drug Discovery Today* **12**, 853-859, doi:10.1016/j.drudis.2007.08.006 (2007).
130 Tarrado-Castellarnau, M., de Atauri, P. & Cascante, M. Oncogenic regulation of tumor metabolic reprogramming. *Oncotarget* **7**, 62726-62753, doi:10.18632/oncotarget.10911 (2016).
131 Gaglio, D. *et al.* Oncogenic K-Ras decouples glucose and glutamine metabolism to support cancer cell growth. *Mol. Syst. Biol.* **7**, 523, doi:10.1038/msb.2011.56 (2011).
132 Romero, R. *et al.* Keap1 loss promotes Kras-driven lung cancer and results in dependence on glutaminolysis. *Nat. Med.* **23**, 1362-1368, doi:10.1038/nm.4407 (2017).
133 Son, J. *et al.* Glutamine supports pancreatic cancer growth through a KRAS-regulated metabolic pathway. *Nature* **496**, 101-105, doi:10.1038/nature12040 (2013).
134 DeBerardinis, R. J. *et al.* Beyond aerobic glycolysis: transformed cells can engage in glutamine metabolism that exceeds the requirement for protein and nucleotide synthesis. *Proc. Natl. Acad. Sci. U. S. A.* **104**, 19345-19350, doi:10.1073/pnas.0709747104 (2007).
135 Sayin, V. I. *et al.* Activation of the NRF2 antioxidant program generates an imbalance in central carbon metabolism in cancer. *eLife* **6**, doi:10.7554/eLife.28083 (2017).
136 Christofk, H. R. *et al.* The M2 splice isoform of pyruvate kinase is important for cancer metabolism and tumour growth. *Nature* **452**, 230-233, doi:10.1038/nature06734 (2008).
137 Christofk, H. R., Vander Heiden, M. G., Wu, N., Asara, J. M. & Cantley, L. C. Pyruvate kinase M2 is a phosphotyrosine-binding protein. *Nature* **452**, 181-186, doi:10.1038/nature06667 (2008).
138 Vander Heiden, M. G. *et al.* Evidence for an alternative glycolytic pathway in rapidly proliferating cells. *Science* **329**, 1492-1499, doi:10.1126/science.1188015 (2010).
139 Mann, T. in *Proc. R. Soc. Lond. B.* 303-315 (The Royal Society).
140 McCord, J. M. & Fridovich, I. Superoxide dismutase an enzymic function for erythrocuprein (hemocuprein). *J. Biol. Chem.* **244**, 6049-6055 (1969).
141 McCord, J. M., Keele, B. B. & Fridovich, I. An enzyme-based theory of obligate anaerobiosis: the physiological function of superoxide dismutase. *Proc. Natl. Acad. Sci. U. S. A.* **68**, 1024-1027, doi:10.1073/pnas.68.5.1024 (1971).
142 Pope, C. R., De Feo, C. J. & Unger, V. M. Cellular distribution of copper to superoxide dismutase involves scaffolding by membranes. *Proc. Natl. Acad. Sci. U. S. A.* **110**, 20491-20496, doi:10.1073/pnas.1309820110 (2013).

143 Suzuki, Y., Ali, M., Fischer, M. & Riemer, J. Human copper chaperone for superoxide dismutase 1 mediates its own oxidation-dependent import into mitochondria. *Nature communications* **4**, 2430, doi:10.1038/ncomms3430 (2013).
144 Leitch, J. M. *et al.* Activation of Cu, Zn-superoxide dismutase in the absence of oxygen and the copper chaperone CCS. *J. Biol. Chem.* **284**, 21863-21871, doi:10.1074/jbc.M109.000489 (2009).
145 Subramaniam, J. R. *et al.* Mutant SOD1 causes motor neuron disease independent of copper chaperone–mediated copper loading. *Nat. Neurosci.* **5**, 301, doi:10.1038/nn823 (2002).
146 Carroll, M. C. *et al.* Mechanisms for activating Cu-and Zn-containing superoxide dismutase in the absence of the CCS Cu chaperone. *Proc. Natl. Acad. Sci. U. S. A.* **101**, 5964-5969, doi:10.1073/pnas.0308298101 (2004).
147 Reaume, A. G. *et al.* Motor neurons in Cu/Zn superoxide dismutase-deficient mice develop normally but exhibit enhanced cell death after axonal injury. *Nat. Genet.* **13**, 43-47, doi:10.1038/ng0596-43 (1996).
148 Wong, P. C. *et al.* An adverse property of a familial ALS-linked SOD1 mutation causes motor neuron disease characterized by vacuolar degeneration of mitochondria. *Neuron* **14**, 1105-1116, doi:10.1016/0896-6273(95)90259-7 (1995).
149 Howland, D. S. *et al.* Focal loss of the glutamate transporter EAAT2 in a transgenic rat model of SOD1 mutant-mediated amyotrophic lateral sclerosis (ALS). *Proc. Natl. Acad. Sci. U. S. A.* **99**, 1604-1609, doi:10.1073/pnas.032539299 (2002).
150 Gurney, M. E. *et al.* Motor neuron degeneration in mice that express a human Cu,Zn superoxide dismutase mutation. *Science* **264**, 1772-1775, doi:10.1126/science.8209258 (1994).
151 Bruijn, L. I. *et al.* ALS-linked SOD1 mutant G85R mediates damage to astrocytes and promotes rapidly progressive disease with SOD1-containing inclusions. *Neuron* **18**, 327-338, doi:10.1016/S0896-6273(00)80272-X (1997).
152 Benov, L. How superoxide radical damages the cell. *Protoplasma* **217**, 33-36 (2001).
153 Flint, D. H., Tuminello, J. & Emptage, M. The inactivation of Fe-S cluster containing hydro-lyases by superoxide. *J. Biol. Chem.* **268**, 22369-22376 (1993).
154 Liochev, S. I. & Fridovich, I. The role of O2.− in the production of HO.: in vitro and in vivo. *Free Radical Biol. Med.* **16**, 29-33, doi:10.1016/0891-5849(94)90239-9 (1994).
155 Gardner, P. R. & Fridovich, I. Superoxide sensitivity of the Escherichia coli aconitase. *J. Biol. Chem.* **266**, 19328-19333 (1991).
156 Liochev, S. I. & Fridovich, I. Fumarase C, the stable fumarase of Escherichia coli, is controlled by the soxRS regulon. *Proc. Natl. Acad. Sci. U. S. A.* **89**, 5892-5896, doi:10.1073/pnas.89.13.5892 (1992).
157 Benov, L. & Fridovich, I. Why Superoxide Imposes an Aromatic Amino Acid Auxotrophy onEscherichia coli : THE TRANSKETOLASE CONNECTION. *J. Biol. Chem.* **274**, 4202-4206, doi:10.1074/jbc.274.7.4202 (1999).
158 Benov, L. & Fridovich, I. Superoxide Imposes Leakage of Sulfite from Escherichia coli. *Arch. Biochem. Biophys.* **347**, 271-274, doi:10.1006/abbi.1997.0343 (1997).
159 Lebovitz, R. M. *et al.* Neurodegeneration, myocardial injury, and perinatal death in mitochondrial superoxide dismutase-deficient mice. *Proc. Natl. Acad. Sci. U. S. A.* **93**, 9782-9787, doi:10.1073/pnas.93.18.9782 (1996).

160 Huang, T.-T. *et al.* Superoxide-Mediated Cytotoxicity in Superoxide Dismutase-Deficient Fetal Fibroblasts. *Arch. Biochem. Biophys.* **344**, 424-432, doi:10.1006/abbi.1997.0237 (1997).
161 Reaume, A. G. *et al.* Motor neurons in Cu/Zn superoxide dismutase-deficient mice develop normally but exhibit enhanced cell death after axonal injury. *Nat. Genet.* **13**, 43, doi:10.1038/ng0596-43 (1996).
162 Elchuri, S. *et al.* CuZnSOD deficiency leads to persistent and widespread oxidative damage and hepatocarcinogenesis later in life. *Oncogene* **24**, 367-380, doi:10.1038/sj.onc.1208207 (2005).
163 Zhang, Y. *et al.* Dietary restriction attenuates the accelerated aging phenotype of Sod1(-/-) mice. *Free Radic. Biol. Med.* **60**, 300-306, doi:10.1016/j.freeradbiomed.2013.02.026 (2013).
164 McFadden, S. L., Ding, D., Reaume, A. G., Flood, D. G. & Salvi, R. J. Age-related cochlear hair cell loss is enhanced in mice lacking copper/zinc superoxide dismutase. *Neurobiol. Aging* **20**, 1-8, doi:10.1016/S0197-4580(99)00018-4 (1999).
165 Ivannikov, M. V. & Van Remmen, H. Sod1 gene ablation in adult mice leads to physiological changes at the neuromuscular junction similar to changes that occur in old wild-type mice. *Free Radic. Biol. Med.* **84**, 254-262, doi:10.1016/j.freeradbiomed.2015.03.021 (2015).
166 Muller, F. L. *et al.* Absence of CuZn superoxide dismutase leads to elevated oxidative stress and acceleration of age-dependent skeletal muscle atrophy. *Free Radic. Biol. Med.* **40**, 1993-2004, doi:10.1016/j.freeradbiomed.2006.01.036 (2006).
167 Shi, Y. *et al.* The Lack of CuZnSOD Leads to Impaired Neurotransmitter Release, Neuromuscular Junction Destabilization and Reduced Muscle Strength in Mice. *PLoS One* **9**, 1-11, doi:10.1371/journal.pone.0100834 (2014).
168 Olofsson, E. M., Marklund, S. L. & Behndig, A. Enhanced age-related cataract in copper-zinc superoxide dismutase null mice. *Clin Exp Ophthalmol* **40**, 813-820, doi:10.1111/j.1442-9071.2012.02794.x (2012).
169 Watanabe, K. *et al.* Superoxide dismutase 1 loss disturbs intracellular redox signaling, resulting in global age-related pathological changes. *BioMed research international* **2014**, 140165, doi:10.1155/2014/140165 (2014).
170 Busuttil, R. A. *et al.* Organ-Specific Increase in Mutation Accumulation and Apoptosis Rate in CuZn-Superoxide Dismutase–Deficient Mice. *Cancer Res.* **65**, 11271-11275, doi:10.1158/0008-5472.can-05-2980 (2005).
171 Matzuk, M. M., Dionne, L., Guo, Q., Kumar, T. R. & Lebovitz, R. M. Ovarian function in superoxide dismutase 1 and 2 knockout mice. *Endocrinology* **139**, 4008-4011, doi:10.1210/en.139.9.4008 (1998).
172 Kimura, N. *et al.* Intrinsic oxidative stress causes either 2-cell arrest or cell death depending on developmental stage of the embryos from SOD1-deficient mice. *Mol. Hum. Reprod.* **16**, 441-451, doi:10.1093/molehr/gaq007 (2010).
173 Homma, T. *et al.* SOD1 deficiency induces the systemic hyperoxidation of peroxiredoxin in the mouse. *Biochem. Biophys. Res. Commun.* **463**, 1040-1046, doi:10.1016/j.bbrc.2015.06.055 (2015).
174 Iuchi, Y. *et al. Elevated oxidative stress in erythrocytes due to a SOD1 deficiency causes anaemia and triggers autoantibody production*. Vol. 402 (2007).
175 Hadjur, S. *et al.* Defective hematopoiesis and hepatic steatosis in mice with combined deficiencies of the genes encoding Fancc and Cu/Zn superoxide dismutase. *Blood* **98**, 1003-1011, doi:10.1182/blood.V98.4.1003 (2001).

176 Dayal, S. *et al.* Deficiency of superoxide dismutase promotes cerebral vascular hypertrophy and vascular dysfunction in hyperhomocysteinemia. *PLoS One* **12**, e0175732, doi:10.1371/journal.pone.0175732 (2017).
177 Troy, C. M., Derossi, D., Prochiantz, A., Greene, L. A. & Shelanski, M. L. Downregulation of Cu/Zn superoxide dismutase leads to cell death via the nitric oxide-peroxynitrite pathway. *J. Neurosci.* **16**, 253-261, doi:10.1523/JNEUROSCI.16-01-00253.1996 (1996).
178 Didion, S. P. *et al.* Increased Superoxide and Vascular Dysfunction in CuZnSOD-Deficient Mice. *Circ. Res.* **91**, 938-944, doi:10.1161/01.res.0000043280.65241.04 (2002).
179 Didion, S. P., Kinzenbaw, D. A., Schrader, L. I. & Faraci, F. M. Heterozygous CuZn superoxide dismutase deficiency produces a vascular phenotype with aging. *Hypertension* **48**, 1072-1079, doi:10.1161/01.HYP.0000247302.20559.3a (2006).
180 Didion, S. P., Kinzenbaw, D. A. & Faraci, F. M. Critical role for CuZn-superoxide dismutase in preventing angiotensin II-induced endothelial dysfunction. *Hypertension* **46**, 1147-1153, doi:10.1161/01.hyp.0000187532.80697.15 (2005).
181 Baumbach, G. L., Didion, S. P. & Faraci, F. M. Hypertrophy of cerebral arterioles in mice deficient in expression of the gene for CuZn superoxide dismutase. *Stroke* **37**, 1850-1855, doi:10.1161/01.STR.0000227236.84546.5a (2006).
182 Sakellariou, G. K. *et al.* Neuron-specific expression of CuZnSOD prevents the loss of muscle mass and function that occurs in homozygous CuZnSOD-knockout mice. *FASEB J.* **28**, 1666-1681, doi:10.1096/fj.13-240390 (2014).
183 Sataranatarajan, K. *et al.* Neuron specific reduction in CuZnSOD is not sufficient to initiate a full sarcopenia phenotype. *Redox Biol* **5**, 140-148, doi:10.1016/j.redox.2015.04.005 (2015).
184 Sakellariou, G. K. *et al.* Comparison of Whole Body SOD1 Knockout with Muscle-Specific SOD1 Knockout Mice Reveals a Role for Nerve Redox Signaling in Regulation of Degenerative Pathways in Skeletal Muscle. *Antioxid. Redox Signal.* **28**, 275-295, doi:10.1089/ars.2017.7249 (2018).
185 Michelotti, G. A., Machado, M. V. & Diehl, A. M. NAFLD, NASH and liver cancer. *Nature reviews. Gastroenterology & hepatology* **10**, 656-665, doi:10.1038/nrgastro.2013.183 (2013).
186 Uchiyama, S., Shimizu, T. & Shirasawa, T. CuZn-SOD deficiency causes ApoB degradation and induces hepatic lipid accumulation by impaired lipoprotein secretion in mice. *J. Biol. Chem.* **281**, 31713-31719, doi:10.1074/jbc.M603422200 (2006).
187 Wang, L., Jiang, Z. & Lei, X. G. Knockout of SOD1 altered murine hepatic glycolysis, gluconeogenesis, and lipogenesis. *Free Radic. Biol. Med.* **53**, 1689-1696, doi:10.1016/j.freeradbiomed.2012.08.570 (2012).
188 Sakiyama, H. *et al.* Cu,Zn-SOD deficiency induces the accumulation of hepatic collagen. *Free Radic. Res.* **50**, 666-677, doi:10.3109/10715762.2016.1164856 (2016).
189 Meissner, F., Molawi, K. & Zychlinsky, A. Superoxide dismutase 1 regulates caspase-1 and endotoxic shock. *Nat. Immunol.* **9**, 866-872, doi:10.1038/ni.1633 (2008).
190 Bhattacharya, A. *et al.* Superoxide Dismutase 1 Protects Hepatocytes from Type I Interferon-Driven Oxidative Damage. *Immunity* **43**, 974-986, doi:10.1016/j.immuni.2015.10.013 (2015).

191 Holmstrom, K. M. & Finkel, T. Cellular mechanisms and physiological consequences of redox-dependent signalling. *Nat. Rev. Mol. Cell Biol.* **15**, 411-421, doi:10.1038/nrm3801 (2014).
192 Mumbengegwi, D. R., Li, Q., Li, C., Bear, C. E. & Engelhardt, J. F. Evidence for a superoxide permeability pathway in endosomal membranes. *Mol. Cell. Biol.* **28**, 3700-3712, doi:10.1128/MCB.02038-07 (2008).
193 Li, Q. *et al.* Nox2 and Rac1 regulate H2O2-dependent recruitment of TRAF6 to endosomal interleukin-1 receptor complexes. *Mol. Cell. Biol.* **26**, 140-154, doi:10.1128/mcb.26.1.140-154.2006 (2006).
194 Harraz, M. M. *et al.* SOD1 mutations disrupt redox-sensitive Rac regulation of NADPH oxidase in a familial ALS model. *J. Clin. Invest.* **118**, 659-670, doi:10.1172/jci34060 (2008).
195 Morikawa, K. *et al.* Pivotal role of Cu,Zn-superoxide dismutase in endothelium-dependent hyperpolarization. *J. Clin. Invest.* **112**, 1871-1879, doi:10.1172/jci19351 (2003).
196 Grzenkowicz-Wydra, J. *et al.* Gene transfer of CuZn superoxide dismutase enhances the synthesis of vascular endothelial growth factor. *Mol. Cell. Biochem.* **264**, 169-181, doi:10.1023/B:MCBI.0000044386.45054.70 (2004).
197 Somwar, R. *et al.* Superoxide dismutase 1 (SOD1) is a target for a small molecule identified in a screen for inhibitors of the growth of lung adenocarcinoma cell lines. *Proc. Natl. Acad. Sci. U. S. A.* **108**, 16375-16380, doi:10.1073/pnas.1113554108 (2011).
198 Papa, L., Hahn, M., Marsh, E. L., Evans, B. S. & Germain, D. SOD2 to SOD1 switch in breast cancer. *J. Biol. Chem.* **289**, 5412-5416, doi:10.1074/jbc.C113.526475 (2014).
199 Glasauer, A., Sena, L. A., Diebold, L. P., Mazar, A. P. & Chandel, N. S. Targeting SOD1 reduces experimental non-small-cell lung cancer. *J. Clin. Invest.* **124**, 117-128, doi:10.1172/jci71714 (2014).
200 Juarez, J. C. *et al.* Copper binding by tetrathiomolybdate attenuates angiogenesis and tumor cell proliferation through the inhibition of superoxide dismutase 1. *Clin. Cancer Res.* **12**, 4974-4982, doi:10.1158/1078-0432.ccr-06-0171 (2006).
201 Huang, P., Feng, L., Oldham, E. A., Keating, M. J. & Plunkett, W. Superoxide dismutase as a target for the selective killing of cancer cells. *Nature* **407**, 390-395, doi:10.1038/35030140 (2000).
202 Lee, K. *et al.* The copper chelator ATN-224 induces peroxynitrite-dependent cell death in hematological malignancies. *Free Radic. Biol. Med.* **60**, 157-167, doi:10.1016/j.freeradbiomed.2013.02.003 (2013).
203 Muscoli, C. *et al.* On the selectivity of superoxide dismutase mimetics and its importance in pharmacological studies. *Br. J. Pharmacol.* **140**, 445-460, doi:10.1038/sj.bjp.0705430 (2003).
204 Younus, H. Therapeutic potentials of superoxide dismutase. *International Journal of Health Sciences* **12**, 88-93 (2018).
205 K., H. A., Lu, M., K., S. C. D. & H., S. C. W. Redox-Modulated Phenomena and Radiation Therapy: The Central Role of Superoxide Dismutases. *Antioxidants & Redox Signaling* **20**, 1567-1589, doi:10.1089/ars.2012.5000 (2014).
206 Brewer, G. J. *et al.* Initial therapy of patients with Wilson's disease with tetrathiomolybdate. *Arch. Neurol.* **48**, 42-47, doi:10.1001/archneur.1991.00530130050019 (1991).

207 Yamaguchi, Y., Heiny, M. E. & Gitlin, J. D. Isolation and characterization of a human liver cDNA as a candidate gene for Wilson disease. *Biochem. Biophys. Res. Commun.* **197**, 271-277, doi:10.1006/bbrc.1993.2471 (1993).
208 Tanzi, R. E. *et al.* The Wilson disease gene is a copper transporting ATPase with homology to the Menkes disease gene. *Nat. Genet.* **5**, 344-350, doi:10.1038/ng1293-344 (1993).
209 Bull, P. C., Thomas, G. R., Rommens, J. M., Forbes, J. R. & Cox, D. W. The Wilson disease gene is a putative copper transporting P-type ATPase similar to the Menkes gene. *Nat. Genet.* **5**, 327-337, doi:10.1038/ng1293-327 (1993).
210 Ranucci, G., Polishchuck, R. & Iorio, R. Wilson's disease: Prospective developments towards new therapies. *World J. Gastroenterol.* **23**, 5451-5456, doi:10.3748/wjg.v23.i30.5451 (2017).
211 Mills, C. F., El-Gallad, T. T. & Bremner, I. Effects of molybdate, sulfide, and tetrathiomolybdate on copper metabolism in rats. *J. Inorg. Biochem.* **14**, 189-207, doi:10.1016/S0162-0134(00)80000-8 (1981).
212 Harris, E. D. A requirement for copper in angiogenesis. *Nutr. Rev.* **62**, 60-64, doi:10.1301/nr.2004.feb.60–64 (2004).
213 Ziche, M., Jones, J. & Gullino, P. M. Role of prostaglandin E1 and copper in angiogenesis. *J. Natl. Cancer Inst.* **69**, 475-482 (1982).
214 Pan, Q. *et al.* Copper deficiency induced by tetrathiomolybdate suppresses tumor growth and angiogenesis. *Cancer Res.* **62**, 4854-4859 (2002).
215 Brewer, G. J. Tetrathiomolybdate anticopper therapy for Wilson's disease inhibits angiogenesis, fibrosis and inflammation. *J. Cell. Mol. Med.* **7**, 11-20, doi:10.1111/j.1582-4934.2003.tb00198.x (2003).
216 Goodman, V. L., Brewer, G. J. & Merajver, S. D. Copper deficiency as an anti-cancer strategy. *Endocr. Relat. Cancer* **11**, 255-263, doi:10.1677/erc.0.0110255 (2004).
217 Brewer, G. J. Anticopper therapy against cancer and diseases of inflammation and fibrosis. *Drug Discov. Today* **10**, 1103-1109, doi:10.1016/s1359-6446(05)03541-5 (2005).
218 Lin, J. *et al.* A non-comparative randomized phase II study of 2 doses of ATN-224, a copper/zinc superoxide dismutase inhibitor, in patients with biochemically recurrent hormone-naive prostate cancer. *Urol. Oncol.* **31**, 581-588, doi:10.1016/j.urolonc.2011.04.009 (2013).
219 Lowndes, S. A. *et al.* Phase I study of copper-binding agent ATN-224 in patients with advanced solid tumors. *Clin. Cancer Res.* **14**, 7526-7534, doi:10.1158/1078-0432.ccr-08-0315 (2008).
220 Antonarakis, E. S. *et al.* Changes in PSA kinetics predict metastasis- free survival in men with PSA-recurrent prostate cancer treated with nonhormonal agents: combined analysis of 4 phase II trials. *Cancer* **118**, 1533-1542, doi:10.1002/cncr.26437 (2012).
221 Berenson, J. R. *et al.* Phase I Study of the [Cu, Zn] Superoxide Dismutase (SOD1) Inhibitor ATN-224 (Bis-Choline Tetrathiomolybdate) in Patients (pts) with Advanced Hematologic Malignancies. *Blood* **108**, 2593-2593 (2006).
222 Xu, M., Casio, M., Range, D. E., Sosa, J. A. & Counter, C. M. Copper Chelation as Targeted Therapy in a Mouse Model of Oncogenic BRAF-Driven Papillary Thyroid Cancer. *Clin. Cancer Res.*, doi:10.1158/1078-0432.ccr-17-3705 (2018).
223 Brady, D. C., Crowe, M. S., Greenberg, D. N. & Counter, C. M. Copper Chelation Inhibits BRAF(V600E)-Driven Melanomagenesis and Counters Resistance to BRAF(V600E) and MEK1/2 Inhibitors. *Cancer Res.* **77**, 6240-6252, doi:10.1158/0008-5472.can-16-1190 (2017).

224 Mukhopadhyay, T. & Roth, J. A. Superinduction of wild-type p53 protein after 2-methoxyestradiol treatment of Ad5p53-transduced cells induces tumor cell apoptosis. *Oncogene* **17**, 241, doi:10.1038/sj.onc.1201909 (1998).
225 Kachadourian, R. *et al.* 2-Methoxyestradiol Does Not Inhibit Superoxide Dismutase. *Arch. Biochem. Biophys.* **392**, 349-353, doi:10.1006/abbi.2001.2455 (2001).
226 The Cancer Genome Atlas Research, N. Comprehensive molecular profiling of lung adenocarcinoma. *Nature* **511**, 543-550, doi:10.1038/nature13385 (2014).
227 Ruzankina, Y. *et al.* Deletion of the developmentally essential gene ATR in adult mice leads to age-related phenotypes and stem cell loss. *Cell stem cell* **1**, 113-126, doi:10.1016/j.stem.2007.03.002 (2007).
228 Zhang, Y. *et al.* CuZnSOD gene deletion targeted to skeletal muscle leads to loss of contractile force but does not cause muscle atrophy in adult mice. *The FASEB Journal* **27**, 3536-3548, doi:10.1096/fj.13-228130 (2013).
229 DuPage, M., Dooley, A. L. & Jacks, T. Conditional mouse lung cancer models using adenoviral or lentiviral delivery of Cre recombinase. *Nat. Protoc.* **4**, 1064, doi:10.1038/nprot.2009.95 (2009).
230 Feil, R., Wagner, J., Metzger, D. & Chambon, P. Regulation of Cre Recombinase Activity by Mutated Estrogen Receptor Ligand-Binding Domains. *Biochem. Biophys. Res. Commun.* **237**, 752-757, doi:10.1006/bbrc.1997.7124 (1997).
231 Artelt, P. *et al.* The prokaryotic neomycin-resistance-encoding gene acts as a transcriptional silencer in eukaryotic cells. *Gene* **99**, 249-254 (1991).
232 Kinnula, V. L. & Crapo, J. D. Superoxide Dismutases in the Lung and Human Lung Diseases. *Am. J. Respir. Crit. Care Med.* **167**, 1600-1619, doi:10.1164/rccm.200212-1479SO (2003).
233 Polimeni, L. *et al.* Oxidative stress: New insights on the association of non-alcoholic fatty liver disease and atherosclerosis. *World Journal of Hepatology* **7**, 1325-1336, doi:10.4254/wjh.v7.i10.1325 (2015).
234 Adams, L. A., Angulo, P. & Lindor, K. D. Nonalcoholic fatty liver disease. *Can. Med. Assoc. J.* **172**, 899-905, doi:10.1503/cmaj.045232 (2005).
235 Sanyal, A. J. Mechanisms of Disease: pathogenesis of nonalcoholic fatty liver disease. *Nat. Clin. Pract. Gastroenterol. Hepatol.* **2**, 46-53, doi:10.1038/ncpgasthep0084 (2005).
236 Farrell, G. C. & Larter, C. Z. Nonalcoholic fatty liver disease: from steatosis to cirrhosis. *Hepatology* **43**, S99-s112, doi:10.1002/hep.20973 (2006).
237 Laurent, A. *et al.* Pivotal role of superoxide anion and beneficial effect of antioxidant molecules in murine steatohepatitis. *Hepatology* **39**, 1277-1285, doi:10.1002/hep.20177 (2004).
238 Ikegami, T. *et al.* Model mice for tissue-specific deletion of the manganese superoxide dismutase (MnSOD) gene. *Biochem. Biophys. Res. Commun.* **296**, 729-736, doi:10.1016/S0006-291X(02)00933-6 (2002).
239 Kessova, I. G., Ho, Y. S., Thung, S. & Cederbaum, A. I. Alcohol-induced liver injury in mice lacking Cu, Zn-superoxide dismutase. *Hepatology* **38**, 1136-1145, doi:10.1053/jhep.2003.50450 (2003).
240 Jiang, Z. G., Robson, S. C. & Yao, Z. Lipoprotein metabolism in nonalcoholic fatty liver disease. *Journal of Biomedical Research* **27**, 1-13, doi:10.7555/JBR.27.20120077 (2013).
241 Fisher, E. A. & Ginsberg, H. N. Complexity in the Secretory Pathway: The Assembly and Secretion of Apolipoprotein B-containing Lipoproteins. *J. Biol. Chem.* **277**, 17377-17380, doi:10.1074/jbc.R100068200 (2002).

242 Horton, J. D., Goldstein, J. L. & Brown, M. S. SREBPs: activators of the complete program of cholesterol and fatty acid synthesis in the liver. *J. Clin. Invest.* **109**, 1125-1131, doi:10.1172/jci15593 (2002).
243 Goldstein, J. L., Rawson, R. B. & Brown, M. S. Mutant mammalian cells as tools to delineate the sterol regulatory element-binding protein pathway for feedback regulation of lipid synthesis. *Arch. Biochem. Biophys.* **397**, 139-148, doi:10.1006/abbi.2001.2615 (2002).
244 Chang, L. Y., Kang, B. H., Slot, J. W., Vincent, R. & Crapo, J. D. Immunocytochemical localization of the sites of superoxide dismutase induction by hyperoxia in rat lungs. *Lab. Invest.* **73**, 29-39, doi:10.3109/10715769709097798 (1995).
245 Coursin, D. B., Cihla, H. P., Oberley, T. D. & Oberley, L. W. Immunolocalization of antioxidant enzymes and isozymes of glutathione S-transferase in normal rat lung. *American Journal of Physiology-Lung Cellular and Molecular Physiology* **263**, L679-L691, doi:10.1152/ajplung.1992.263.6.L679 (1992).
246 Xu, X. *et al.* Evidence for type II cells as cells of origin of K-Ras–induced distal lung adenocarcinoma. *Proc. Natl. Acad. Sci. U. S. A.* **109**, 4910-4915, doi:10.1073/pnas.1112499109 (2012).
247 Sutherland, K. D. *et al.* Multiple cells-of-origin of mutant K-Ras–induced mouse lung adenocarcinoma. *Proc. Natl. Acad. Sci. U. S. A.* **111**, 4952-4957, doi:10.1073/pnas.1319963111 (2014).
248 Borchelt, D. R. *et al.* Superoxide dismutase 1 with mutations linked to familial amyotrophic lateral sclerosis possesses significant activity. *Proc. Natl. Acad. Sci. U. S. A.* **91**, 8292-8296, doi:10.1073/pnas.91.17.8292 (1994).
249 Gongora, M. C. *et al.* Loss of extracellular superoxide dismutase leads to acute lung damage in the presence of ambient air: a potential mechanism underlying adult respiratory distress syndrome. *Am. J. Pathol.* **173**, 915-926, doi:10.2353/ajpath.2008.080119 (2008).
250 Van Remmen, H. *et al.* Life-long reduction in MnSOD activity results in increased DNA damage and higher incidence of cancer but does not accelerate aging. *Physiol. Genomics* **16**, 29-37, doi:10.1152/physiolgenomics.00122.2003 (2003).
251 Neumann, C. A. *et al.* Essential role for the peroxiredoxin Prdx1 in erythrocyte antioxidant defence and tumour suppression. *Nature* **424**, 561-565, doi:10.1038/nature01819 (2003).
252 Chu, F.-F. *et al.* Bacteria-induced intestinal cancer in mice with disrupted Gpx1 and Gpx2 genes. *Cancer Res.* **64**, 962-968, doi:10.1158/0008-5472.CAN-03-2272 (2004).
253 Goh, J. *et al.* Mitochondrial targeted catalase suppresses invasive breast cancer in mice. *BMC Cancer* **11**, 191, doi:10.1186/1471-2407-11-191 (2011).
254 Mustacich, D. *et al.* Increased skin carcinogenesis in a keratinocyte directed thioredoxin-1 transgenic mouse. *Carcinogenesis* **25**, 1983-1989, doi:10.1093/carcin/bgh195 (2004).
255 Ran, Q. *et al.* Reduction in glutathione peroxidase 4 increases life span through increased sensitivity to apoptosis. *The Journals of Gerontology Series A: Biological Sciences and Medical Sciences* **62**, 932-942, doi:10.1093/gerona/62.9.932 (2007).
256 Khor, T. O. *et al.* Nrf2-deficient mice have an increased susceptibility to dextran sulfate sodium-induced colitis. *Cancer Res.* **66**, 11580-11584, doi:10.1158/0008-5472.can-06-3562 (2006).

257 Khor, T. O. *et al.* Increased susceptibility of Nrf2 knockout mice to colitis-associated colorectal cancer. *Cancer Prev. Res. (Phila.)* **1**, 187-191, doi:10.1158/1940-6207.capr-08-0028 (2008).
258 Sporn, M. B. & Liby, K. T. NRF2 and cancer: the good, the bad and the importance of context. *Nature reviews. Cancer* **12**, 10.1038/nrc3278, doi:10.1038/nrc3278 (2012).
259 Vichai, V. & Kirtikara, K. Sulforhodamine B colorimetric assay for cytotoxicity screening. *Nat. Protoc.* **1**, 1112, doi:10.1038/nprot.2006.179 (2006).
260 Weydert, C. J. & Cullen, J. J. Measurement of superoxide dismutase, catalase and glutathione peroxidase in cultured cells and tissue. *Nat. Protocols* **5**, 51-66, doi:10.1038/nprot.2009.197 (2010).
261 Dobin, A. *et al.* STAR: ultrafast universal RNA-seq aligner. *Bioinformatics* **29**, 15-21, doi:10.1093/bioinformatics/bts635 (2013).
262 Breese, M. R. & Liu, Y. NGSUtils: a software suite for analyzing and manipulating next-generation sequencing datasets. *Bioinformatics* **29**, 494-496, doi:10.1093/bioinformatics/bts731 (2013).
263 Liao, Y., Smyth, G. K. & Shi, W. featureCounts: an efficient general purpose program for assigning sequence reads to genomic features. *Bioinformatics* **30**, 923-930, doi:10.1093/bioinformatics/btt656 (2013).
264 Ewels, P., Magnusson, M., Lundin, S. & Käller, M. MultiQC: summarize analysis results for multiple tools and samples in a single report. *Bioinformatics* **32**, 3047-3048, doi:10.1093/bioinformatics/btw354 (2016).
265 Robinson, M. D., McCarthy, D. J. & Smyth, G. K. edgeR: a Bioconductor package for differential expression analysis of digital gene expression data. *Bioinformatics* **26**, 139-140, doi:10.1093/bioinformatics/btp616 (2010).
266 Itoh, K. *et al.* Keap1 represses nuclear activation of antioxidant responsive elements by Nrf2 through binding to the amino-terminal Neh2 domain. *Genes Dev.* **13**, 76-86 (1999).
267 Li, L. *et al.* Nrf2/ARE pathway activation, HO-1 and NQO1 induction by polychlorinated biphenyl quinone is associated with reactive oxygen species and PI3K/AKT signaling. *Chem. Biol. Interact.* **209**, 56-67, doi:10.1016/j.cbi.2013.12.005 (2014).
268 Valentine, J. S., Doucette, P. A. & Zittin Potter, S. Copper-zinc superoxide dismutase and amyotrophic lateral sclerosis. *Annu. Rev. Biochem.* **74**, 563-593, doi:10.1146/annurev.biochem.72.121801.161647 (2005).
269 Ratovitski, T. *et al.* Variation in the biochemical/biophysical properties of mutant superoxide dismutase 1 enzymes and the rate of disease progression in familial amyotrophic lateral sclerosis kindreds. *Hum. Mol. Genet.* **8**, 1451-1460, doi:10.1093/hmg/8.8.1451 (1999).
270 Corson, L. B., Strain, J. J., Culotta, V. C. & Cleveland, D. W. Chaperone-facilitated copper binding is a property common to several classes of familial amyotrophic lateral sclerosis-linked superoxide dismutase mutants. *Proc. Natl. Acad. Sci. U. S. A.* **95**, 6361-6366, doi:10.1073/pnas.95.11.6361 (1998).
271 Crapo, J. D., Oury, T., Rabouille, C., Slot, J. W. & Chang, L. Y. Copper,zinc superoxide dismutase is primarily a cytosolic protein in human cells. *Proc. Natl. Acad. Sci. U. S. A.* **89**, 10405-10409, doi:10.1073/pnas.89.21.10405 (1992).
272 Tsang, C. K., Liu, Y., Thomas, J., Zhang, Y. & Zheng, X. F. S. Superoxide dismutase 1 acts as a nuclear transcription factor to regulate oxidative stress resistance. *Nature communications* **5**, doi:10.1038/ncomms4446 (2014).
273 Li, X. *et al.* Role for KAP1 Serine 824 Phosphorylation and Sumoylation/Desumoylation Switch in Regulating KAP1-mediated Transcriptional

Repression. *J. Biol. Chem.* **282**, 36177-36189, doi:10.1074/jbc.M706912200 (2007).
274 Tsunoda, S., Kibe, N., Kurahashi, T. & Fujii, J. Differential responses of SOD1-deficient mouse embryonic fibroblasts to oxygen concentrations. *Arch. Biochem. Biophys.* **537**, 5-11, doi:10.1016/j.abb.2013.06.008 (2013).
275 Rufini, A., Tucci, P., Celardo, I. & Melino, G. Senescence and aging: the critical roles of p53. *Oncogene* **32**, 5129-5143, doi:10.1038/onc.2012.640 (2013).
276 Chen, J. The Cell-Cycle Arrest and Apoptotic Functions of p53 in Tumor Initiation and Progression. *Cold Spring Harb. Perspect. Med.* **6**, a026104, doi:10.1101/cshperspect.a026104 (2016).
277 Bieging, K. T., Mello, S. S. & Attardi, L. D. Unravelling mechanisms of p53-mediated tumour suppression. *Nature Reviews Cancer* **14**, 359, doi:10.1038/nrc3711 (2014).
278 Muller, F. L., Liu, Y. & Van Remmen, H. Complex III releases superoxide to both sides of the inner mitochondrial membrane. *J. Biol. Chem.* **279**, 49064-49073, doi:10.1074/jbc.M407715200 (2004).
279 Goldsteins, G. *et al.* Deleterious role of superoxide dismutase in the mitochondrial intermembrane space. *J. Biol. Chem.* **283**, 8446-8452, doi:10.1074/jbc.M706111200 (2008).
280 Kawamata, H. & Manfredi, G. Import, maturation, and function of SOD1 and its copper chaperone CCS in the mitochondrial intermembrane space. *Antioxid. Redox Signal.* **13**, 1375-1384, doi:10.1089/ars.2010.3212 (2010).
281 Kawamata, H. & Manfredi, G. Different regulation of wild-type and mutant Cu,Zn superoxide dismutase localization in mammalian mitochondria. *Hum. Mol. Genet.* **17**, 3303-3317, doi:10.1093/hmg/ddn226 (2008).
282 Bihlmaier, K., Mesecke, N., Kloeppel, C. & Herrmann, J. M. The disulfide relay of the intermembrane space of mitochondria: an oxygen-sensing system? *Ann. N. Y. Acad. Sci.* **1147**, 293-302, doi:10.1196/annals.1427.005 (2008).
283 Hanahan, D. & Weinberg, Robert A. Hallmarks of Cancer: The Next Generation. *Cell* **144**, 646-674, doi:10.1016/j.cell.2011.02.013 (2011).
284 Ying, H. *et al.* Oncogenic Kras maintains pancreatic tumors through regulation of anabolic glucose metabolism. *Cell* **149**, 656-670, doi:10.1016/j.cell.2012.01.058 (2012).
285 Morgan, B., Sobotta, M. C. & Dick, T. P. Measuring E(GSH) and H2O2 with roGFP2-based redox probes. *Free Radic. Biol. Med.* **51**, 1943-1951, doi:10.1016/j.freeradbiomed.2011.08.035 (2011).
286 Chang, L. Y., Slot, J. W., Geuze, H. J. & Crapo, J. D. Molecular immunocytochemistry of the CuZn superoxide dismutase in rat hepatocytes. *The Journal of Cell Biology* **107**, 2169-2179, doi:10.1083/jcb.107.6.2169 (1988).
287 Ziv, Y. *et al.* Chromatin relaxation in response to DNA double-strand breaks is modulated by a novel ATM- and KAP-1 dependent pathway. *Nat. Cell Biol.* **8**, 870, doi:10.1038/ncb1446 (2006).
288 Mita, P. *et al.* URI Regulates KAP1 Phosphorylation and Transcriptional Repression via PP2A Phosphatase in Prostate Cancer Cells. *J. Biol. Chem.* **291**, 25516-25528, doi:10.1074/jbc.M116.741660 (2016).
289 Bürck, C. *et al.* KAP1 is a host restriction factor that promotes HAdV E1B-55K SUMO modification. *J. Virol.*, doi:10.1128/jvi.01836-15 (2015).
290 Li, X. *et al.* SUMOylation of the transcriptional co-repressor KAP1 is regulated by the serine and threonine phosphatase PP1. *Sci Signal* **3**, ra32, doi:10.1126/scisignal.2000781 (2010).

291 Wallace, M. A. *et al.* Superoxide inhibits 4Fe-4S cluster enzymes involved in amino acid biosynthesis. Cross-compartment protection by CuZn-superoxide dismutase. *J. Biol. Chem.* **279**, 32055-32062, doi:10.1074/jbc.M403590200 (2004).
292 Srinivasan, C., Liba, A., Imlay, J. A., Valentine, J. S. & Gralla, E. B. Yeast lacking superoxide dismutase(s) show elevated levels of "free iron" as measured by whole cell electron paramagnetic resonance. *J. Biol. Chem.* **275**, 29187-29192, doi:10.1074/jbc.M004239200 (2000).
293 White, M. F. & Dillingham, M. S. Iron–sulphur clusters in nucleic acid processing enzymes. *Curr. Opin. Struct. Biol.* **22**, 94-100, doi:10.1016/j.sbi.2011.11.004 (2012).
294 Netz, D. J. *et al.* Eukaryotic DNA polymerases require an iron-sulfur cluster for the formation of active complexes. *Nat. Chem. Biol.* **8**, 125-132, doi:10.1038/nchembio.721 (2011).
295 Paul, V. D. & Lill, R. Biogenesis of cytosolic and nuclear iron–sulfur proteins and their role in genome stability. *Biochim. Biophys. Acta* **1853**, 1528-1539, doi:10.1016/j.bbamcr.2014.12.018 (2015).
296 Boal, A. K. *et al.* Redox signaling between DNA repair proteins for efficient lesion detection. *Proc. Natl. Acad. Sci. U. S. A.* **106**, 15237-15242, doi:10.1073/pnas.0908059106 (2009).
297 Kelley, S. O. & Barton, J. K. Electron Transfer Between Bases in Double Helical DNA. *Science* **283**, 375-381, doi:10.1126/science.283.5400.375 (1999).
298 Núñez, M. E., Hall, D. B. & Barton, J. K. Long-range oxidative damage to DNA: Effects of distance and sequence. *Chem. Biol.* **6**, 85-97, doi:10.1016/S1074-5521(99)80005-2 (1999).
299 Genereux, J. C. & Barton, J. K. Mechanisms for DNA Charge Transport. *Chem. Rev.* **110**, 1642-1662, doi:10.1021/cr900228f (2010).
300 Boal, A. K. *et al.* DNA-Bound Redox Activity of DNA Repair Glycosylases Containing [4Fe-4S] Clusters. *Biochemistry* **44**, 8397-8407, doi:10.1021/bi047494n (2005).
301 Weyemi, U. *et al.* ROS-generating NADPH oxidase NOX4 is a critical mediator in oncogenic H-Ras-induced DNA damage and subsequent senescence. *Oncogene* **31**, 1117-1129, doi:10.1038/onc.2011.327 (2012).
302 García-Santamarina, S., Boronat, S. & Hidalgo, E. Reversible Cysteine Oxidation in Hydrogen Peroxide Sensing and Signal Transduction. *Biochemistry* **53**, 2560-2580, doi:10.1021/bi401700f (2014).
303 Winterbourn, C. C. & Hampton, M. B. Thiol chemistry and specificity in redox signaling. *Free Radical Biol. Med.* **45**, 549-561, doi:10.1016/j.freeradbiomed.2008.05.004 (2008).
304 Veal, E. A., Day, A. M. & Morgan, B. A. Hydrogen Peroxide Sensing and Signaling. *Mol. Cell* **26**, 1-14, doi:10.1016/j.molcel.2007.03.016 (2007).
305 McDonagh, B., Sakellariou, G. K., Smith, N. T., Brownridge, P. & Jackson, M. J. Differential Cysteine Labeling and Global Label-Free Proteomics Reveals an Altered Metabolic State in Skeletal Muscle Aging. *J. Proteome Res.* **13**, 5008-5021, doi:10.1021/pr5006394 (2014).
306 Zaccarin, M. *et al.* Quantitative label-free redox proteomics of reversible cysteine oxidation in red blood cell membranes. *Free Radical Biol. Med.* **71**, 90-98, doi:10.1016/j.freeradbiomed.2014.03.013 (2014).
307 Murray, C. I. & Van Eyk, J. E. Chasing Cysteine Oxidative Modifications: Proteomic Tools for Characterizing Cysteine Redox-Status. *Circulation.*

Cardiovascular genetics **5**, 591-591, doi:10.1161/CIRCGENETICS.111.961425 (2012).

308 van der Reest, J., Lilla, S., Zheng, L., Zanivan, S. & Gottlieb, E. Proteome-wide analysis of cysteine oxidation reveals metabolic sensitivity to redox stress. *Nature communications* **9**, 1581, doi:10.1038/s41467-018-04003-3 (2018).

309 Gould, Neal S. *et al.* Site-Specific Proteomic Mapping Identifies Selectively Modified Regulatory Cysteine Residues in Functionally Distinct Protein Networks. *Cell Chemical Biology* **22**, 965-975, doi:10.1016/j.chembiol.2015.06.010 (2015).

310 Bar-Peled, L. *et al.* Chemical Proteomics Identifies Druggable Vulnerabilities in a Genetically Defined Cancer. *Cell* **171**, 696-709.e623, doi:10.1016/j.cell.2017.08.051 (2017).

APPENDICS: PUBLISHED PAPER

Identification of a non-gatekeeper hot spot for drug-resistant mutations in mTOR kinase

TJ Wu, X Wang, Y Zhang, L Meng, JE Kerrigan, SK Burley, XFS Zheng

Cell reports 2015, 11 (3), 446-459